FORCED RESPONSE OF SFDs OPERATING WITH A BUBBLY (AIR/OIL) MIXTURE

Sergio Diaz
Dr. Luis San Andrés

April 1997

TRC-SFD-1-97

Texas A&M University
Mechanical Engineering Department

FORCED RESPONSE OF A SQUEEZE FILM DAMPER OPERATING WITH A
BUBBLY (AIR/OIL) MIXTURE

by

Sergio Diaz
graduate student
Luis San Andrés
Associate Professor, P.I.
1997 Plank Co. Faculty Fellow

Subject: squeeze film dampers

April 1997

TABLE OF CONTENTS

NOMENCLATURE

A amplitude of journal motion (fit) [m].

C *SFD* nominal clearance [0.343 mm].

D journal diameter [129.4 mm].

e journal orbit radius or eccentricity [0.216 mm].

f $f_r + if_t$, squeeze film force per unit length (at Z_j) [N/m].

f_r, f_t radial and tangential components of squeeze film force [N/m].

FFT   Fast Fourier Transform.

h $C + e\ cos(\omega t)$. Local film thickness [m].

Hz Hertz

i $\sqrt{-1}$. Imaginary unit.

L *SFD* journal length [31.1 mm].

LPM   liters per minute.

n number of full periods of journal motion.

O offset of journal motion (fit) [m].

$P(t)$ period-averaged or instantaneous film pressure at location (Z_j, θ). [Pa].

$p\text{-}p$ peak-to-peak amplitude.

PG   pressure gauge.

PP   displacement sensor.

PT   pressure transducer.

R journal radius [64.7 mm].

rpm   revolutions per minute.

r, t radial and tangential coordinates.

SLPM   standard liters per minute.

t time [sec].

t_o time of minimum film thickness at $0°$ [sec].

T $2\pi/\omega$. Journal period of motion [sec].

TT   temperature transducer.

X, Y horizontal and vertical coordinates and journal center displacements [m].

X_j $A \cdot cos(\Omega t - \phi) + O$. Journal horizontal displacement (fit) [m].

Z_j axial location of pressure measurements [mm]. Z_1 (5.16 mm), Z_2 (16.7 mm).

Z_a inlet *SFD* plane.

Z_3 discharge *SFD* plane.

β angle between squeeze film force and the radial direction.

$\delta h / \delta t$ local time rate of change of the film thickness.

ϕ phase of journal motion (fit) [rad].

λ mixture void fraction (air volume/total volume).

φ mixture quality (air mass/total mixture mass).

θ angular location of pressure measurements [rad].

Ω journal whirl frequency (fit) [rad/sec].

ω journal whirl frequency [rad/sec].

LIST OF FIGURES

EXECUTIVE SUMMARY

Squeeze film dampers (*SFDs*) are effective means to reduce vibrations and to suppress instabilities in rotor-bearing systems. Most dampers operate with low levels of external pressurization allowing for lubricant vaporization in the regions where the local film thickness is increasing. However, at operating conditions while traversing critical speeds with large orbital whirl motions, ingestion of an external gaseous media (air) into the squeeze film lands leads to a bubbly (air on oil) mixture. This pervasive phenomena, known as *dynamic gaseous cavitation*, lacks proper physical understanding and sound analytical modeling, although it is generally accepted that it affects greatly the dynamic force capability of *SFDs*.

Progress is reported on an experimental investigation to determine the performance of a *SFD* operating with *gaseous cavitation* (air ingestion into the fluid film). Tests are conducted in a constrained circular orbit, open end *SFD* supplied with a controlled bubbly mixture of air and oil. Detailed measurements of the *dynamic* squeeze film pressures and journal motion, film temperatures, electrical power, air and lubricant flow rates are performed at two whirl frequencies (8.33 and 16.67 Hz) as the air content in the mixture increases from 0% to 100%. A review of the literature indicates that theoretical models are yet to account for the physical aspects of bubble dynamics and its effects on squeeze film damper performance.

At fixed whirl frequency and mixture void fraction, the experimental *dynamic* film pressures for different periods of shaft speed have a noisy character associated to the non-homogeneous nature of the bubbly mixture. The analysis of *period-averaged dynamic* film pressures from many cycles of journal motion reveals a zone of uniform low pressure (*gaseous cavitation*) with a magnitude equal to the damper discharge pressure, independently of the mixture composition. The *gaseous cavitation* zone extends as the mixture void fraction increases and develops around the position of local maximum film thickness. Similitude of the *dynamic* pressures measured around the damper circumference makes evident a pressure field rotating at a frequency equal to the shaft speed. Then, a simple kinematic relation allows the estimation of *SFD* forces (resulting from the action of the film pressure on the journal surface) from the test *dynamic* pressures measured at a fixed angular location. The resulting damper forces, peak-to-peak film pressures, and drive power decrease as the air content in the bubbly mixture rises, evidencing a notable reduction in the damping capability of the *SFD*. The line of action of the damper force undergoes a shift from the tangential direction for pure oil towards the radial direction as the air volume fraction increases. This radial centering force is produced by the axial flow through the damper and still apparent even without journal whirl motion.

AN APPRAISAL OF THE LITERATURE ON GASEOUS CAVITATION IN SQUEEZE FILM DAMPERS

The two most commonly recurring problems in rotordynamics are excessive steady-state synchronous vibration levels and subsynchronous rotor instabilities. Squeeze film dampers (*SFDs*) have been successfully used to remedy these problems, stabilizing otherwise unstable units [Childs, 1993]. However, although *SFDs* are widely used in high speed turbomachinery, their operation is yet not fully understood [2].

The incompressible-fluid Reynolds equation is generally used to model hydrodynamic bearings, including squeeze film dampers. However, Childs[1993], Walton et al.[1987], Zeidan and Vance[1989a, 1990a], and many others establish that the correlation between theory and experiment is considerably less compelling for dampers than bearings due to *dynamic lubricant* cavitation. To this date the onset and extent of *dynamic* cavitation or film rupture are difficult to predict, and its effects on squeeze film damper performance are not known adequately. Lack of proper physical understanding on the phenomena of dynamic fluid film rupture appears to be generalized.

Squeeze film dampers derive their behavior from a lubricant being squeezed in the annular space between a non-rotating journal and a bearing housing. The journal, typically mounted on the outer race of rolling element bearings, whirls due to the forces exerted on the rotating shaft. The squeeze film action generates hydrodynamic pressures and damping forces at the film locations where the instantaneous local gap is decreasing. Analyses also predict suction pressures in regions where the film thickness is locally increasing. In these

1

zones, simple analytical models assume the lubricant to cavitate, *i. e.*, to undergo an *instantaneous* phase change since an ideal fluid is unable to sustain tension. In actuality, air ingestion is most likely to occur, generating a bubbly (air on oil) mixture that resembles a foam.

Zeidan and Vance [1989b, 1990b,c], Walton et al.[1987], and Hibner and Bansal [1979] report the occurrence of two different mechanisms of cavitation in squeeze film dampers, namely, vapor cavitation and gaseous cavitation. *Vapor cavitation* in a fluid film bearing occurs when the fluid pressure drops to its saturation value and a phase change (vaporization) follows. *Gaseous cavitation* occurs when the relative movement between the damper journal and housing drags air into the film or releases air dissolved in the lubricant, eventually leading to a two phase mixture. This last mechanism of film rupture is intimately related to the kinematics of motion, and is the one most commonly to appear in commercial applications of squeeze film dampers. Yet, to this date, there is no accurate model for predicting the effects of air ingestion on *SFD* performance.

Zeidan and Vance [1990b,c], and Walton et al. [1987] perform observations of open ends *SFD* film flows with high speed motion pictures, and find that the occurrence of gaseous cavitation leads to a two phase (non-homogeneous) **bubbly** mixture within the dampers. The air present in the mixture forms bubbles persisting even in the high pressure zone generated by the squeeze motion. Zeidan and Vance's experiments show typical dynamic pressures due to gas cavitation, and qualitatively describe the differences between a gaseous cavitation pressure field and that due to lubricant vapor cavitation.

The traditional modeling of cavitation inception and extent calls for boundary conditions, and specifically treats the fluid as a single component material. A detailed review of these boundary conditions is presented by Braun and Hendricks[1984] and Ku and Tichy[1990] for hydrodynamic bearings. The simplest model, the infamous half-Sommerfeld or π-film condition, replaces a uniform *cavitation* pressure for any negative pressures resulting from solution of the Reynolds equation since *no real fluid can support tension*. Later, the Swift-Stieber (or Reynolds) condition devices a null pressure gradient at the cavitation inception zone to account for flow continuity on the cavitation zone. The recognition of measured sub-atmospheric pressures within hydrodynamic journal bearings brings the need to account for the flow carried through the cavitation zone. The *separation model* considers that the lubricant moves under and/or over the cavitation zone, and requires of a null velocity gradient across the film, a condition equivalent to the inception of secondary flows. This condition causes a flow reversal region where dissolved gases can congregate and results in a negative pressure gradient at the cavitation boundary. The *Floberg cavitation model* postulates the conservation of lubricant mass flow through the cavitation zone, and without mass transfer between the liquid lubricant and the cavity at uniform pressure. Next, Olsson modified the Floberg condition for a moving boundary in dynamically loaded bearings constituting the *JFO model (Jakobsson- Floberg-Olsson)*. Both, the separation and the Floberg models account for sub-atmospheric pressures in the film.

The validity of these last cavitation models can not be questioned in steadily loaded journal bearings. Braun and Hendricks [1984] determine that in an eccentric journal bearing the extension of the gas-vapor filled cavity is well predicted by the Floberg model. Ku and Tichy [1990] develop a simplified formulation of the *JFO condition*, predict the size and location of the vapor cavity in a tightly sealed *SFD*, and show good agreement with their own experiments. Boedo and Booker [1994] study the negative squeeze motion of two parallel plates separating and conclude that the *JOF condition* is suitable for gaseous cavitation prediction. Jung and Vance [1993a,b] use the *Swift-Stieber conditions* to predict vapor cavitation effects in a long *SFD* executing circular centered orbits. This cavitation model allows them to produce good comparisons between their measured dynamic pressures and the computed predictions. In general, the boundary conditions discussed above seem to be suitable to predict the occurrence (onset and extent) of either vapor cavities or stationary gas or gas-vapor cavities. On the other hand, gaseous cavitation in *SFD*s is characterized by a **bubbly** mixture where the air bubbles are dispersed and persist even in high pressure zones. Thus, the physics of the gaseous cavitation in squeeze film flows does not allow the implementation of the conventional cavitation models.

Undaunted by the complexity of this phenomenological problem, several authors have addressed the importance of air entrainment on fluid film bearing performance. It appears reasonable to expect that small concentrations of air dissolved within the lubricant do not appreciably affect the oil properties. On the other hand, a two phase system where large amounts of air are mechanically captured as discrete bubbles (entrained air) leads to a mixture with properties different from those of the original lubricant (Chamniprasart et al.,1993). The two material properties of importance for an air/oil mixture are its viscosity and density, and must be related directly to the local instantaneous hydrodynamic pressure which must be related to the kinematics of journal motion. The general approach has been to model the (air/oil) mixture by estimating its effective or equivalent viscosity and density, while still using a Reynolds-like lubrication equation to determine the resulting pressure field. Several attempts to estimate the mixture properties lead to sometimes contradictory models. Feng and Hahn [1986] and Pinkus [1990] present an extensive compilation of expressions for the mixture viscosity. These are, namely:

- *Owens model*, the mixture viscosity is equal to the base liquid viscosity;
- *Cicitti model*, the mixture viscosity is a linear combination of liquid and gas viscosities based on their respective volume fractions;
- *Dukler model*, the mixture viscosity is a linear combination of the component viscosities based on the volume fractions and the relative densities, enlarging the effect of the lower viscosity;
- *Isbin model*, the reciprocal of Cicitti's relation.

Owens model is obviously limited to small amounts of air, while the other three models provide relationships that decrease smoothly from the liquid viscosity to the gas viscosity as the gas volume fraction in the mixture increases. Pinkus[1990] reveals that experience shows that the viscosity of the mixture lays between those predicted by *Owens* and *Isbin* models. The models mentioned predict dissimilar values over a wide range of mixture void fractions, but do not exhaust the possibilities. For example, Hayward [1961] finds experimentally that the viscosity of the mixture increases for small amounts of air. *Hayward model* is based on the Taylor [1932] approximation of the Einstein [1906] theoretical relation for two phase mixtures viscosity.

It is important to note that the available models for the viscosity of binary (i.e., two-component) mixtures, whether these predict increasing, decreasing, or constant viscosity, have been developed for conditions in which the shear stress in the fluid remains small in comparison to the surface tension acting on the oil-gas interfaces. Then, these models are probably suspect under the lubrication conditions prevalent in *SFDs*, where the kinematics of motion cause large shear stresses within the thin film and the bubbles' size is as large or larger than the local film thickness.

Estimation of the density of the mixture is even more intricate. The presence of gas bubbles introduces a compressibility to the lubricant, Pinkus [1990]. Hence, models relating the effective density to the mixture conditions (in particular the pressure) need to be accounted for.

Zeidan and Vance [1990a] detail an approach to determine the squeeze film pressure in *SFDs* operating with bubbly oils so as to reproduce measured pressure profiles. The authors use an experimentally determined density distribution and some of the available viscosity correlations (*Isbin, Owens and Hayward*) in a Reynolds equation of lubrication modified to include effective values of the mixture properties.

If the flow in squeeze film dampers showing gaseous cavitation is regarded as a uniform two phase mixture of oil and air bubbles, then it is natural to introduce the continuum theory of mixtures to model the phenomena. Important research has been developed in this area for over forty years and an attempt to cover all the important works would be beyond the scope of this work. Nevertheless, Atkin and Crane [1976] and Rajagopal and Tao [1995] present remarkable summaries and offer and introduction to the basis of the continuum theory of mixtures. Within the context of this continuum theory, a mixture is defined as a homogeneous combination of two or more immiscible components in solid, liquid or gaseous state. Just as it is done in classical chemistry for mixtures of ideal gases under quasi-static conditions, every component is assumed to occupy the full volume itself, i.e., every spatial point of the mixture contains particles of all the components

in the same proportion (*Principle of Equiprescence*) and the concepts of partial pressures and densities apply.

In the case of ideal gases, it is usually assumed that the interaction between the gaseous components is negligible. Then, the contributions of every component can be computed independently and added together to obtain the resultant property of the mixture. In the general continuum theory of mixtures the interaction between the components is taken into account, and the equations of momentum, continuity and energy of each component are averaged to assemble the corresponding equations for the mixture. There is a certain consensus in the averaging procedures, but the constitutive equations that represent the interaction between components and the nature of the components themselves are still a matter of discussion. As pointed out elsewhere (Atkin and Crane [1976], Rajagopal and Tao [1995]), the frame indifference of the constitutive equations can be forced by a full orthogonal group or by just a proper orthogonal group, either procedure leading to different results. Furthermore, the second law of thermodynamics needs to be introduced, with all the polemics intrinsic to the entropy definition [Tao and Rajagopal, 1997].

In the continuum theory of mixtures, the equations of motion and those of the constituents are complex in nature, and more mathematical expressions than physical relations. A typical problem in a binary mixture can require the solution of 46 simultaneous equations in some cases. An attempt by Tao and Rajagopal [1997] to overcome the uncertainty contained in the entropy inequality for the specific case of bubbly liquids consists on substituting the second law by a dissipation inequality. The authors argue that it should be easier to agree in the fact that energy is dissipated in any process.

Despite the mathematical complexity of the continuum theory of mixtures, the literature presents a series of applications of the mixture theory on the field of tribology. Al-Sharif, et al. [1992], and Wang, et al. [1992] study lubrication films with liquid-liquid emulsions. The authors develop a set of constitutive equations and combine them with the flow equations of motion, to obtain an extended Reynolds equation for binary mixtures in thin film flows. Wang et al. [1992] apply this approach to elasto-hydrodynamic lubrication films with an oil in water emulsion. Chamniprasart et al. [1993] extended the analysis to render a Reynolds equation that accounts for a multiphase continua of a Newtonian liquid (oil) and an ideal gas (air), i.e., a bubbly oil. The modified Reynolds equation is applied to the solution of a finite length loaded journal bearing and compared to some available experimental data given by Braun and Hendricks [1984]. Recently, Szeri [1996] provides a detailed summary of his research with liquid emulsions and bubbly mixtures.

In general, the results of the theory of mixtures present qualitative agreement with some practical observations, but there are still limitations on the application of the theory, in particular with squeeze film flows. A number of yet unknown experimental parameters are needed for predictable results and construction of the constitutive equations. The theory demands homogeneous mixtures and requires the components to be present in such proportions that, according with their densities, the *equipresence principle* can be considered valid. It is worth to note that (so far) the lubrication mixture models do not account for mass transfer between phases. That is, no vaporization or condensation can be considered within them.

Some other approaches start the analysis of bubbly mixtures from a microscale point of view, as opposed to the macroscale standpoint taken by the theory of mixtures. Basically, these models study the dynamics of a single bubble, considering the effects of the bubble composition, size, shape, solubility, change of phase, surface tension, damping, thermal effects, and in general, its interaction with a surrounding fluid regarded as an infinite medium. Subsequently, the main assumption to model the mixture is uniformity in the distribution of the bubbles (constant number of bubbles per unit volume of liquid). Then, the mixture density can be computed and its viscosity estimated as a function of the local size of the bubbles, thus resulting in a formulation equivalent to that of a compressible fluid. It is noted that, due to the general nature of the mixture theory, this approach can be considered as a particular case where the constitutive equation is that governing the dynamics of a single bubble.

The most general model for the dynamics of a bubble is that described by the *Rayleigh-Plesset differential equation*, exhaustively discussed by Plesset and Prosperetti [1977], Hsieh [1988], and Brennen [1995].

Rayleigh first used the momentum equations to describe the motion of the boundary of a gas-filled spherical bubble while studying the cavitation phenomena and the cavitation damage due to the bubble collapse. Plesset includes terms corresponding to the liquid viscosity and surface tension. Later, terms to account for a number of parameters such as temperature, vaporization or change of phase, compressibility of the liquid, non-spherical shapes, etc., have been added to the original *Rayleigh-Plesset* model, thus rendering a complete and general model. The liquid surrounding the bubble is considered as Newtonian and a state equation needs to be assumed for the gas (usually that of an ideal gas). The study of single bubble dynamics with the *Rayleigh-Plesset* equation can give light to the analysis of cavitation in terms of its inception and nucleation. Other effects such as those due to viscosity, bubble collapse, effect of contaminant gas, surface roughness, and many others can currently be modeled. Brennen [1995] presents an excellent compilation of results and discussions regarding these points.

One of the issues relevant to the phenomenology of *gaseous cavitation* in squeeze film flows relates to the behavior of a bubble within a pressure field varying both in time and space. The presence of a contaminant gas will lead to bubbles filled with a mixture of gas and lubricant vapor and whose internal pressure is the sum of the partial pressures. If the concentration of gas provides sufficiently large pressures, the bubble will grow at liquid pressures greater than the vapor pressure and the tensile strength could be negative. This prediction coincides with the experimental observations of persisting bubbles in the high pressure zone of squeeze film dampers as reported by Zeidan and Vance [1989,1990] and Walton, et al. [1987]. In early stages of gaseous cavitation inception, i.e., formation of the bubbly mixture, when the bubbles are small, a rectified mass diffusion can result in the growth of the bubble during successive cycles of pressure until a dynamic equilibrium is reached. Some parallel can be found with the observations of the gaseous cavitation development in *SFDs*. For a given pressure, a critical radius exists above which the bubble will grow (unstable). That is, for a given radius if the pressure drops below a certain value the bubble becomes unstable and grows without bounds. This growth, however, can be stopped by an increase in the pressure, and the collapse of the bubble will be faster than its development. This could explain the ability of squeeze films to support negative (absolute) pressures for short periods of time

Sun and Brewe [1992] compare, in a theoretical analysis, the typical times required to fill a cavity with vapor by evaporation, and with gas by diffusion. They show that vapor can fill the cavity in a time that can be considered instantaneous when compared to the time required to fill it by diffusion. These results support the assumption made in the derivation of the *Rayleigh equation* that the partial pressure of the vapor is constant and equal to the corresponding vapor pressure of the oil at the bubble temperature while the air mass is considered constant.

The known applications of the *Rayleigh-Plesset equation* to lubrication thin films are based on overly simplified versions (most commonly not even referenced as related to their parent model, i.e. the *Rayleigh-Plesset* equation). For example, neglecting the dynamic terms in the general *Rayleigh-Plesset* equation leads to a simple equilibrium relation between the internal bubble pressure, the surface tension, and the pressure of the external fluid, and equivalent to a quasi-static assumption for the bubble motion (i.e. that occurring at excitation frequencies much lower than the bubble natural frequency). Pinkus [1990] applies this formulation to a circular thrust bearing and reports good agreement between predictions of load capacity and experiments for mixtures with as much as 90% air volume injection. However, Pinkus also notes a negligible variation on the bearing performance and attributes it to an early expulsion of the air from the bearing pads due to centrifugal forces. Braun and Hendricks [1984] use the same equilibrium relation in conjunction with several sets of boundary conditions to predict the cavity location and extent in a *gaseous cavitated* steadily loaded journal bearing. The authors report reasonable agreement with their experiments in the case of the Floberg boundary condition.

The works of Pinkus [1990], and Braun and Hendriks [1984] for steadily loaded bearings support the viability of using the Rayleigh-Plesset equation in squeeze film flows. However in this later case, there is no sound reason to neglect the dynamics of the bubble. In *SFDs*, the bubbles are subjected to the cyclic motion of the journal, compressing and expanding periodically. This fact is confirmed by Parkins and May-Millers [1984] with detailed experiments on the dynamic behavior of a bubble in the squeeze motion between two parallel

plates. In conclusion, a systematic way to model a squeeze bubbly flow with *the Rayleigh-Plesset equation* needs to be addressed.

Brennen [1995] provides a comprehensive study of *homogeneous bubbly flows*. In separated flows, the streams of the two phases (or components) can travel at different speeds. On the other hand, in homogeneous mixture flows, one phase is very finely dispersed within the other, with sufficiently small particle sizes and so well mixed that their relative motion is negligible. For homogeneous mixtures without relative motion, the governing mass and momentum equations reduce to forms similar to those for single-phase compressible fluids with effective mixture properties. The effective local density may be defined as the weighted average of the phases' densities according to their local volume fraction as given by the concentration of bubbles per unit volume of liquid (usually a constant) and the size of the bubbles (governed by the *Rayleigh-Plesset equation*). The local effective mixture viscosity could be estimated by one of the available expressions based on the local volume fraction.

An adequate barotropic relationship for the mixture density provides closure for the mass and momentum transport equations replacing the *Rayleigh-Plesset equation*. This means that the two-phase mixture could be modeled as a single-phase compressible fluid with such a barotropic relation, and thus, the whole spectrum of phenomena observed in single-phase gas dynamics can also be expected in two-phase flows. That is, we could expect to find some similitude between the lubrication with bubbly mixtures and the gas lubrication theory. In some multiple phase flows it is possible to explicitly establish such a barotropic relation using the *Rayleigh-Plesset* equation. However, a barotropic relation requires some thermodynamic property like the temperature or the entropy to be held constant. And then, only for highly simplified cases (both mixture phases are considered in thermodynamic equilibrium, dynamics of the bubbles is neglected, surface tension is neglected and/or many other simplifications on the component densities, mixture density definition, etc.), the sonic speed of the mixture can be estimated and the associated barotropic relation can be obtained explicitly. However, when the mixture components are not in equilibrium at all times and the dynamics of the bubbles have an important role, it becomes very difficult or in some cases impossible to find a barotropic relation. In such cases, the *full Rayleigh-Plesset equation* describing the dynamics of individual bubbles should be incorporated into a flow model which also accounts for the mixture transport of mass and momentum equations along with the appropriate density and viscosity models.

Hsie [1988] applies the averaging scheme of Drew [1971] along with the *Rayleigh-Plesset equation* to derive a set of governing equations for general bubbly flows. This mathematically rigorous as well as physically plausible model is able to predict the behavior of mixtures with relative motion between its components, with bubbles of different natures (components, sizes, shapes, etc.). The major limitation stems from the fact that the *Rayleigh-Plesset equation* models the dynamics of each bubble independent from others and thus, no interactions with the flow boundaries are likely to be implemented. Furthermore, Humes and Holmes [1978] and Sun et al.[1993] note that fluid cavitation is not a stable phenomenon. The inception and extent of cavitation can be more severe in one case than in others even under the same test conditions, or it can even simply not occur and the lubricant may be able sustain substantial tensile forces.

Sun and Brewe [1992] state that *air entrainment is device dependent, its occurrence requires the presence of adequate leak path(s)*. The effects of air ingestion (*gaseous cavitation*) on the performance of squeeze film dampers, although well known because of its pervasiveness in the commercial applications, have defied accurate analysis. Prediction of gaseous cavitation inception and the extent of its influence on damper forces are unknown. Hence, it becomes necessary to initiate a systematic experimental research along with theoretical developments to produce reliable models for reliable design of squeeze film dampers.

Progress is reported on an experimental investigation to determine the performance of a *SFD* operating with *gaseous cavitation* (air ingestion into the fluid film). Tests are conducted in a constrained orbit *SFD* supplied with a controlled bubbly mixture of air and oil. Detailed measurements of the *dynamic* squeeze film pressures and journal motion, film temperatures, electrical power, lubricant flow and mixture composition are performed to identify the parameters affecting most the performance of the *SFD*. In addition, important performance parameters like the peak-to-peak *dynamic* pressures and squeeze film forces are derived from

the measurements. The current experiments and comprehensive analysis complement earlier test results of Diaz and San Andrés [1997].

EXPERIMENTAL FACILITY

The test rig has been successfully used in 10 years of continuous research activities. Detailed descriptions of the apparatus can be found in Arauz and San Andrés [1993, 1996]. The squeeze film damper test apparatus is shown in Figure 1a. The test section consists of a journal (length, L=31.1 mm, outer diameter, D=129.4 mm) mounted on an eccentric sleeve with a ball bearing to provide a controlled circular orbit (Figure 1b). This eccentric is mounted on a rigid shaft supported by precision ball bearings in an overhung configuration. The journal has four anti-rotation pins allowing it to whirl but not to spin. A variable speed electrical motor drives the shaft and damper journal through a toothed belt. The whirl frequency (equal to shaft speed) is measured by an optical sensor. The nominal radial clearance (C) of the damper is 0.343 mm (13.5 mils), and the nominal journal eccentricity or orbit radius (e) is 0.216 mm (8.5 mils), (e/C=0.63) for an unpressurized condition.

The lubricant employed on the tests is an ISO VG 68 of density (ρ) equal to 0.87 gr/cm^3 and measured viscosity (μ) equal to 77.5 and 25.8 centipoise at 28 and 50.9 °C, respectively. The oil is stored in a 113.6 liters (30 gallons) reservoir and delivered to the SFD test section via a gear pump. The damper is lubricated with a bubbly mixture of oil and air. The flow rates of oil and air are regulated by setting the valves in the oil line, air line, and oil bypass (Figure 2). The mixture is produced at the sparger (mixer element) in the junction of air and oil lines. The static (feed) pressures of oil and air are displayed in Bourdon type pressure gauges, PG_1 and PG_2, respectively. An additional gauge (PG_3) allows measurement of the air-oil mixture pressure just before its entrance to the damper test section. There are two windows made of transparent hoses to monitor the condition of the mixture. These are located at the inlet and outlet ports of the SFD. A thermal mass flowmeter (0-100 SLPM[1]) is employed to measure the air flow rate, and a positive displacement gear flowmeter (up to 4 LPM[2]) for the oil volumetric flow rate. The lubricant inlet and outlet temperatures, the film temperature, and the air supply temperature are measured with K-type thermocouples (TT).

The lubricant is fed to the damper left end (Z_o) through two holes at the top and bottom sections (180° apart from each other). The damper left end is sealed with an O-ring so there is no leakage in this direction (see Figure 1b). The right end (Z_3) opens to a plenum. This configuration maximizes the axial pressure variation and results in a constant pressure at the right end of the damper. In the test rig, the plenum pressure is displayed on a pressure gauge installed in the housing cap as indicated in Figure 1a. The test damper configuration resembles actual configurations used in commercial SFDs.

The motion of the journal is measured with two non-contact eddy current sensors (PP_x and PP_y) located in the horizontal and vertical directions. Four piezoelectric pressure transducers (PT) are flush mounted at the plane of Z_2 (16.7 mm from the left end) on the circumferential locations 0°, 120°, 180°, and 240°, measured clockwise from the positive x axis (see Figures 1b and 2). As the piezoelectric transducers can only measure dynamic variations of the pressure, two strain gage pressure transducers are flush mounted at 330° on two different axial locations (Z_1 and Z_2) to measure absolute film pressures. The location Z_1 (5.6 mm from the left end) is nearer to the sealed end of the SFD, and Z_2 is a location half way between Z_1 and the open end of the damper (see Figure 1b). The signals of the pressure transducers and displacement sensors are monitored with oscilloscopes, conditioned with the aid of amplifiers, and recorded simultaneously with a 16 bits, A/D board to a computer.

EXPERIMENTAL PROCEDURE

Prior to the tests, a calibration of the instrumentation is performed. Manufacturer values for sensitivity and precision of the flowmeters, pressure transducers, proximity probes, pressure gauges and thermocouples are

---

[1] SPLM: standard liters per minute
[2] LPM: liters per minute

verified. An error analysis of the mixture air/oil volume ratio, a derived parameter, establishes the overall uncertainty on its measurement based on the individual uncertainties of the measured parameters.

The mixture void fraction is defined as the air volumetric flow rate divided by the total volumetric flow rate (air plus oil). The oil flow rate is obtained directly from the meter display, but the air meter provides a mass measurement (*SLPM*). So, air temperature and pressure are required to obtain the actual air volumetric rate from that at standard conditions. These four measurements are taken into account to estimate the void fraction uncertainty. The individual calibration errors are: oil flow meter, 1% of measurement, air flow meter, 0.5% of full scale (100 *SLPM*), pressure gauge, 3% of full scale (150 psi), and thermocouple, 1% of full scale (200 °F). The void fraction uncertainty is depicted as error bars on the corresponding graphs given later.

The experiments consist of two sets of measurements taken at two shaft speeds, 500 rpm (8.34 Hz) and 1000 rpm (16.67 Hz). On both cases, the mixture void fraction is increased from 0 to 1, with air and oil at constant supply pressures of 6.8 bar (100 psi), and constant feed temperatures equal to room temperature (25 °C). The mixing of oil and air is produced in a sparger, where a diameter reduction accelerates the oil and locally decreases its pressure below that of the air. The mixture void fraction is regulated by valves on the oil and air feeding lines, and which makes necessary some elapsed time before a uniform mixture condition is achieved (usually less than 2 minutes). The power supply to the drive motor needs to be reset for each test mixture void fraction value in order to keep a constant shaft speed due to variations on the damper power consumption.

For each test case, the values of the temperatures and feed pressures of air, oil, and mixture, the air and oil flow rates, and the journal speed are manually recorded, as well as the voltage and current supplied to the drive motor. The time signals of the pressure transducers at the axial location Z_2 and the horizontal (X) journal displacement sensor are acquired simultaneously, at a rate of 500 samples per second, and a total of 1,024 data points for each signal (34 cycles of journal motion for 1,000 rpm, and 17 cycles for 500 rpm). The tests performed at 500 rpm also include the pressure transducer at location Z_1 and the vertical (Y) journal displacement sensor. The digital data is stored as ASCII files (one per pressure transducer for a given whirl speed and mixture void fraction), for later analysis with a dedicated data processing software.

ANALYSIS OF THE MEASUREMENTS

Most of the significant results of this study are derived from a sophisticated and extensive data processing and analysis from the directly measured variables, journal displacement and squeeze film pressures. It is convenient to subdivide the measured quantities into *steady* and *dynamic* to better understand the process of analysis. A *steady* variable does not vary during each of the test cases, and a *dynamic* variable is that which changes with time within each journal motion cycle.

In the following, the procedure devised for processing the test measurements is described, from the acquisition of the steady variables identifying every test case to the estimation of damper forces on the whirling journal. Intermediate steps encompass units conversion, signal conditioning, period and ensemble averaging, graphical representation and analysis, parameter identification, data smoothing, frequency analysis, and numerical integration of pressures. A flow chart sketching the processing analysis is depicted in Figure 3.

THE MEASUREMENTS AND THEIR UNCERTAINTIES

Steady or *stationary variables*, like lubricant temperatures, journal speed, supply and discharge pressures, and power supply voltage and current, are manually recorded from the measuring instruments as a single number, considered representative for the whole time span of the test. In this case, the main source of measurement uncertainty is that of the instrument itself, and whose calibration and precision are verified in the laboratory against manufacturer values. This measurement uncertainty reflects on the uncertainty of the derived *steady* parameters such as drive power or mixture composition. The estimation of this uncertainty is performed by the standard methodology for error propagation in single-sample measurements as given by Kline and McClintock [1953].

Dynamic variables, i.e., film pressures and journal displacements, are measured and stored digitally in a computer as discrete functions of time. In this case, two types of uncertainties are present. As in any experimental measurement the instrumentation precision, or better said lack of precision, produces measurement uncertainties. In the present experiments the analog to digital conversion is the main component of instrumentation uncertainty, and which is on the order of hundredths of a bar for pressure for example. However, the time dependency of the measured variables and the temporal fluctuations associated with the nature of the bubbly mixtures result in another kind of uncertainty, referred to as first-order uncertainty by Moffat [1982]. This uncertainty is related to changes in the repeated measurement of the same variable, as occurs in a test when values of the sampled *dynamic* variable from different periods of journal motion are compared to each other. In the current experiments the temporal fluctuations of the peak-to-peak squeeze film dynamic pressures from cycle to cycle of journal motion can be as high as one bar. These variations largely overcome the instrumentation uncertainty (by about two orders of magnitude). Therefore, the resultant uncertainties are presented in terms of temporal fluctuations. No attempt is done to include instrumentation uncertainty in the analysis of the *dynamic* variables.

MIXTURE QUALITY AND VOID FRACTION

The mixture composition is determined from the *static* measurements of oil flow rate, air mass flow rate, and local temperature and pressure of the mixture. The mixture quality (φ) defined as the ratio of air mass flow to total mass flow (air plus oil) is calculated from the flowmeter readings and the value of oil density. This ratio is a good estimate of quality if both phases in the mixture travel with the same velocities and the release of air previously dissolved in the oil is minimal. Both assumption are reasonable based on the visual observation of the bubbly mixture. The mixture void fraction (λ) or air volume fraction changes with the mixture conditions (temperature and pressure) given that the mixture quality remains constant. The void fraction is defined as the ratio of the local air volume to the total volume. The oil volumetric flow rate is directly measured from a flow meter, but the air volume is computed using the mass flow and assuming that the bubbles are in equilibrium at the local mixture pressure and temperature (the surface tension is neglected in this calculation). This assumption results in an estimate of the mixture void fraction which gives an excellent approximation or reference value, though not the real one. Three locations on the test rig are selected to compute the mixture void fraction. These are at the sparger (mixer), the damper inlet, and the damper exit (plenum), given that these are the most representative of the mixture condition and that the available instrumentation provides full description of the local conditions.

DRIVE POWER CONSUMPTION

The drive power to the test rig is calculated as the product of the voltage and current supplied to the electrical motor. *Steady* variables digitally measured in the power source are voltage within ±0.1 Volts, and current within ±1 amperes.

PEAK-TO-PEAK PRESSURES AND JOURNAL ORBIT SIZE

The measurements recorded as discrete functions of time are processed in several steps, each one associated with a particular procedure. The first procedure accounts for the transformation of the discrete data into their respective physical units, and regroups the data into one file per location of pressure measurement per whirl frequency. This file includes all the different mixture void fraction cases. At this step, a recurrent 60 Hz noise introduced by the transducer power supply in the measurement of the absolute pressure at (Z_1, 330°) is digitally filtered (See Figure 5 later).

The second procedure, takes the data file of each pressure measurement and finds the temporal average of the peak-to-peak pressure. This average peak-to-peak pressure is defined as the difference between the average of the maximum pressure peaks in the whole test time (32 periods of journal motion at 1,000 rpm, and 16 periods for 500 rpm), and the average of the minimum pressure peaks over the same period of time. Estimates of the fluctuations on the instantaneous peak-to-peak pressure are also determined by finding the *lowest ever* and *highest ever* values over the sampled time. The *static* pressure component is computed as the overall average of the absolute pressures measured with the strain gauge transducers. Additionally, since

the *SFD* configuration presents circumferential symmetry and the pressure field is suspected to rotate synchronously with the whirling journal, a *spatial average* is also computed by ensemble averaging the average peak-to-peak pressures of the pressure transducer located at the same axial location (Z_2).

A similar treatment is given to the journal displacements in the horizontal (X) and vertical (Y) directions. The maximum and minimum peak displacement averages are computed for each direction. Half the difference between the maximum peak displacement average and the minimum peak displacement average provides the time averaged orbit radius. The largest and lowest differences give the level of temporal fluctuations on the orbit radius. The overall average of the measured *dynamic* displacements provides the *static* displacement of the orbit center within the damper clearance.

RANDOM FLUCTUATIONS AND TIME AVERAGING

The random temporal fluctuations in the measurements of *dynamic* squeeze film pressures and journal displacements are significant due to the nature of the bubbly mixtures. For the sake of analysis simplicity it is convenient to apply a time averaging procedure able to suppress or at least minimize the effect of the random temporal fluctuations. To this end, the time span of the measured *dynamic* functions is divided into "n" periods of the journal whirling motion (32 periods for the tests at 1,000 rpm, and 16 for those at 500 rpm). The "n" periodic *dynamic* functions are averaged in time and the resulting function is considered to be typical over a full period of journal motion. This averaged function shows minimal effects of the random fluctuations, thus making it representative of the "n" periods of journal motion. However, the effectiveness of this averaging requires the exact knowledge of each period for a journal cycle. Furthermore, the computation of the squeeze film forces, as discussed later, requires precise estimates of the phase lag of the *dynamic* pressure measurements with respect to the minimum film thickness. Additionally, uniformity in frequencies and phases enhances the graphical representation of the test *dynamic* measured variables.

The identification of this phase lag is limited by several factors. First, the discrete nature of the *dynamic* measurements with a given time step size limits the resolution on phase angle identification. Second, the measurements for different mixture compositions are not simultaneous events, and so the frequency of journal motion is not exactly the same in all the tests. Even more, the shaft speed varies slightly during the sampling time giving cycles of different periods for the same test. This prevents good estimation of the phase and frequencies by just using the first and last maximum peaks of the of the *dynamic* periodic function, or the times when this function crosses the zero value. Thus, the discrete *dynamic* function values over the entire time span of a test must be used for the identification of phase lags and frequencies. A non-linear multiple variable curve fitting is applied to the horizontal (X) journal *dynamic* displacement of each test case, i.e.

$$X_j(t) = A. \cos(\Omega t - \phi) + O \tag{1}$$

where the fitting parameters A, Ω, ϕ, and O denote the amplitude, frequency, phase lag and offset. Once the curve fitting is performed, Ω gives the best approximation for the frequency of all the *dynamic* measurements taken simultaneously with the given X-displacement (i.e., one case per speed, per mixture void fraction). Additionally, the ratio ϕ/Ω gives the time for the first occurrence of the minimum film thickness at the circumferential location $0°$ (positive X-axis).

The time averaging scheme is then applied to the *dynamic* pressures, but the origin (in time) of the resulting digital functions is displaced, forcing all the independent averaged functions to concur with the minimum film thickness. Also, the small differences in rotational speed (on the order of 1%) are accounted for by independently scaling the time axis of the averaged functions in such a way that all of them result with the same frequency as the one measured for the case of pure oil operation (i.e., void fraction equals zero). As sometimes the value of the functions is required at times not coinciding with measured points, a linear interpolation scheme, which also helps smoothing the data, is implemented. Calculation of the *FFT* amplitude and phase spectra of the original and time-averaged function is performed for comparison and verification of the goodness of the fit and the smoothing of the function.

Waterfall-like graphs of pressure as a function of the mixture void fraction are generated. These summarize the development of the pressure field at every location of measurement. This process is applied to both, averaged and unprocessed signals, but the most significant information arises from the time-averaged ones. The results are plotted as a *3D* surface, with time in one axis, pressure in other, and mixture void fraction in the third one. This treatment allows visualization of the development of the squeeze film gaseous cavitation from different (spatial) points of view. More importantly, the *3D* surface representation leads to the application of contour plots that facilitate the identification of pressure levels and *gaseous cavitation* zones. As will be discussed later, *gaseous cavitated* films present a zone of uniform or constant pressure that starts during the negative squeeze motion (increasing film thickness) and persists until part of the positive squeeze (decreasing film thickness) takes place [Diaz and San Andrés, 1996, 1997]. The *gaseous cavitation* zone is approximately centered around the point of maximum film thickness.

EVALUATION OF SQUEEZE FILM FORCES

The ultimate objective of the experimental study is to evaluate the effects of air entrainment in the lubricant film and the dynamic forces generated by the journal motion. Hence, the relationship between journal kinematics and ensuing squeeze film pressures needs to be addressed. The forces acting on the rotor are the resultant of the pressure acting on the journal surface. Thus, spatial integration of the squeeze film pressure field would yield the desired forces. However, the test rig configuration does not allow for measurement of pressure at enough different spatial locations (axial and circumferential). Fortunately, the cyclic characteristic of the journal motion and the damper rotational symmetry (for circular centered orbits) allow to correlate the pressure profile around the journal to the *dynamic film* pressures at a fixed angular location during one cycle of journal motion. In this case, the pressure field rotates synchronously with the journal whirl speed, i.e. the pressure profile is *stationary* for an observer rotating with the drive shaft. Therefore, the *dynamic* pressure variations detected by a *stationary* observer (at a fixed angular location in the damper housing) have a unique correspondence to the values of the *stationary* pressure field as this rotates with an angular speed equal to the journal whirl frequency. To verify this assertion, the pressure profile measured by a *stationary* transducer for one cycle of journal motion is plotted in polar coordinates and superimposed to the pressures measured simultaneously with other pressure transducers at other angular locations around the damper circumference (see the section *Results*).

Damper forces (F_r, F_t) in the radial and tangential directions arise from integration of the pressure field around the journal surface. A well known (simple) kinematic relation between the *stationary* (though rotating) pressure field and the *dynamic* pressure field at a fixed location is used to transform the spatial integration around the journal circumference into an integration in time. Thus, the *dynamic* pressure profiles are integrated for every test, rendering estimated radial and tangential forces $(f_r, f_t)_{(Z)}$ per unit length at the axial location of measurement. The relationship is:

$$ f_{(Z)} = (f_r + i \cdot f_t)_{(Z)} = \frac{-\omega \frac{D}{2}}{n} \cdot \int_{t_0}^{t_0 + n \cdot T} P_{(t,Z)} \cdot e^{-i \left[\omega \cdot (t - t_0) + \theta \right]} \, dt $$

(2)

Refer to the *Nomenclature* for a proper definition of all variables. The procedure also computes the test *ensemble* average radial and tangential forces (f_r, f_t) by averaging the forces computed from the pressures at different angular locations of measurement on the same axial plane.

MEASURED RESULTS AND DISCUSSION

Two sets of measurements are presented, one for a shaft speed of 500 rpm (journal whirl frequency equal to 8.33 Hz), and the other at a speed of 1,000 rpm (whirl frequency equal to 16.67 Hz). On both cases, measurements are presented for mixture compositions ranging from pure oil to pure air. The volumetric mixture

composition (i.e., mixture void fraction) is controlled at the mixer element or sparger but it changes along the test rig as noted below.

MIXTURE QUALITY AND VOID FRACTION

Figure 4 relates the mixture void fraction (air volume per unit mixture volume) at the damper inlet and damper outlet (plenum) vs. the void fraction at the sparger. The figure also includes the mixture quality (air mass per unit mixture mass). The mixture quality or mass ratio is assumed to remain invariant along the test rig based on the assertions of no relative movement between phases and negligible release of dissolved air from the oil. The large difference between oil and air densities makes the mixture quality fairly low for the whole range of void fractions, except for very high void fractions. On the other hand, the mixture void fraction increases along the test rig due to the pressure drop and the consequent air expansion. The pressure drop is very small from the mixer to the damper inlet and the mixture void fraction is nearly the same at both locations. However, the pressure drops across the injection holes and axially through the damper are considerable higher (more than 6 bars). Thus, the mixture void fraction at the damper exit or plenum is larger than at the inlet for all the test cases except the two extremes (pure oil and pure air).

Physically, the mixture appearance is different at the inlet and outlet windows. At the inlet section before the *SFD*, the bubbles are small and dispersed on the oil matrix for the entire range of mixture void fractions. At the exit section on the damper discharge, the bubbles are larger and the mixture is foamy. The value of the mixture void fraction at the sparger or mixer element is used as the reference for each test. From here on all results are referred to the mixture void fraction without explicitly specifying its location.

DIGITALLY FILTERED PRESSURE MEASUREMENTS

Figure 5 illustrates one of the difficulties that need to be addressed when analyzing experimental measurements. In this case, one of the strain gauge pressure transducers (the one installed at $330°$, Z_i) introduced systematically a 60 Hz noise to the measured signal. The persistence of this noise on all the measurements allow it to be filtered by using *FFT*s and a digital band-stop filter function. Figure 5 shows one of the measured *dynamic* pressures vs. time and its corresponding frequency spectrum before and after the digital filtering.

MEASURED DYNAMIC PRESSURES AND TEMPORAL RANDOM FLUCTUATIONS

In *SFD*s executing circular centered orbits a cycle of motion comprises of two regions, each lasting half the period of motion. For a fixed observer, the first region occurs when the journal moves toward the bearing (positive squeeze) decreasing the local film thickness, and the other when the journal moves away providing negative squeeze or enlarging the local gap or film thickness.

The measured *dynamic* squeeze film pressures are presented in Figure 6 for 500 rpm (8.33 Hz), and Figure 7 for 1,000 rpm (16.67 Hz). The figures are conformed by several waterfall-like plots, each one corresponding to one pressure transducer and identified by its physical circumferential and axial location. Every one of these plots presents the history of the pressure fields at its particular location when the mixture void fraction increases from zero to one, i.e. pure oil to pure air. The pressure is noted in the vertical axis, the time in the horizontal axis and the mixture void fraction on the in-plane axis. The *noisy* condition of the *dynamic* pressure measurement is the clearest outcome from these results. Each one of the pressure waves depicted presents noticeable variations from one cycle of journal motion to another along with the appearance of random pressure spikes. These temporal fluctuations are almost imperceptible for mixture compositions close to the pure oil condition, though they increase dramatically with the mixture void fraction independently of the transducer location. The pressure spikes may represent the collapse of air bubbles on the zone of high pressure generation (positive squeeze).

The *noise* in the *dynamic* pressure fields is most certainly related to the non-homogeneous nature of the bubbly oil mixture, and whose composition is not exactly the same in every cycle of journal motion. Even more, it is speculated that the pressure of an air bubble is not the same as that of the surrounding oil due to surface tension and the dynamic characteristics of the bubble itself. If a large enough bubble is in front of the

12

pressure transducer, this will sense the bubble pressure rather than the *mixture pressure* (note that the size of the pressure *spikes* seems to be related to the position on the pressure wave at which it occurs). This fact allows to correlate the collapse of bubbles with the random spikes on the measured pressures. A closer look to the results reveals that the pressures appear *noisier* at the measurement locations closest to the lubricant injection holes located at the top (270°) and bottom (90°) of the damper housingt. Therefore, the pressure waves at 120° and 240° are less repetitive in time and present more *spikes* than the ones recorded at the other angular locations more distant form the lubricant inlets. It seems that there are more bubbles and of more different sizes in the neighborhood of the lubricant inlets, as if the mixture tends to become more uniform as it moves away from the injection points. It is speculated, based on observations on a *SFD* with a transparent housing[3], that the larger bubbles are expelled of the film earlier, perhaps due to their lower viscosity, and not reaching film locations distant from the injection point. However, other factors like differences in the local static feed pressures could also induce variations in the measured pressure fields (see section under).

PEAK-TO-PEAK PRESSURES AND FIRST ORDER UNCERTAINTY

Figures 8 and 9 present a compilation of the test results (shown in Figures 6 and 7), and in terms of peak-to-peak (p-p) values of the squeeze film pressure for 500 rpm and 1,000 rpm respectively. The figures show the time-averaged p-p pressure as a function of the mixture void fraction for each physical location on the damper circumference. The vertical bars represent the first-order uncertainty on the estimate of average p-p pressure as given by the time fluctuations in this value over each test with n periods of journal motion. The horizontal bars represent the uncertainty in the measurement of the mixture void fraction. The p-p pressures follow similar trends around the damper circumference at both test frequencies. The introduction of a very small amount of air in the mixture produces a sharp reduction of the p-p pressures (low void fraction). Further increments of the mixture void fraction (from $\lambda=0.02$ to $\lambda=0.85$ approximately) produce a quasi-linear reduction on the p-p pressures at a slower rate than in the lower range of void fractions. Above a mixture void fraction $\lambda>0.85$, the peak-to-peak pressure drops faster, achieving an almost zero value for the case of pure air.

The temporal fluctuations of the p-p pressures are relatively small ($\pm 2\%$) at zero mixture void fraction, and increase to about $\pm 45\%$ at mixture void fractions in the neighborhood of 0.85. Then the variations decrease to about $\pm 15\%$ for a mixture void fraction (λ) close to one (i.e., pure air).

The similitude between the squeeze film pressures measured at different angular locations confirms the assertion of a pressure field rotating synchronously with the journal, as the circumferential symmetry of the damper and the journal motion (circular centered orbit) at first instance would suggest. Figures 10a and 10b present the time-averaged peak-to-peak (p-p) pressures measured at different circumferential positions at the axial location Z_2 for 500 rpm and 1,000 rpm respectively. The spatial or *ensemble average* of the time-averaged p-p pressures is superimposed as a thick line showing an excellent correlation with the p-p pressures at the different angular locations. The *ensemble average* peak-to-peak pressures represent the individual p-p pressures within 10% for the case of 500 rpm, and 8% for 1,000 rpm.

The axial variation of the peak-to-peak pressure at the circumferential angle of 330° is presented in Figure 11. The time-averaged p-p pressures at axial locations Z_1 (5.6 mm) and Z_2 (16.7 mm) are shown versus the mixture void fraction. Both pressures follow the same trend, and as expected, the one closer to the sealed end (Z_1) presents larger dynamic pressures.

IDENTIFICATION OF PHASES AND FREQUENCIES OF JOURNAL MOTION AND PERIOD-AVERAGED FILM PRESSURES

Figure 12 exemplifies the result of the curve fitting implemented to find the frequency (Ω) and phase angle (ϕ) of the journal orbital motion. The figure shows the measured and fitted harmonic function for the X (horizontal) journal displacement at 500 rpm vs. time for a mixture void fraction equal to 0.067. The figure

---

[3] There are concurrent experiments carried out on a small scale rotor kit test apparatus with a *SFD*.

reveals the changes in journal speed during the experiment. This procedure provides the frequency for all the measurements taken simultaneously with the curve fitted X-displacement (i.e., all the ones at the same journal speed and mixture void fraction). It also provides the phase lag between the measurements not taken simultaneously (i.e., at the same speed but different mixture void fraction).

Using this information, the measured digital functions representing *dynamic* pressures are divided into *n* periods of journal motion. These *periods* are averaged in time and one period-averaged pressure function is obtained from each measurement. The averaged functions are scaled in time to have the same period, arbitrarily chosen to be the measured period at a mixture void fraction equal to zero[4]. The time origins of the *dynamic* pressure waves are also displaced to have all measurements coinciding with the minimum film thickness, regardless of when the actual trigger of the data acquisition takes place relative to a period of journal motion. Figure 13 shows the period-*averaged dynamic* pressure to simulate well the actual *dynamic* measurements over consecutive cycles. Figure 14 demonstrates that the period-averaging procedure not only smoothes the data for analysis in the time domain but also in the frequency domain. A frequency analysis of the period-averaged *dynamic* pressures allows identification of harmonic components and provides a coherent phase diagram that seemed lost when directly analyzing the *dynamic* measured data.

PERIOD-AVERAGED DYNAMIC PRESSURES AND GASEOUS CAVITATION ZONE

Figures 15 and 16 present the period-averaged *dynamic* pressures corresponding to the *dynamic (instantaneous)* pressures depicted in Figures 5 and 6, for 8.33 Hz and 16.67 Hz, respectively. The *noise* or temporal fluctuations and spikes are removed by the period-averaging procedure described above. This allows the focus of study to be the analysis of the pressure wave shapes. Note that the averaging does not remove the effects of closeness to the lubricant injection point. The pressure fields at 120° and 240° for both operational speeds are different from those at the angular locations far from the inlet holes. The pressure waves at 120° and 240° resemble the compressible fluid *SFD* solution [Constantinescu, 1969] at smaller mixture void fractions than at any other location of measurement.

The appearance of a zone in which the film pressure remains constant, i.e., null squeeze pressure generation, is common in all the *dynamic* pressures. This zone is named as *gaseous cavitation* [Diaz and San Andrés, 1996, 1997] and reported as typical of bubbly lubricants in *SFDs* [Zeidan and Vance, 1990]. The extent of the *gaseous cavitation* zone is shown to increase with the mixture void fraction as depicted approximately in Figures 15 and 16. The time history of the pressures reveals that, within every journal motion cycle, the local film pressure reaches a maximum during the positive film squeeze ($\partial h/\partial t < 0$), then decreases rapidly, and reaches a minimum peak during the negative film squeeze ($\partial h/\partial t > 0$). After the minimum pressure, and still during the negative film squeeze region, the pressure starts to raise. But, as the mixture void fraction increases, the rate of pressure increase is reduced by the appearance of the *gaseous cavitation zone* (where the film pressure remains constant). After the cavitation zone, and during the positive film squeeze, the pressure starts to raise (again) until reaching the maximum peak value. This sequence repeats for every cycle of journal motion. However, there is a range of mixture void fractions in which the *gaseous cavitation* zone appears randomly in some cycles of journal motion, not in all of them. This condition is known as an *incipient gaseous cavitation regime*, and is followed by the *fully developed gaseous cavitation regime* as the mixture void fraction increases [Diaz and San Andrés, 1997]. In this last regime, the *gaseous cavitation zone* does appear in all the cycles, but its extent is not exactly the same in every period of journal motion.

Inside the *gaseous cavitation* zone, the mechanical work performed by the journal motion is related to a change of volume of the lubricant mixture at constant pressure, instead of a change of pressure at constant fluid density as would be the case for an ideal incompressible fluid. This provides a rationale for the reduction in the squeeze film pressure generation as evidenced by the decreasing peak-to-peak pressures.

---

[4] Note that the tests are essentially performed at a constant speed, either 500 or 1,000 rpm. However, minute variations of the nominal speed are found to be significant enough to alter the derived *SFD* forces. Hence then the need to refer all other experiments to a unique normalized or baseline period for easiness in presentation and manipulation of results.

To gain a better understanding on the development of the pressure fields and gaseous cavitation zone with the mixture void fraction, the results of Figures 15 and 16 are reproduced as *3D* surfaces that can be displayed from different view perspectives. Figures 17 and 18 show the pressure surface plots for 500 rpm and 1,000 rpm, respectively. In every 3D-graph it is clear that the difference between maximum and minimum pressures decreases with the mixture void fraction. However, the most relevant finding is that the *gaseous cavitation* zone lays in a horizontal plane, i.e., it takes place at the same magnitude of pressure independently of the mixture void fraction (note that the pressures at $330°$ (Z_1 and Z_2) are absolute).

Figures 19 and 20 show contour plots of the *3D*-pressure-surfaces just described. The graphs present the isobaric lines in the plane of mixture void fraction and time. The local film thickness is graphed with the same time scale at the bottom of each figure. From the plots at $330°$ (absolute pressure), the *gaseous cavitation* zone presents the same absolute pressure independently of the mixture void fraction and develops around the time of maximum film thickness when going from negative film squeeze (increasing film thickness) to positive film squeeze (decreasing film thickness). The cavitation zone extent during a period of motion increases with the mixture void fraction. Thus, based on the assertion of a pressure field rotating synchronously with the journal whirling motion, it can also be asserted that the physical extent of the *gaseous cavitation zone* around the journal circumference also increases. The maximum peak pressure displaces towards the location of minimum film thickness when the mixture void fraction increases, approaching the condition of an ideal gas. Similar conclusions can be drawn from the measurements at all other angular locations even though the represented pressures are dynamic instead of absolute.

Figures 21a,b are waterfall plots of the frequency content (amplitude and phase) of the period-averaged-*dynamic* pressure for the location ($0°,Z_2$) at 500 rpm and 1,000 rpm respectively. The harmonic content of the pressures is manifest. The main frequency component is at the journal whirl frequency, and up to five harmonics are important. The first two harmonics (*1x* and *2x*) decrease with the mixture void fraction over its whole range, from pure oil to pure air. However, the other frequency components remain almost invariant up to a mixture void fractions equal to ~0.85, after which they drop abruptly. The phase diagram is found to remain nearly invariant up to a mixture void fraction of about 0.80. Figure 21 includes a comparison between the phase diagrams of the pressures corresponding to mixture void fractions equal to 0.00 and 0.25, respectively.

STATIC, INLET, EXIT, AND CAVITATION PRESSURES

The *static* film pressure is defined as the overall average of the film pressures over the sampled time (17 and 34 cycles of journal motion for 500 and 1,000 rpm respectively), i.e., this is the zero frequency component of the squeeze film pressure. The *gaseous cavitation* pressure is estimated as the pressure at the point of maximum film thickness, and around which the cavitation zone develops as previously discussed. Both the *static* and the *gaseous cavitation* pressures are calculated from the absolute pressures measured with the transducers located at $330°$, and depicted versus the mixture void fraction in Figure 22 for axial locations Z_1 and Z_2 at 500 rpm, and axial location Z_2 at 1,000 rpm. The Figure also includes the exit (plenum) pressures.

The static film pressure at both axial locations is identical to the discharge pressure at the plenum, and only small differences appear for mixture void fractions above 0.85. In the upper range of mixture void fractions, the pressure recovered by deceleration of the exit flow seems to be important due to the lower density of the mixture and the larger fluid speeds. The *gaseous* cavitation zone pressure is consistently lower than the exit pressure by a constant value over the entire range of mixture void fractions. The axial pressure gradient within the cavitation zone is negative as the sealed end is approached from the exit (discharge) edge, i.e., the pressure decreases from the exit plane to Z_2, and then to Z_1. Neither the *static* film pressure nor the *gaseous cavitation* pressure appear to depend on the amount of air entrained to the mixture, but rather seem to be related to the pressure at the open end plenum (boundary condition).

VARIATIONS ON THE JOURNAL MOTION ORBIT: AMPLITUDE AND CENTER

The journal orbital motion is mechanically fixed by an eccentric mounted in a rigid shaft. However, the test measurements show changes in the journal orbit size, shape, and position. Figure 23 sketches the averaged journal orbits for the two extreme cases of mixture void fraction equal to zero (pure oil) and one (pure air)

at an operational speed of 500 rpm. The orbit corresponding to the damper operating with pure air at ambient pressure (i.e., no pressurization or air through flow) is given as reference corresponding to the nominal value of journal orbit radius ($e=0.216$ mm). It is important to note that for mixture void fractions $\lambda \leq 0.85$ the change on the measured orbit radius from that at the pure oil condition is minor when compared to the changes above $\lambda=0.85$.

The journal orbit radius is determined as one half the peak-to-peak amplitude of the measured journal *dynamic* displacements. However, the displacement signals present differences from one period of journal motion to another. The displacements are not as *noisy* as the film pressures in the sense that they do not present sharp changes like *spikes*. However, the amplitude of journal motion does change from cycle to cycle evidencing, once more, the effects of the non-homogeneous and non-steady nature of the bubbly mixture. Figure 24 presents the average orbit radius along with the maximum and minimum values (vertical bars) versus the mixture void fraction for the test cases at 500 rpm. These results are based on the measurements in the horizontal-X and vertical-Y directions. Figure 25 shows the orbit radius based on measurements of horizontal displacements versus the mixture void fraction for the test cases at 1,000 rpm. The largest orbit radius are achieved at the highest mixture void fractions where the mixture viscosity is presumably small. The temporal fluctuations of the orbit radius are relatively small ($\pm2\%$) at zero mixture void fraction, and increase to about $\pm15\%$ at mixture void fractions in the neighborhood of 0.85. The variations decrease to about $\pm3\%$ for a mixture void fraction equal to one (i.e., pure air).

Figure 26 presents the locus of the journal orbit center for the whole range of mixture void fractions along with the reference orbit (without any lubricant) and its center. The displacement of the orbit center, though small when compared to the orbit size, persists in all the tests. Figures 27 and 28 relate the orbit center displacements with the supply and discharge (plenum) pressures. Journal orbit center displacements in both directions (horizontal[X] and vertical [Y]) are measured for 500 rpm and depicted in Figure 27. The journal orbit center displacement in the horizontal direction-X at 1,000 rpm is depicted in Figure 28. The top graphs suggest that the horizontal [X]displacement of the orbit center is related to the discharge pressure at the plenum. This pressure exerts an axial force and pushes the journal against the housing end plate (see Figure 1a). It is suspected that a minute misalignment between the journal and housing results in an asymmetric force distribution that affects the support reactions and displaces the orbit center. This assertion is confirmed by observations performed controlling the plenum pressure while keeping the journal static (zero whirling) and no through oil flow (exit valve closed).

The bottom graph of Figure 27 indicates the vertical [Y] displacement of the orbit center is related to the lubricant supply pressure to the *SFD*. The injection holes are located at the top and bottom of the damper ($270°$ and $90°$, respectively). Variations in the flow resistances in the film lands and injection holes due to changes in the local film thickness could result in a *hydrostatic* circumferential pressure field generating a vertical force able to move the journal orbit center.

The variations or changes in the journal orbit size and center are thought not to produce significant variations in the squeeze film dynamic pressures and do not affect the conclusions drawn from the experiments [Diaz and San Andrés, 1996, 1997]. However, although these variations may be small, their study reveals the effects of the test damper feed arrangement as conducive to generate static fluid film pressures.

HYDROSTATIC PRESSURE FIELD RELATED TO THE JOURNAL POSITION

The journal orbit radius is found to decrease when oil is fed to the damper even when the journal is not whirling ($\omega=0$). A test in which a pure oil is fed to the *SFD* at the nominal value of supply pressure (7.8 bar [115 psia]) and discharge pressure (1.7 bar[25 psia]) is performed for a non-whirling journal. The shaft is manually rotated and a *hydrostatic* film pressure is measured with the strain gauge pressure transducers. The *hydrostatic* pressure (absolute value - solid line) is depicted in Figures 29 to 31versus the angular location of the journal center measured from the transducer location ($330°$, Z_1 and Z_2). The Figures also include the local film thickness and the measured *dynamic* pressure for pure oil ($\lambda=0$) at 500 rpm (Z_1, in Figure 29, Z_2 in

Figure 30) and 1,000 rpm (Z_2 in Figure 31). These *dynamic* film pressures represent the largest pressures measured for each whirl frequency.

The local *hydrostatic* film pressure depends on the angular location of the journal, i.e., on the local film thickness. This pressure does not depend on journal motion (*hydrodynamic*) but on the disposition of the feed holes and the local film thickness which acts as a flow resistance constraining the local axial flow. For example, at a local (static) position of small film thickness, the film and orifice flow resistances increase ($\sim 1/c^3$) and the local pressure rises. The opposite effect occurs on the other side of the journal, i.e. the local film increases, reduces the flow resistance and the local pressure drops. Then, the *hydrostatic* pressure is maximum at the minimum film thickness, and minimum at the maximum film thickness.

The magnitude of the *hydrostatic* circumferential pressure when the journal is manually rotated (at $\omega=0$) is significant when compared to the largest peak-to-peak *dynamic* pressure measured when the journal whirls at 500 and 1,000 rpm. It is speculated that this *hydrostatic* pressure profile, related to the instantaneous journal position instead of the journal center squeeze velocity, is also present when the damper whirls. Therefore, the *dynamic* film pressures should be the superposition of the *hydrodynamic* pressures due to the squeeze journal motion and a component related to the *hydrostatic* pressure profile just described. This discussion will be retaken later when the squeeze film forces are presented.

The film force per unit axial length due to the *static* circumferential pressure field (at a given axial location) is estimated by numerical integration of the pressure around the journal circumference. In this case, the computed forces due to the *azimuthal pressure* related to the static journal position are 3,372 N/m at Z_2 acting 6.4° from the radial direction, and 7,275 N/m at Z_1 and 8.0° from the radial direction. Thus, these forces are essentially radial inward, i.e., centering forces. Therefore, the damper at zero whirl speed produces a restoring (spring-like) force similar to that in annular pressure seals due to the *Lomakin effect*.

As seen in Figure 23, the journal orbits are not completely circular but rather elliptical with the major and minor axes oriented in the horizontal and vertical directions, respectively. Figure 24 shows the difference between amplitudes in the two directions to be consistent over the whole range of mixture void fractions. However, without lubricant pressurization the journal orbit is a perfect circle. In the test damper, the lubricant mixture is injected through holes at the top and bottom of the housing, and from here it flows through the film lands. The pressure losses related to this flow render *average feed* pressures higher at the top and bottom of the damper (near the injection holes) than at the horizontal sides (distant from the injection holes). Thus, the flattened orbits are a result of the feeding arrangement for the test damper.

In an earlier discussion[5], it was noted that the *dynamic* film pressures in the neighborhood of the lubricant inlets present a *noisier* condition and a slightly different shape. There, the non-uniformity of the mixture at the inlet feed holes is identified as a probable cause for the noted differences in the test pressures. However, the presence of the *hydrostatic* film pressure around the damper provides an independent rationale for the differences between the *dynamic* pressures[6]. At the feed ports, it is also probable that the larger absolute pressure levels (preventing unstable growth of the air bubbles) or larger flow rates (availability of oil) delay the onset and generation of the *gaseous cavitation zone* at the top and bottom sections of the damper.

SQUEEZE FILM FORCES

The rotordynamic characteristics of a *SFD* are given by the forces it exerts on the journal. These forces can be estimated by integrating the measured circumferential pressure profiles to obtain forces per unit length at the given axial location of measurement. However, this integration is performed under the assumption of a pressure field rotating synchronously with the journal. As previously discussed, the pressure wave shapes are similar at the locations of measurement but shifted (in time) by a constant value equal to the angle between the transducers divided by the whirl frequency (ω). Also the peak-to-peak pressures are shown to be similar over the entire journal circumference. However, the most convincing evidence of a rotating pressure field is

---

[5] see section on *Measured dynamic pressures and temporal random fluctuations*

[6] The argument holds whether the bubbly mixture is homogeneous or not

shown in Figure 32, where the circles denote pressures measured simultaneously with different pressure transducers (located at the angular positions shown) at the instantaneous journal position sketched. The continuous line depicts the pressure profile recorded at a fixed angular location (the one coinciding with the radial direction on the figure) over one period of journal motion. In these figures, the pressure values as well as the film thickness correspond to the *period-averaged* measurements. The continuous line passes through the circles, and confirms that the pressure field does rotate with an angular speed equal to the journal whirl frequency. The same conclusion can be drawn from other measurements using other transducers and at different mixture qualities than the ones presented in Figure 32. These results are not included for brevity.

Figures 33 and 34 show the radial (f_r) and tangential (f_t) forces per unit length as a function of the mixture void fraction (λ). The forces are calculated by time integration of the *period-averaged* pressure fields, as given in equation (2). The similitude between the estimated forces using the pressures at different angular locations verifies, once more, the circumferential symmetry of the pressure distribution. This also allowing for the application of an *ensemble average* of the forces. The *ensemble-averaged* forces are also presented in the figures and show fair correlation with the forces from different angular locations. The estimates of tangential force lay all within a narrow band around the *ensemble average*. The estimates of the radial force are also close to the *ensemble average*, but the dispersion of the force estimates is a little larger for mixture void fractions around 0.85.

Figures 35 and 36 show the *ensemble-averaged* forces versus the mixture void fraction for the test speeds of 500 rpm and 1,000 rpm respectively. The figures provide two representations of the squeeze film damper force, one using the radial and tangential components, and the other using the total force and its angle with the radial direction. Figure 35 also includes the estimates of squeeze film force from the transducer located at ($330°$, Z_2).

The total squeeze film force decreases with the mixture quality in a way more or less proportional to the reduction in the peak-to-peak pressures (see Figures 8 to 11). The introduction of a very small amount of air ($\lambda \sim 0$) produces a sharp reduction of the force. Further increments of the mixture void fraction (from 0.02 to 0.85 approximately) produce a quasi-linear reduction on the total force at a slower rate than in the lower range of void fractions. Above a mixture void fraction of 0.85, the total force drops abruptly, achieving a negligible value for the case of pure air. At the same time, the angle between the force and the radial direction goes from $80°$ to $0°$. That is, the force begins mainly as tangential (direct damping force) and ends as a pure radial (centering) force.

Close scrutiny of the force components helps to understand the changes in the squeeze film force. The tangential force, larger for the condition of pure oil and practically zero for mixture void fraction equal to one, varies more or less linearly with the void fraction evidencing a reduction in the mixture viscosity. The radial force starts from a small value, for small amounts of air ($\lambda < 0.02$) it increases rapidly, then remains almost constant with a light tendency to increase up to mixture void fractions around 0.85. Further increments of mixture void fraction cause the radial force to diminish, reaching a null value for pure air. For both test speeds, the tangential force per unit length at the axial location Z_2 is larger than the radial force up to a mixture fraction $\lambda \sim 0.70$. The radial force is larger above this value of λ. At the axial location Z_1, the tangential force is larger than the radial only up to a mixture void fraction of about 0.40.

A simple hydrodynamic theory for incompressible fluid, full film *SFDs*, would predict damper forces directly proportional to the lubricant viscosity, whirl frequency, and journal orbit radius. Thus, for a constant mixture composition (or at least for the pure oil condition), the forces at 1,000 rpm should be twice their counterparts at 500 rpm. Yet, this is not the case in the present experiments. For the pure oil condition, the estimated total force at 16.6 Hz is less than 1.5 times the force at 8.33 Hz . However, it is well known that a non-cavitated oil lubricated *SFD* executing circular centered orbits renders a pure tangential (damping) force opposing the journal center speed. Furthermore, in all the test cases the radial forces have a non-zero value

18

at a mixture void fraction equal to zero (pure oil)[7]. Still, at 16.6 Hz the tangential force is only 1.4 times the tangential force at 8.33 Hz, while the radial force is 2.6 times its counterpart at 8.33 Hz for the pure oil condition. Since the test results correspond to similar operating conditions in journal orbit radius, supply pressure, and fluid temperature (i.e., viscosity), the empirical evidence leads to the manifest appearance of lubricant *vapor cavitation*, which reduces the magnitude of the tangential (damping) force, and gives rise to a radial force.

Figures 29 to 31 show the *period-averaged* pressures corresponding to a null mixture void fraction (pure oil) at the two test speeds (and the two axial locations of measurement). The test results indicate the minimum *dynamic* pressure drops (slightly) below the zero absolute value, and thus, the fluid is subjected to tension. This induces the lubricant to cavitate by changing its phase *(vapor cavitation)* affecting the symmetry and magnitude of the pressure field, and thus producing radial forces[8]. The effect of *vapor cavitation* is more pronounced at 1,000 rpm than at 500 rpm. Thus, the film forces at 1,000 rpm can not be exactly twice the value of forces at 500 rpm. Nevertheless, at 500 rpm the radial force component is still appreciable, though not due to vapor cavitation. Therefore, another source generating the radial force must be present.

The radial force per unit length at Z_2 is 8,033 N/m at 1,000 rpm, and 3,091 N/m at 500 rpm. The radial force per unit length at Z_1 at 500 rpm is 8,877 N/m. It stands out that the radial forces at 500 rpm (where *vapor cavitation* is nearly absent) are singularly close to the values of the centering force due to the circumferential hydrostatic pressure gradient related to the axial lubricant flow. Recall that this pressure profile, depicted in Figures 29 to 31, is related to the static position of the journal. If the superposition principle is valid and the hydrostatic pressure field of Figures 29 and 30 is subtracted from the corresponding measured *dynamic* pressures, the resulting force for pure oil at $(Z_1$, 500 rpm) is displaced from 73.8° to 87.0°, while its counterpart at Z_2 goes from 82.7° to 91.5° from the radial direction. That is, the remaining component of the force is nearly tangential, i.e., a direct damping force as expected for full film (uncavitated) *SFDs*. It seems plausible that the dynamic pressure profile is constituted by the contributions of a hydrodynamic pressure related to the squeeze velocity of the journal center plus a hydrostatic pressure profile related to the position of the journal (and independent of the journal speed). Thus, the radial centering force (due to a hydrostatic pressure distribution) appears to be inherent to the test damper configuration. Hence, it constitutes, along with lubricant *vapor cavitation*, a likely source of the unexpected radial forces as $\lambda \rightarrow 0$.

DRIVE POWER

Figure 37 shows measurements of the electrical power (current × voltage) supplied to the drive motor. The vertical bars represent uncertainty in the measurement of power, while the horizontal bars represent uncertainty in the measurement of mixture void fraction. The roller bearings on which the test rig is mounted are sealed grease packed bearings. Thus, the changes in the mechanical power required to drive the test rig at a given speed should only depend on the squeeze film forces. The other identified parameter affecting the drive power is the plenum pressure. As it was discussed, this pressure pushes axially the journal against the housing plate, changing the normal contact forces, and therefore the friction forces. However, the plenum discharge pressure is controlled over the experiment and its changes are relatively small (see Figures 27 and 28). Overall, the driving power shows a similar reduction as the film forces do with increases in the mixture void fraction.

CONCLUSIONS

The effects of controlled air/oil bubbly mixtures on the force performance of an experimental open end *SFD* describing circular centered journal orbits are of interest to advance the state of the art in the design and analysis of *SFDs*. A complete set of experimental measurements and comprehensive analysis reveal the effects of a bubbly mixture on generating a *gaseous cavitation* zone affecting the squeeze film pressures and

---

[7] Prior experiments (1989-1995) conducted on the same test rig were performed with low values of supply pressure, typically less than 25 psi. Consequently, the radial forces due to the feed arrangement and *hydrostatic* pressure field are small and of no consequence in those tests.

[8] Recall that the pressures are the period-averaged ones and that the averaging procedure tends to smooth sharp variations that do not appear in all the cycles.

damper forces. The composition of the mixture is controlled and varied from pure oil to pure air (i.e. mixture void fraction varies from 0 to 1). Experiments to measure the *dynamic* squeeze film and *static* pressures, the journal displacements, film temperatures, and the drive power are conducted at two journal speeds (500 and 1,000 rpm) and over the full range of mixture void fractions. The most relevant findings of the experiments and analysis derive in the following conclusions:

- The squeeze film forces decrease as the mixture void fraction increases. The rate of decrement is larger for mixture void fractions below 0.02 and above 0.85. In the mid range, the total force decreases almost linearly with the mixture void fraction. The squeeze film force is nearly tangential for pure oil, and moves toward the radial direction as the mixture void fraction increases.
- The tangential component of the force continuously decreases with the mixture void fraction, but the radial component increases in the first instance and then remains constant up to a mixture void fraction approximately equal to 0.85. Both force components drop to a nil value for the pure air condition.
- The drive power decreases for increasing mixture void fractions, and is consistent with the reduction of the *SFD* forces.
- The *dynamic* film pressures present temporal fluctuations. That is, they are different from one period of journal motion to another, and show pressure spikes randomly distributed. The temporal fluctuations are attributed to the non-homogenous nature of the bubbly mixture.
- The peak-to-peak (p-p) pressures decrease with the mixture void fraction in a way similar to that of the forces. The temporal fluctuations reach a maximum around a mixture void fraction of 0.85, and are as large as 45% in some cases.
- The generation of squeeze film dynamic pressures (as measured by the p-p pressure) is higher at the axial location Z_1 (closer to the damper sealed end) than at Z_2 (closer to the open end) for the entire range of mixture void fractions.
- The similitude of the *dynamic* pressure measurements around the damper circumference confirms the existence of a pressure field rotating synchronously with the shaft speed. Comparisons between the pressure fields measured simultaneously at different angular locations and the pressure field recorded at a given location during one period of journal motion give excellent agreement. However, subtle differences can be noticed in the pressure waves in the neighborhood of the injection holes.
- A period averaging procedure is effective to eliminate the random temporal fluctuations in the *dynamic* pressures, and unveils important information hidden by the "*noise*" in the measurements.
- A zone of no squeeze film pressure generation (constant pressure zone) appears in the pressure waves and its extent increases with the mixture void fraction. This region is recognized as a *gaseous cavitation zone*.
- The pressure at the *gaseous cavitation* zone is constant in time, independent of the mixture void fraction, and seems to be related to the discharge plenum pressure.
- The *static* component of the *dynamic* film pressure is identical to the discharge plenum pressure.
- The journal motion orbit presents small changes from one operating condition to another as well as temporal fluctuations like those of the pressure waves. The feed arrangement and the plenum pressure affect the journal orbit radius.
- Not only the *dynamic* squeeze film pressure gradients are important. A circumferential pressure gradient is found to develop when the journal is stationary producing a radial restoring force by a mechanism similar to the one present in annular pressure seals.

The comprehensive tests and analysis characterize the performance of a *SFD* operating with a bubbly mixture of air on oil as lubricant. The numerous experiments performed replicate successfully actual working conditions in *SFDs*. However, empirical facts are not the sole outcome of the tests. The praxis gained in the experiments serves as a benchmark to derive a sound mathematical model able to predict (qualitatively and quantitatively) the performance of *SFDs* operating with *gaseous cavitation* due to air ingestion. The measured film pressures and estimated damper forces provide fundamental empirical evidence for validation of a theory for squeeze film flows with bubbly mixtures.

The dynamics of the air bubbles in the mixture become of importance in the formulation of such a model. This model should include periodic bubble expansion and compression, as well as the growth of the bubbles

at constant pressure and bubble collapse at large pressures. The *Rayleigh-Plesset* equation appears as a firm physical model to undertake along with the use of a *homogeneous two component mixture* formulation for the mass and momentum equations (where the relative movement between phases is neglected). Simplifications to this general model and appropriate for thin film flows will result in a modified *Reynolds* equation for the compressible mixture. Here, the mixture viscosity is determined by one of the available empirical correlations, and the mixture density by the local size of the bubbles governed by the *Rayleigh-Plesset* equation. The model then requires the solution of two simultaneous partial differential equations in a coordinate frame rotating with the whirl frequency, and where the flow field appears as stationary for circular centered journal orbits. Appropriate boundary conditions must be natural to the physics of the mixture coming and leaving the *SFD*. As an alternative, and depending on the results of the prior approach, the modeling of additional features accounting for the relative motion between the phases should be addressed as in the general formulation of Hsie [1988].

ACKNOWLEDGEMENTS

REFERENCES

Al-Sharif, A., Chamniprasart, K., Rajagopal, K. R., Szeri, A. Z., 1992, "Lubrication with Binary Mixtures: Liquid-Liquid Emulsion," *ASME* Journal of Tribology, Vol. 115, pp. 46-55.

Arauz, G. L., and San Andrés, L., 1993, "Experimental Pressures and Film Forces in a Squeeze Film Damper," *ASME* Journal of Tribology, Vol. 115,1, pp. 134-140.

Arauz, G. L., and San Andrés, L., 1996, "Experimental Study on the Effect of a Circumferential Feeding Groove on the Dynamic Force Response of a Sealed Squeeze Film Damper," *ASME* Journal of Tribology, Vol. 118, 4, pp. 900-905.

Atkin, R. J., and Craine, R. E., 1976, "Continuum Theories of Mixtures: Basic Theory and Historical Development," Quarterly Journal of Mechanics and Applied Mathematics, Vol. 29, pp. 209-244.

Boedo, S., and Booker, J. F., 1994, "Cavitation in Normal Separation of Square and Circular Plates," *ASME* paper 94-Trib-57.

Braun, M. J. and Hendricks, R. C., 1984, "An Experimental Investigation of the Vaporous/Gaseous Cavity Characteristics of an Eccentric Journal Bearing," *ASLE* Transactions, Vol. 27, 1, pp. 1-14.

Brennen, C. E., 1995, "Cavitation and Bubble Dynamics," Oxford Engineering Series 44, Oxford University Press, New York.

Chamniprasart, K., Al-Sharif, A., Rajagopal, K.R., and Szeri, A. Z., 1993, "Lubrication With Binary Mixtures: Bubbly Oil," *ASME* Journal of Tribology, Vol. 115, pp. 253 - 260.

Childs, D. , 1993, "Turbomachinery Rotordynamics," John Wiley & Sons, New York.

Constantinescu, V. N., 1969, "Gas Lubrication," ASME United Engineering Center, New York, pp. 349-420.

Diaz, S. E., and San Andrés, L. A., 1996, "Effects of Air/Oil Bubbly mixtures on the Performance of Squeeze Film Dampers," TAMU Turbomachinery Research Consortium Report, TRC-*SFD*-1-96, May.

Diaz, S. E., and San Andrés, L. A., 1997, "Measurements of Pressure in a Squeeze Film Damper with an Air/Oil Bubbly Mixture," accepted for publication in the *STLE* Tribology Transactions, to be presented at *I World Tribology Congress*, London, United Kingdom.

Drew, D. A., 1971, "Averaged Field Equations for Two-Phase Media," Studies in Applied Mathematics, Vol. 50, pp. 205-231.

Einstein, A., 1906, "Eine neue Bestimmung der Molekul-Dimension," ("A new Approach to the Molecular Dimension") Ann. Physik, Vol. 19, p. 289.

Feng, N.S., and Hahn, E. J., 1986, "Density and Viscosity Models for Two-Phase Homogeneous Hydrodynamic Damper Fluids," *ASLE* Transactions, Vol. 29, No. 3, p. 361.

Hayward, A. T., 1961, "The viscosity of Bubbly Oil," N.E.L. Fluids Report No. 99, National Engineering Laboratory, UK.

Hibner, D., and Bansal, P., 1979, "Effects of Fluid Compressibility on Viscous Damper Characteristics," Proceedings of the Conference on the Stability and Dynamic Response of Rotors with Squeeze Film Bearings, University of Virginia, pp. 116-132.

Hsie, D. Y., 1988, "On Dynamics of Bubbly Liquids," Advances in Applied Mechanics, Vol. 26, Academic Press INC., pp. 63-133.

Humes, B., and Holmes, R., 1978, "The Role of Subatmospheric Film Pressures in the Vibration Performance of Squeeze Film Bearings," Journal of Mechanical Engineering Science, Vol. 20, No. 5, pp. 283-289.

Jung, S. Y., and Vance, J. M., 1993a, "Effects of Vapor Cavitation and Fluid Inertia on the Force of a Squeeze Film Damper Part I - Analysis of a Long SFD," STLE Tribology Transactions, Vol. 36, 4, pp. 597-604.

Jung, S. Y., and Vance, J. M., 1993b, "Effects of Vapor Cavitation and Fluid Inertia on the Force of a Squeeze Film Damper Part II - Experimental Comparisons," STLE Tribology Transactions, Vol. 36, 4, pp. 700-706.

Kline, S. J., and McClintock, F.A., 1953, "Describing Uncertainties in Single-Sample Experiments," ASME Mechanical Engineering, Vol. 75.

Ku, C. P., and Tichy, J. A., 1990, "An experimental and Theoretical Study of Cavitation in a Finite Submerged Squeeze Film Damper," ASME Journal of Tribology, Vol. 112, pp. 725-733.

Moffat, R. J., 1982, "Contributions to the Theory of Single-Sample Uncertainty Analysis," ASME Journal of Fluids Engineering, Vol. 104, pp.250-260.

Parkins, D. W., May-Miller, R., 1984, "Cavitation in an Oscillatory Oil Squeeze Film," ASME Transactions, Vol. 106, pp. 360-367.

Pinkus, O., 1990, "Thermal Aspects of Fluid Film Tribology," ASME Press, New York, pp. 317-326.

Plesset, M. S., and Prosperetti, A., 1977, "Bubble Dynamics and Cavitation," Annual Review of Fluid Mechanics, Vol. 9, pp. 145-185.

Rajagopal, K. R., and Tao, L., 1995, "Mechanics of Mixtures," Series on Advances in Mathematics for Applied Sciences - Vol. 35, World Scientific, Singapore.

Sun, D. C., and Brewe, D. E., 1992, "Two Reference Time Scales for Studying the Dynamic Cavitation of Liquid Films," ASME Transactions, Vol. 114, pp. 612-615.

Sun, D. C., Brewe, D. E., and Abel, P.B., 1993, "Simultaneous Pressure Measurement and High-Speed Photography Study of Cavitation in a Dynamically Loaded Journal Bearing," ASME Transactions, Vol. 115, pp. 88-95.

Tao, L., and Rajagopal, K. R., 1997, "Flows of Bubbly Liquids," submitted for publication on the Journal of Multiphase Flow.

Taylor, G. I., 1932, "The Viscosity of a Fluid Containing Small Drops of Another Fluid," Proc. Roy. Soc., Series A138, p. 41.

Walton, J., Walowit, E., Zorzi, E., and Schrand, J., 1987, "Experimental Observation of Cavitating Squeeze Film Dampers," ASME Journal of Tribology, 109, pp. 290-295.

Wang, S.H., Al-Sharif, A., Rajagopal, K. R., Szeri, A. Z., 1992, "Lubrication with Binary Mixtures: Liquid-Liquid Emulsion in an EHL Conjunction," ASME Journal of Tribology, Vol. 115, pp. 515-522.

Zeidan, F. Y., and Vance, J. M., 1989a, "Experimental Investigation of Cavitation Effects on The Squeeze Film Force Coefficients", Rotating Machinery Dynamics, DE-vol. 18-1, ASME Conference on Mechanical Vibration and Noise, pp. 237-242.

Zeidan, F. Y., and Vance, J. M., 1989b, "Cavitation Leading to a Two Phase Fluid in a Squeeze Film Damper," STLE Tribology Transactions, Vol. 32, 1, pp. 100-104.

Zeidan, F. Y., and Vance, J. M., 1990a, "A Density Correlation for a Two-Phase Lubricant and its Effect on the Pressure Distribution," STLE Tribology Transactions, Vol. 33, pp. 641 - 647.

Zeidan, F. Y., and Vance, J. M., 1990b, "Cavitation Regimes in Squeeze Film Dampers and Their Effect on the Pressure Distribution," STLE Tribology Transactions, Vol. 33, pp.447-453.

Zeidan, F. Y., and Vance, J. M., 1990c, "Cavitation and Air Entrainment Effects on the Response of Squeeze Film Supported Rotors," ASME Journal of Tribology, Vol. 112, pp. 347 - 353.

REFERENCES

1.- HOUSING END PLATE
2.- HOUSING
3.- JOURNAL
4.- END PLATE
5.- ECCENTRIC
6.- ECCENTRIC HOLDER
7.- SHAFT
8.- KEY
9.- HOUSING CAP
10.- LIP SEAL
11.- LEFT SEAL PLATE
12.- HOUSING SUPPORT
13.- SHAFT SUPPORT
14.- SHAFT BEARINGS
15.- JOURNAL BEARING
16.- PRESSURE NUTS
17.- PROXIMITY PROBE
18.- BASE PLATE

PP: displacement sensor
PT: pressure transducer
TT: thermocouple

dimensions
$Z_1 = 5.6$ mm (0.22 in) $L = 31.1$ mm (1.22 in)
$Z_2 = 16.7$ mm (0.66 in) $D = 129.4$ mm (5.10 in)
$Z_3 = 37.1$ mm (1.46 in) $C = 0.343$ mm (0.0135 in)

$L/D = 0.24$; $R/C = 189$
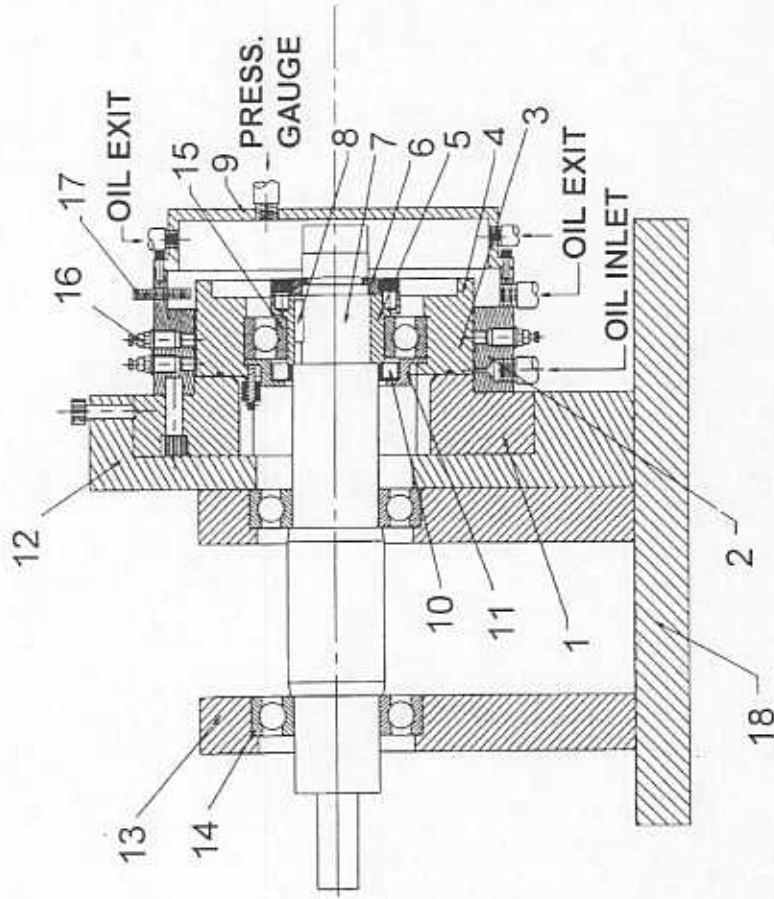
(a) General assembly
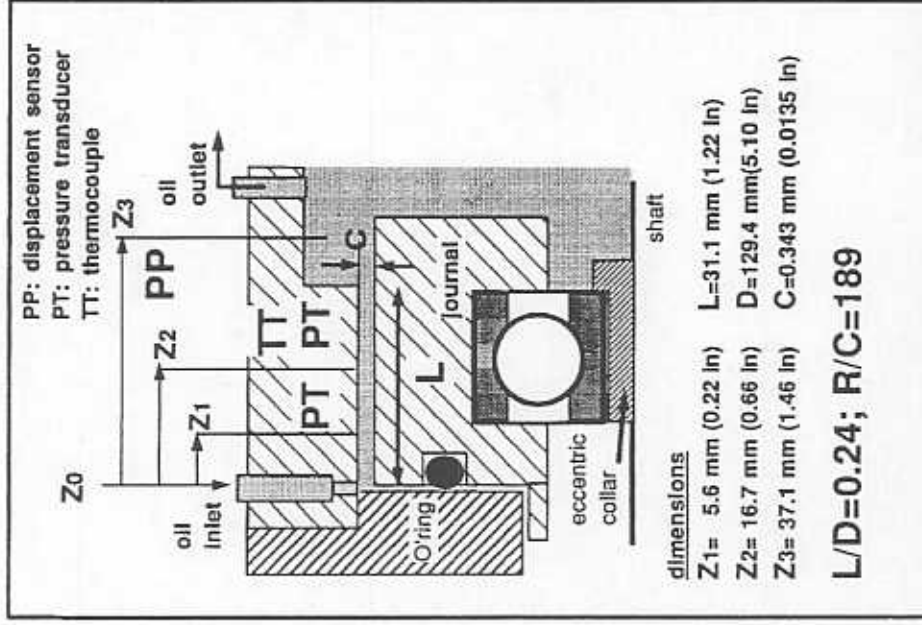
(b) Squeeze film damper detail

Figure 1.- Squeeze film damper test apparatus
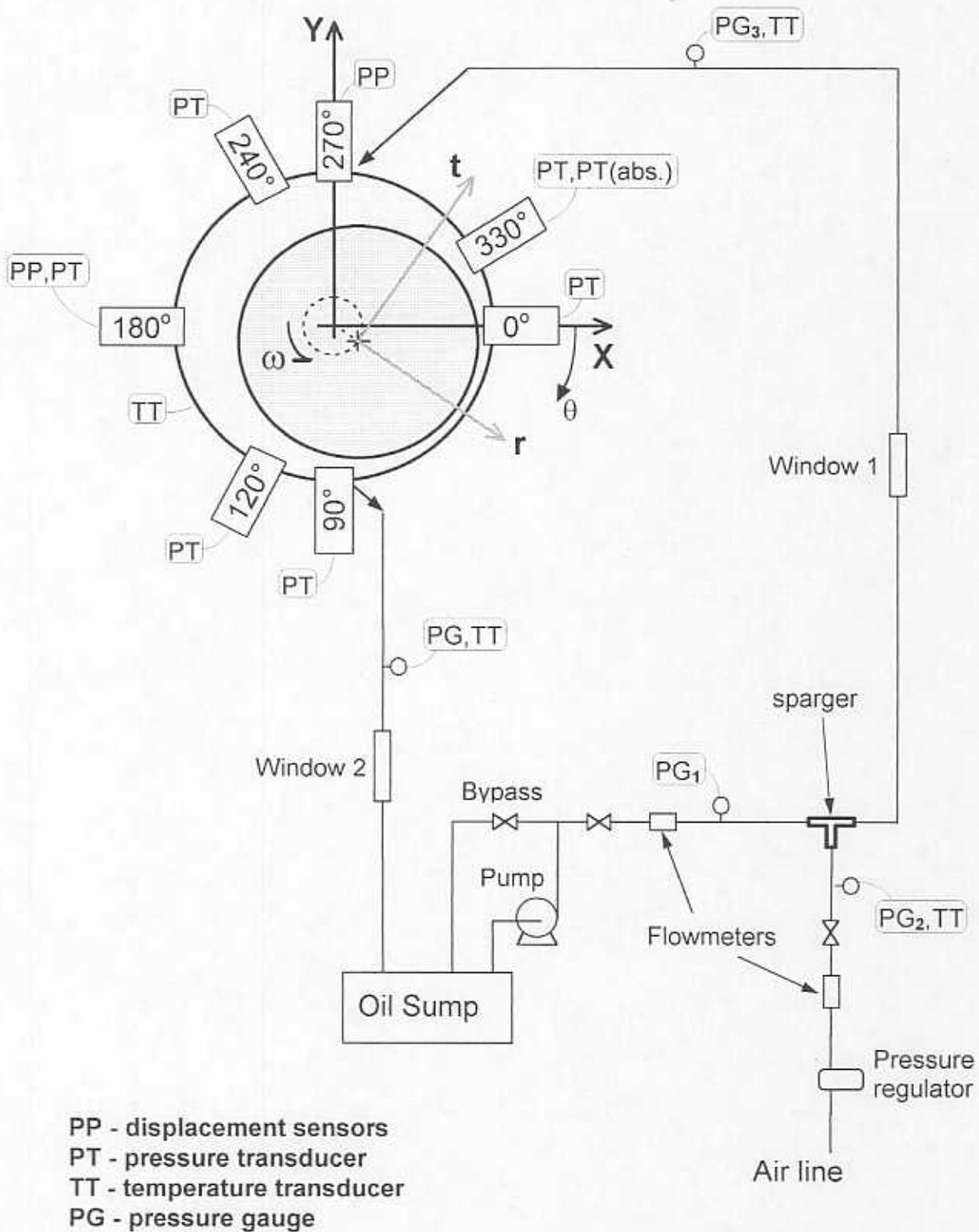
Fig. 2.- Schematic of test rig and instrumentation.
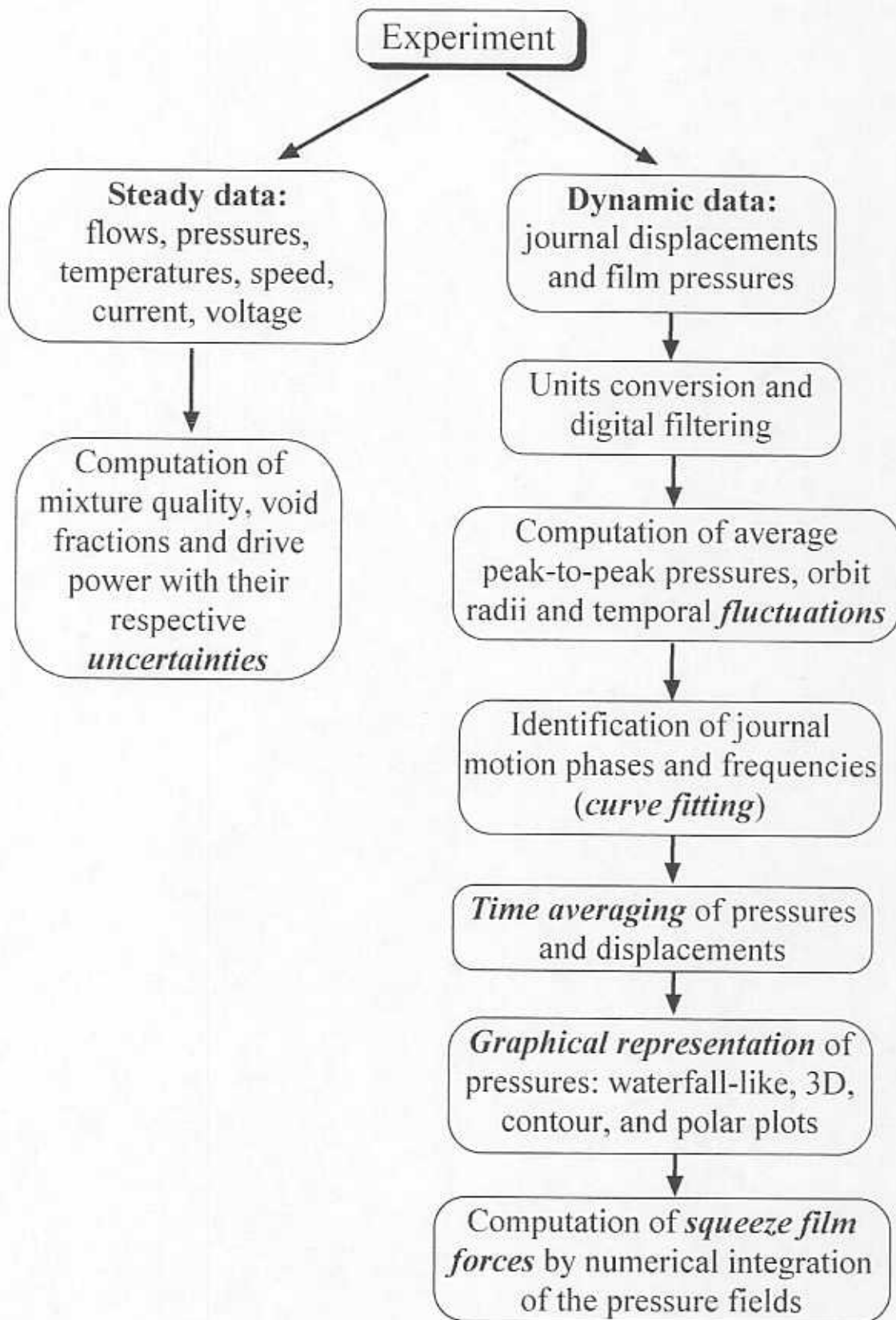
Fig. 3.- Data processing flow chart
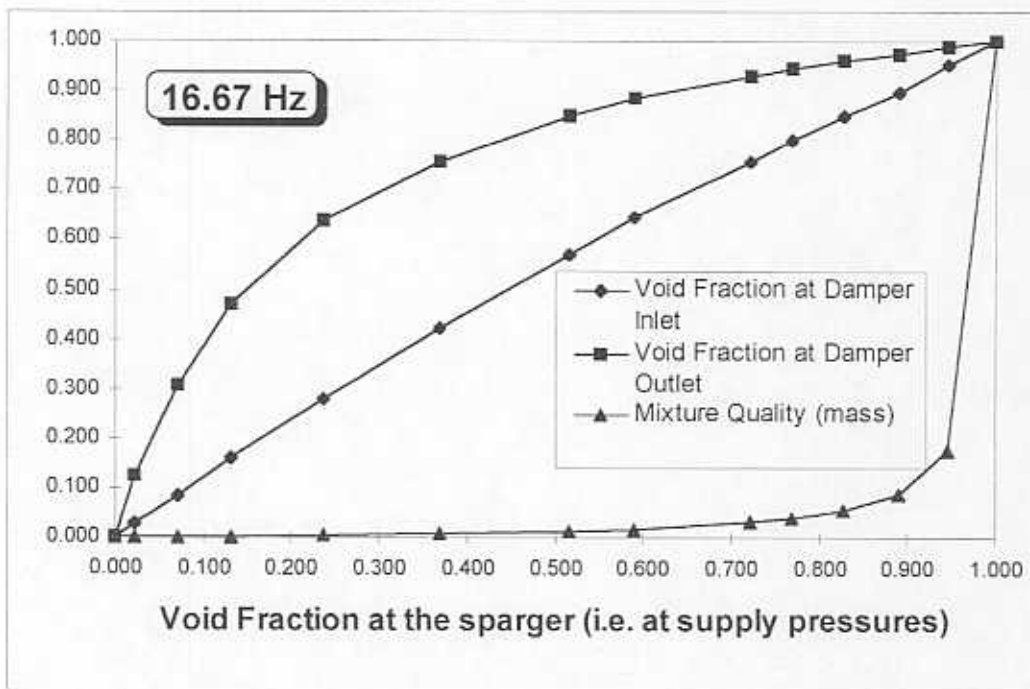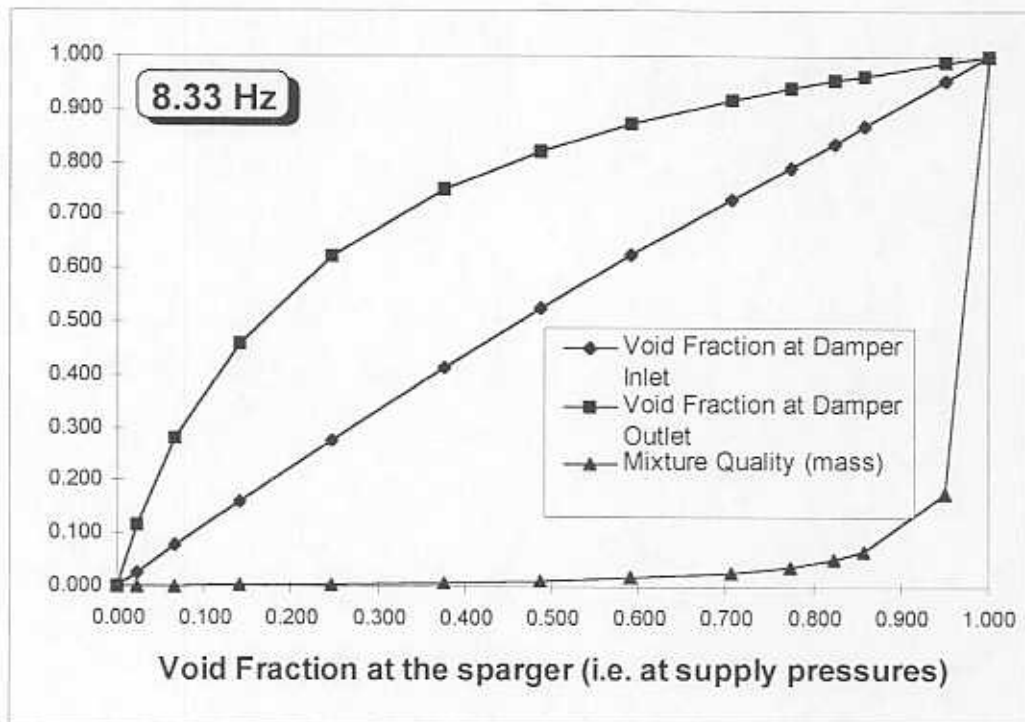
Fig. 4.- Mixture composition (void fraction and mixture quality) along the test rig for two different sets of measurements (whirl frequency equals 8.33 Hz and 16.67 Hz) with the supply conditions as reference (horizontal axis).
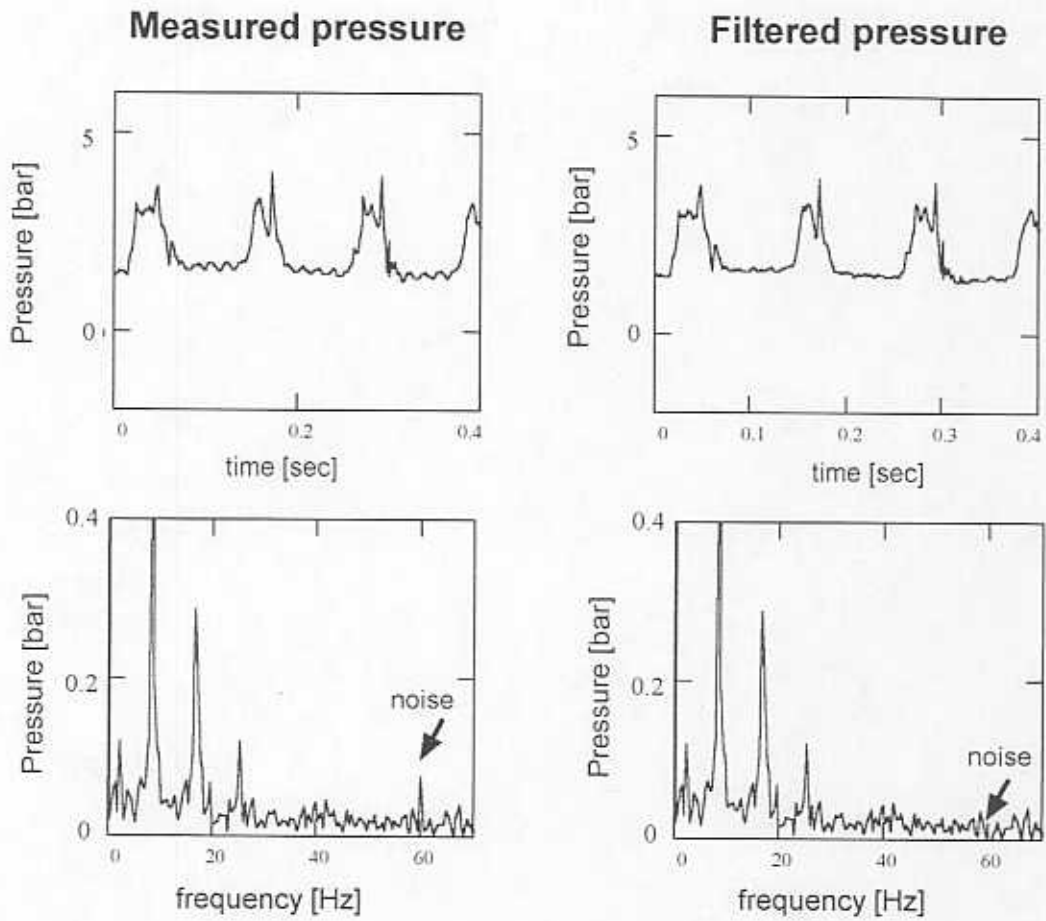
Fig. 5.- Comparison between measured and filtered pressure signal with 60 Hz noise in time and frequency domain. (absolute pressure transducer at Z_1, $330°$, 8.33 Hz, $\lambda=0.86$).
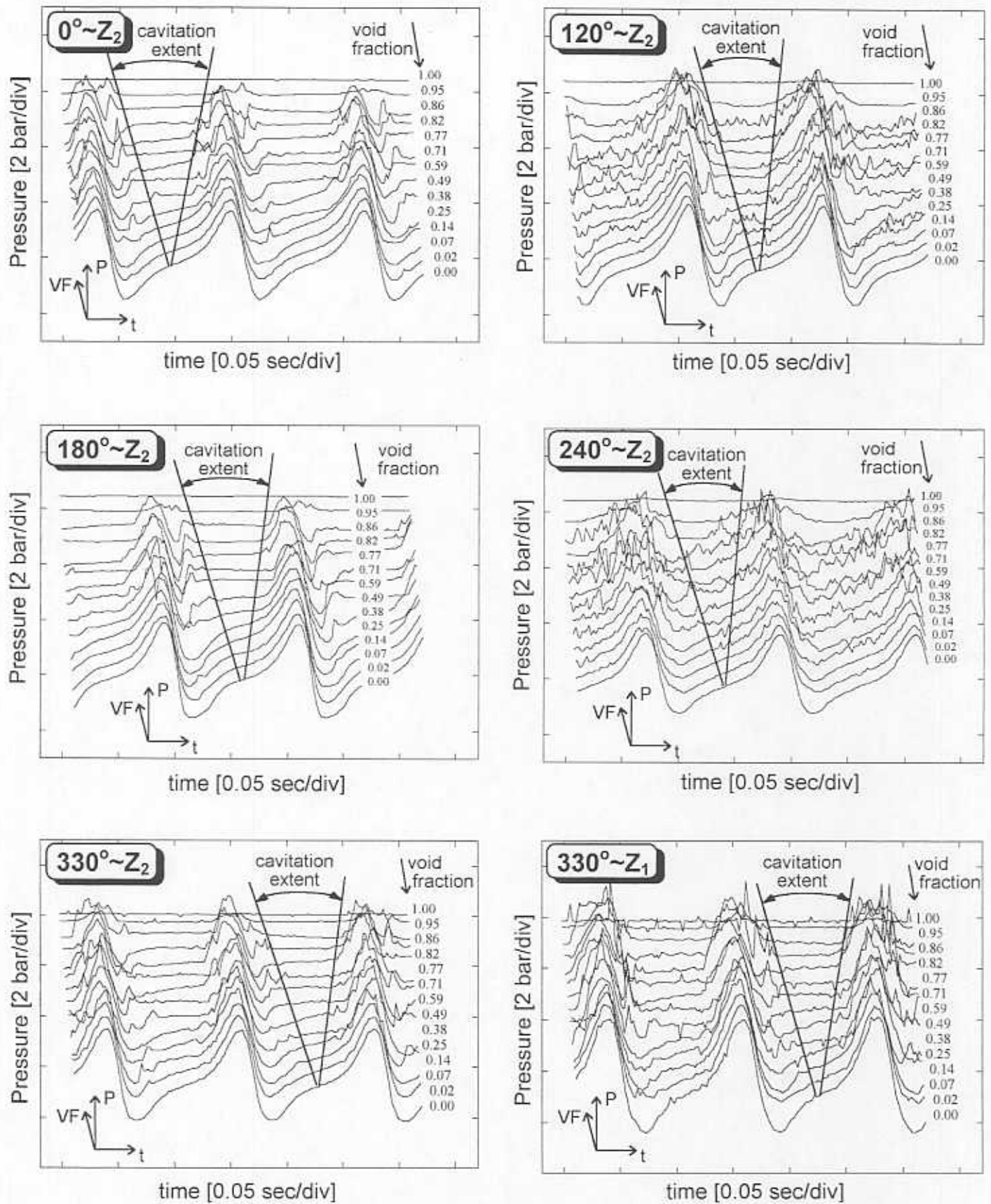
Fig. 6.- Development of the instantaneous pressure field and *gaseous cavitation zone* with the mixture void fraction (VF) for a whirl frequency of 8.33 Hz at different circumferential and axial locations.
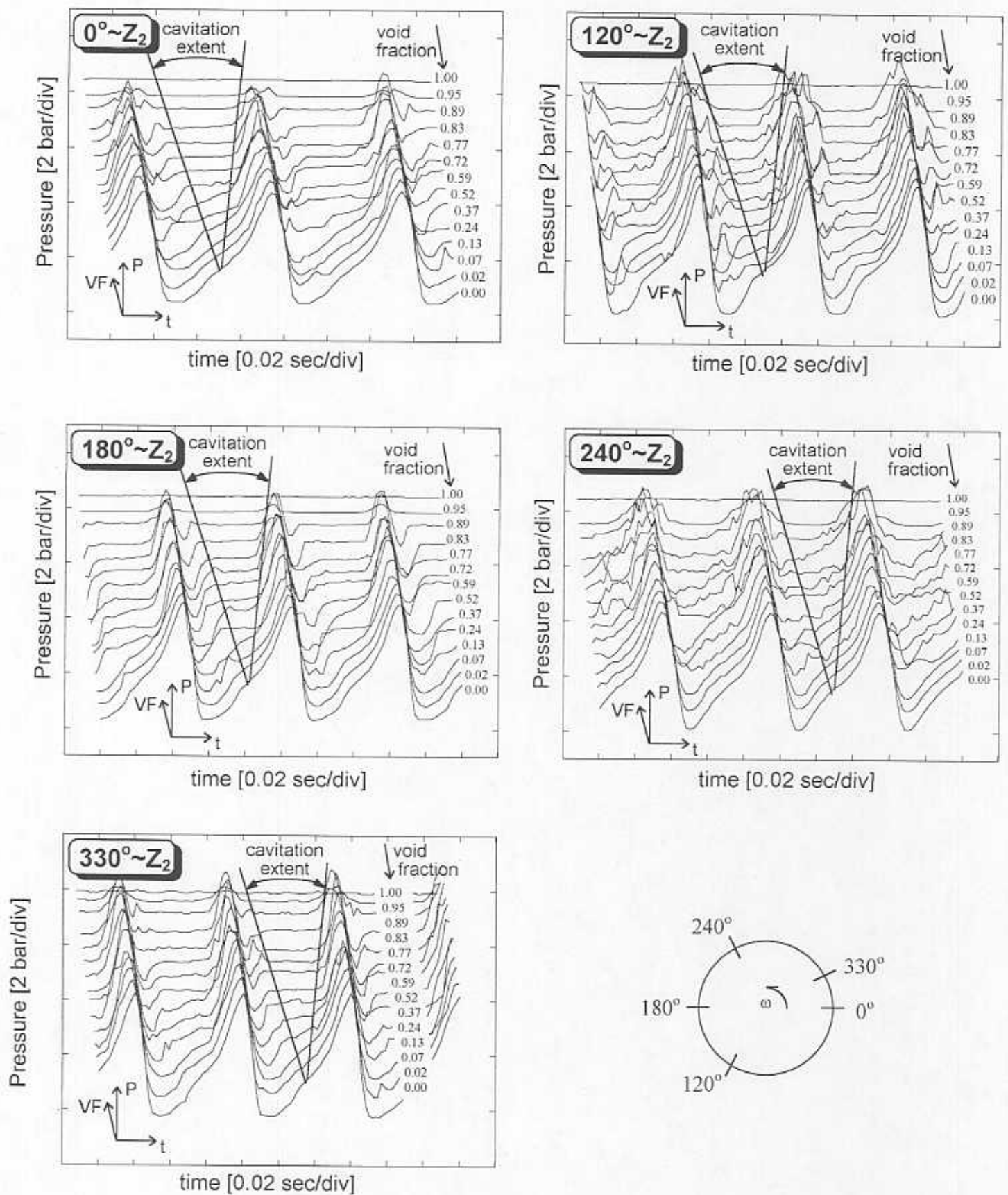
Fig. 7.- Development of the instantaneous pressure field and *gaseous cavitation zone* with the mixture void fraction (VF) for a whirl frequency of 16.67 Hz at different circumferential locations.
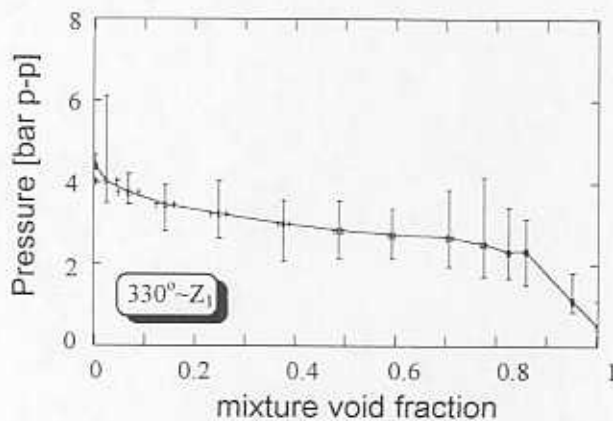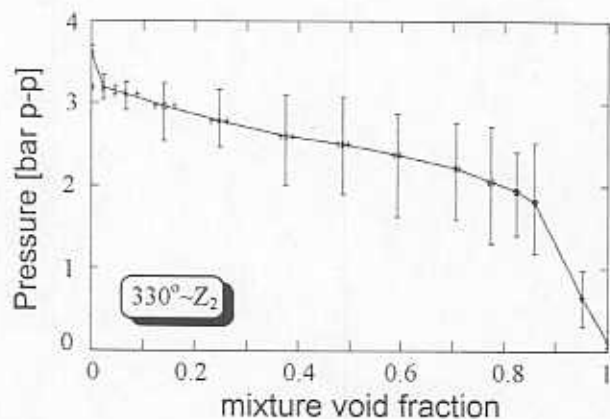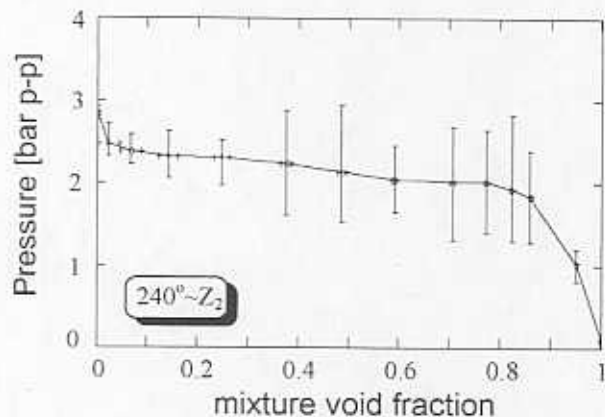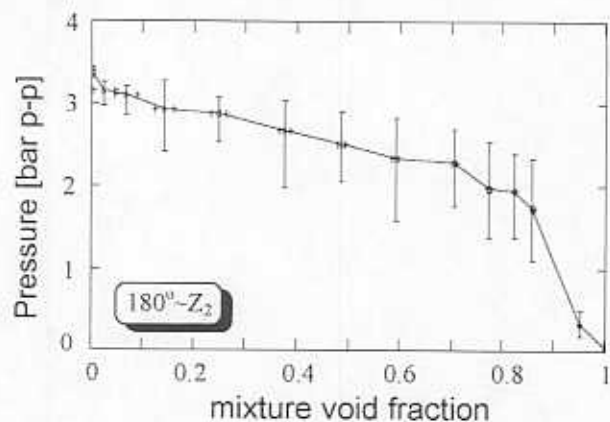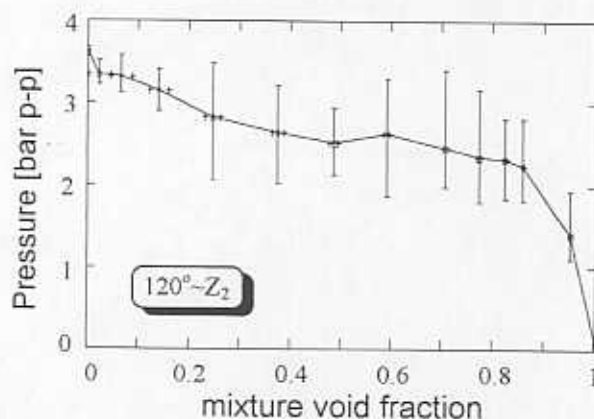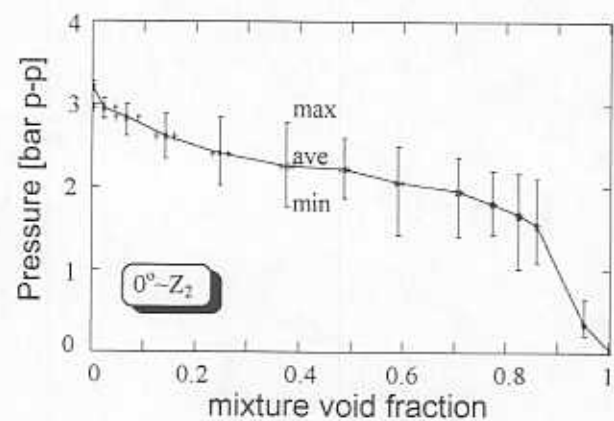
Fig. 8.- Peak-to-peak film pressures vs. mixture void fraction at different circumferential and axial locations for tests at 8.33 Hz.
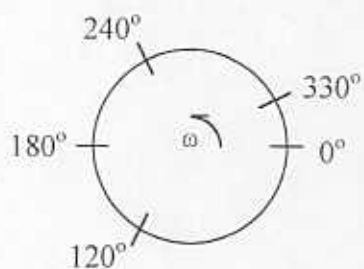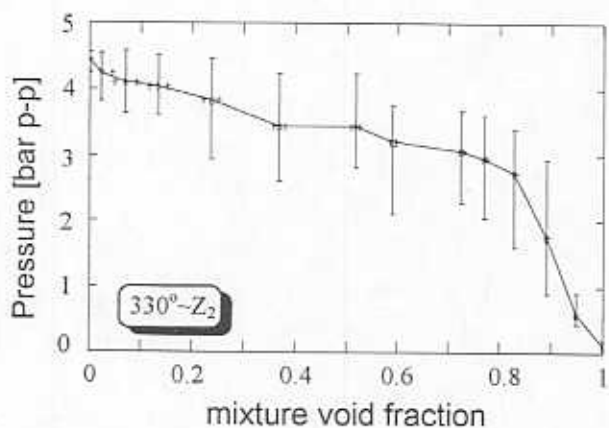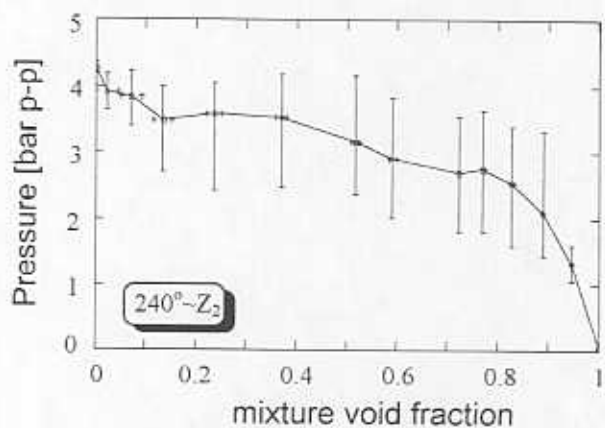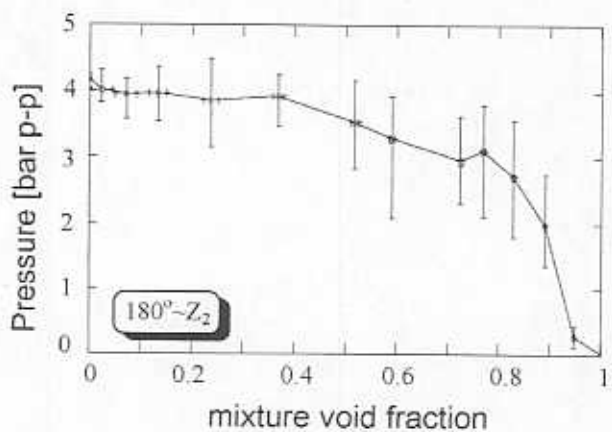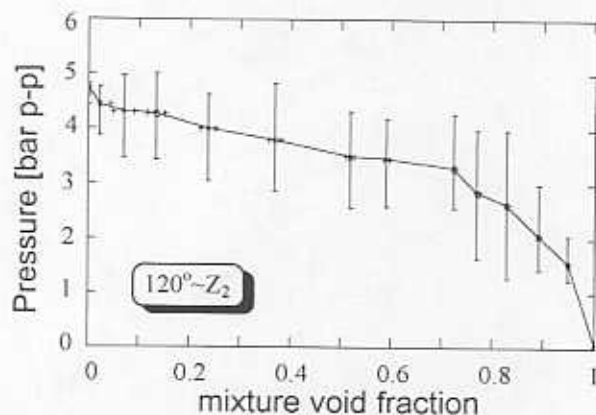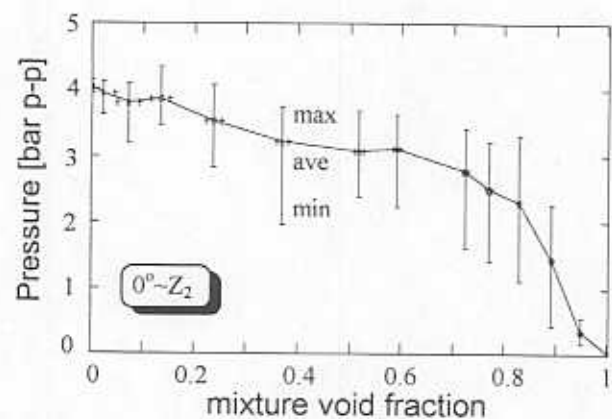
Fig. 9.- Peak-to-peak film pressures vs. mixture void fraction at different circumferential locations for tests at 16.67 Hz.
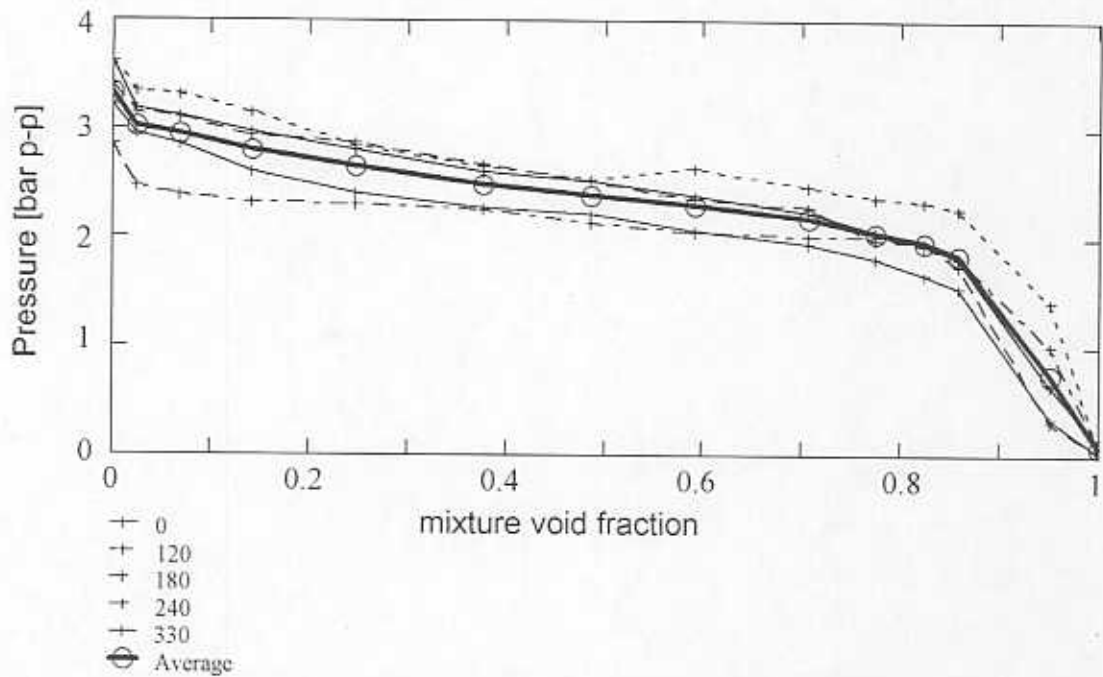
(a) Peak-to-peak pressure vs. mixture void fraction at 8.33 Hz
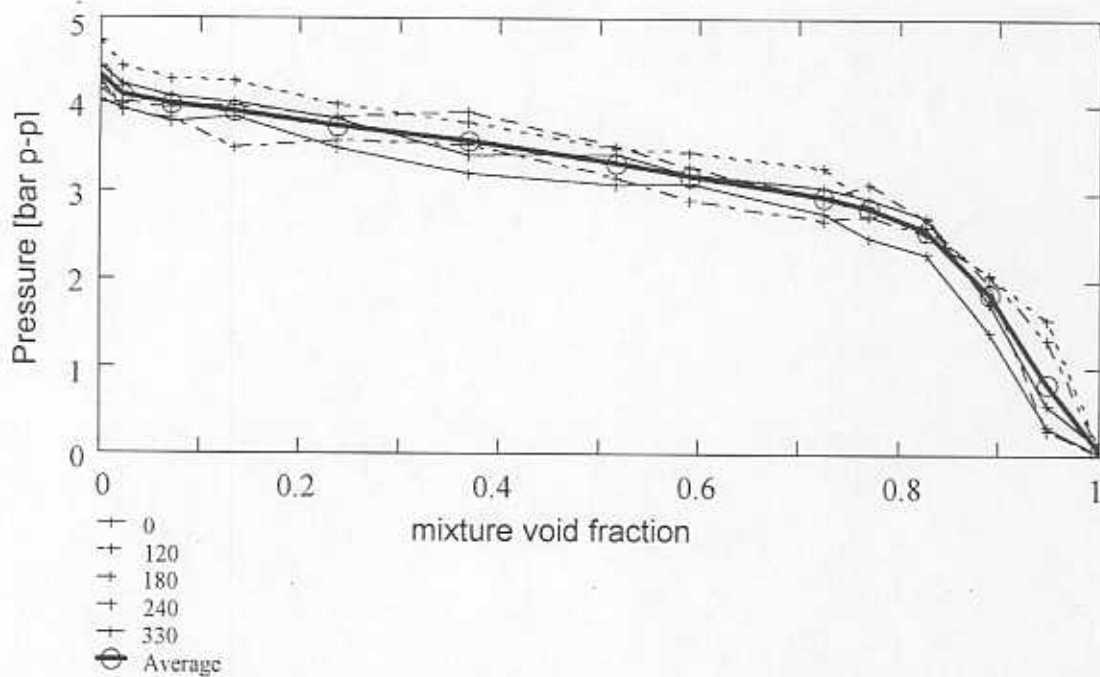
(b) Peak-to-peak pressure vs. mixture void fraction at 16.67 Hz

Fig. 10.- Ensemble averaged peak-to-peak film pressures vs. mixture
void fraction at two different whirl frequencies
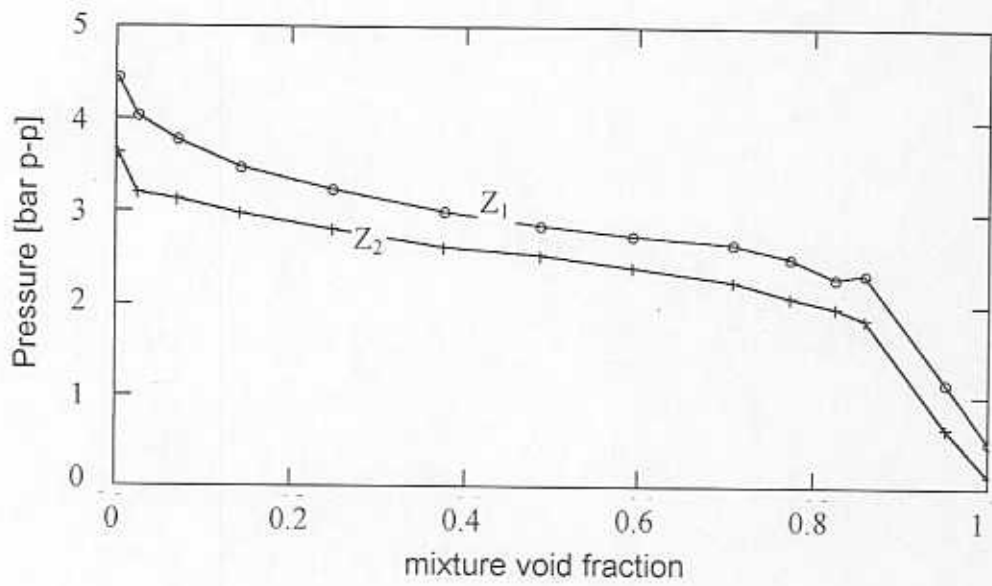
Fig. 11.- Peak-to-peak film pressure at two different axial
locations vs. mixture void fraction at a whirl frequency
of 8.33 Hz (measurements at 330º).
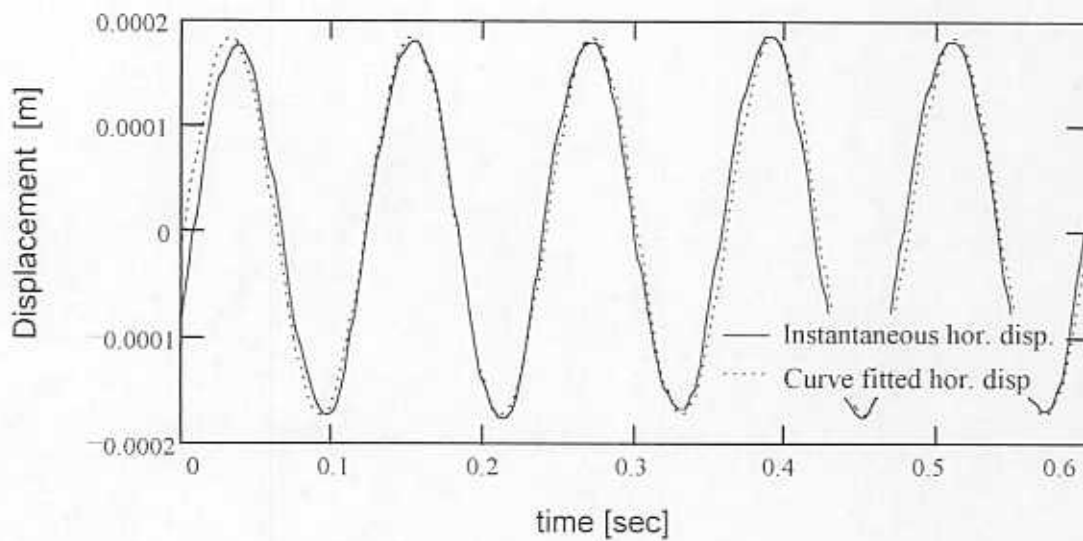
Fig. 12.- Measured and curve fitted horizontal journal displacement for the test at 8.33 Hz, with a mixture void fraction equals to 0.067.
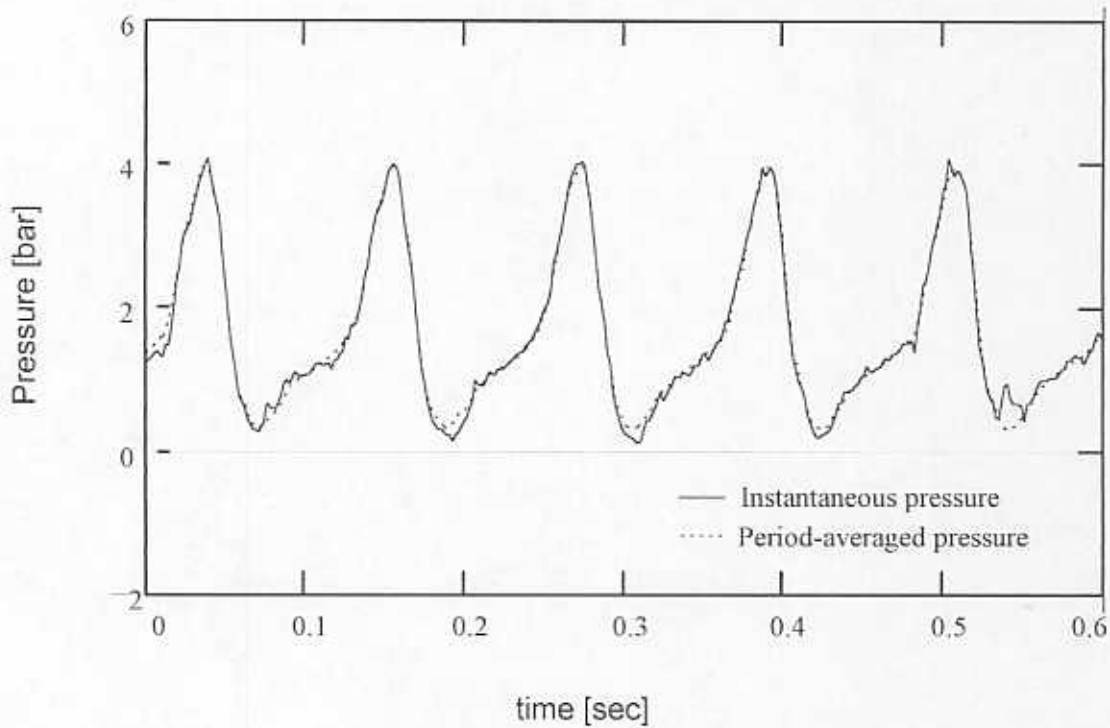
Fig. 13.- *Period-averaged* and instantaneous film pressure at $(330°, Z_1)$ vs. time for the test at 8.33 Hz, mixture void fraction equals 0.067.
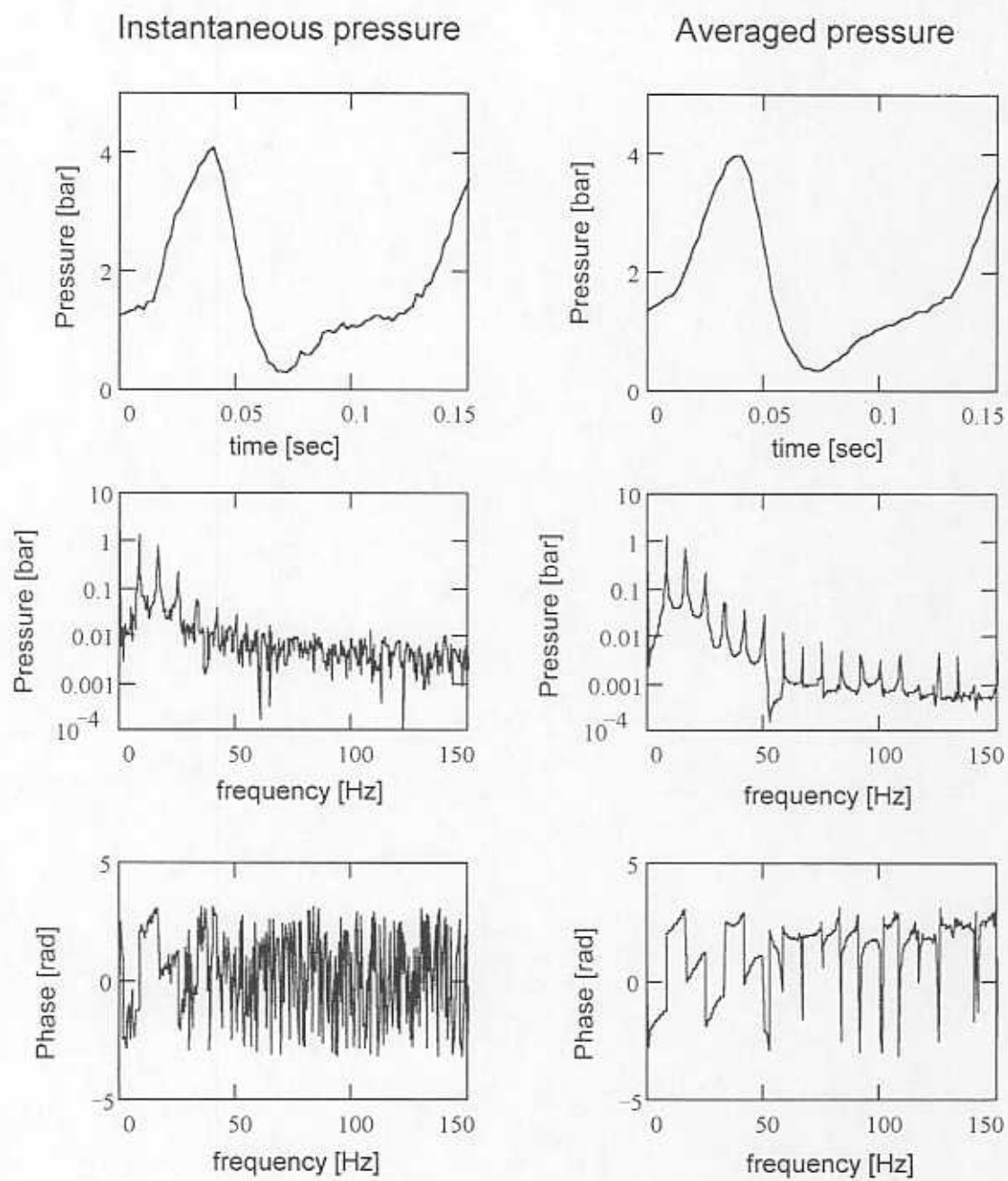
Fig. 14.- Comparison between instantaneous and *period-averaged* pressures in time and frequency domain.
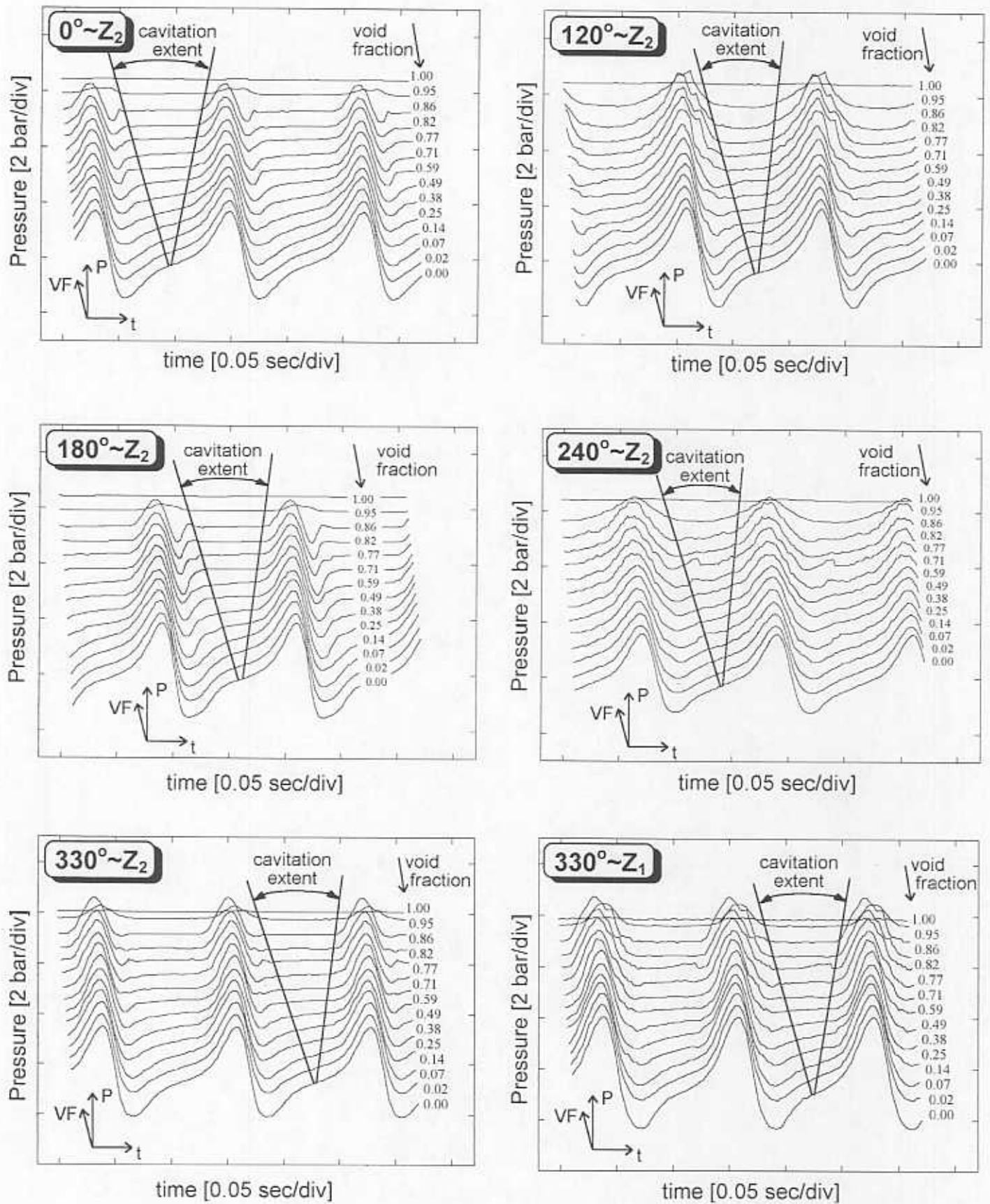
Fig. 15.- Development of the *period-averaged* pressure fields and *gaseous cavitation zone* with the mixture void fraction for a whirl frequency of 8.33 Hz at different circumferential and axial locations.
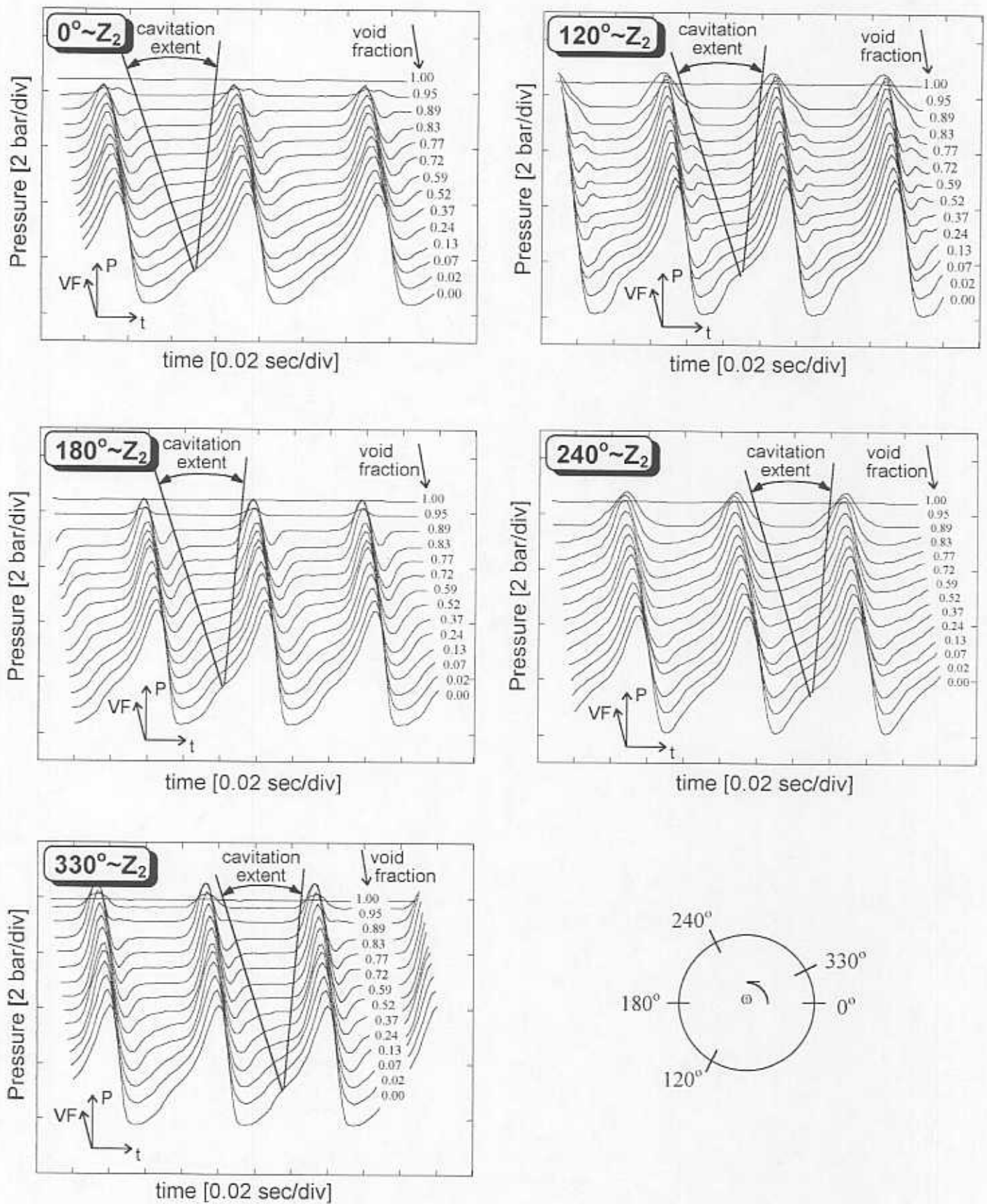
Fig. 16.- Development of the *period-averaged* pressure fields and *gaseous cavitation zone* with the mixture void fraction for a whirlfrequency of 16.67 Hz at different circumferential locations.
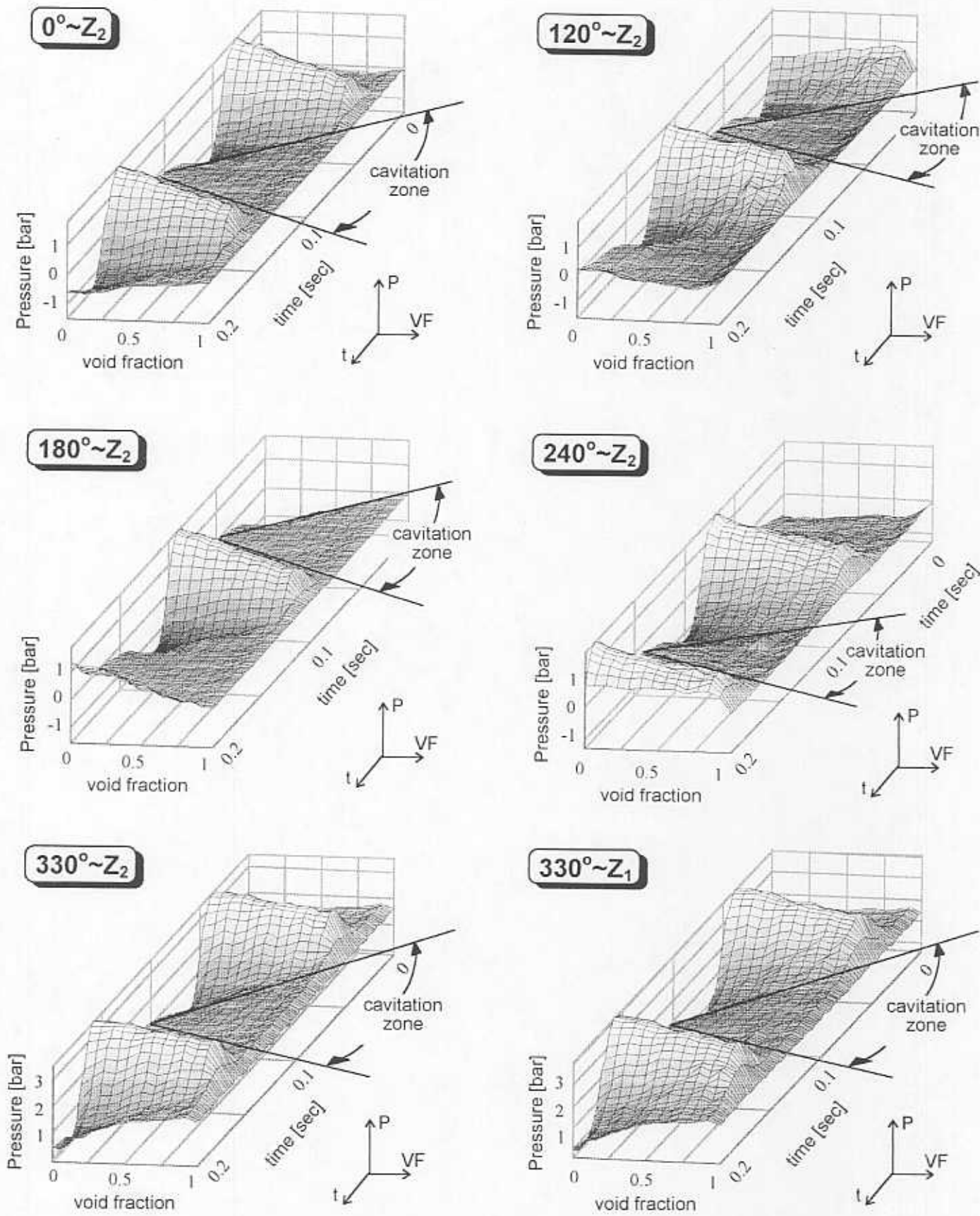
Fig. 17.- 3-D plots of the pressure fields versus the mixture void fraction for a whirl frequency of 8.33 Hz at different circumferential and axial locations.
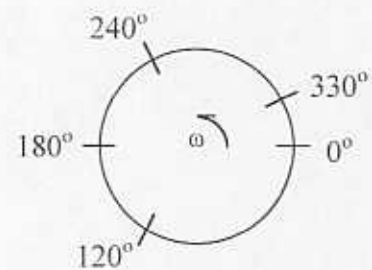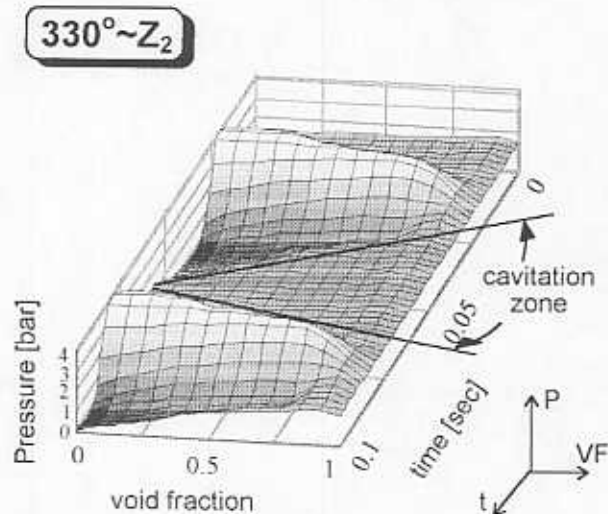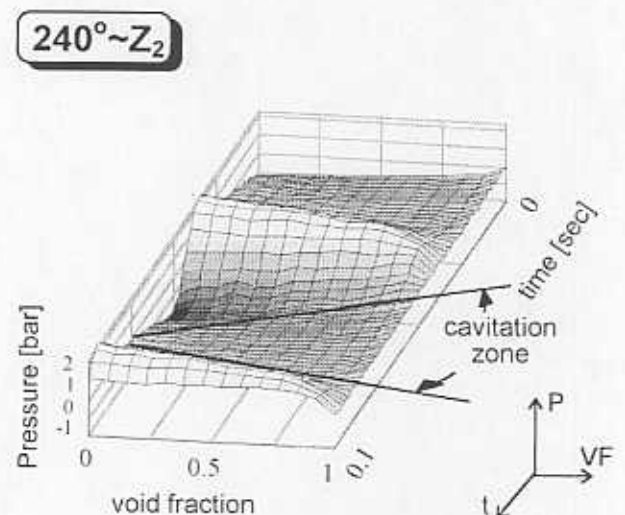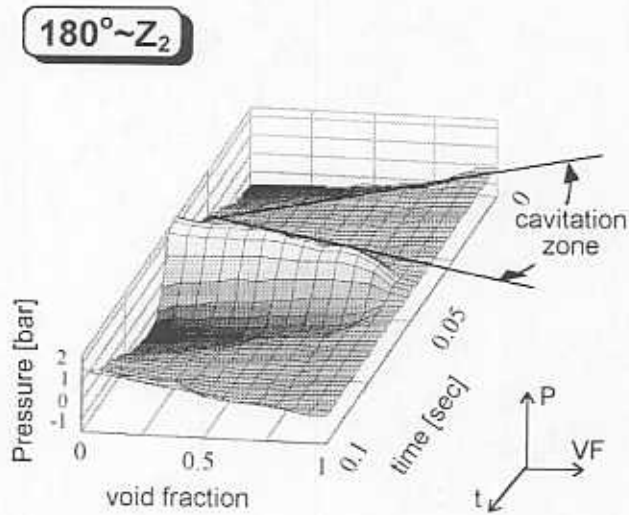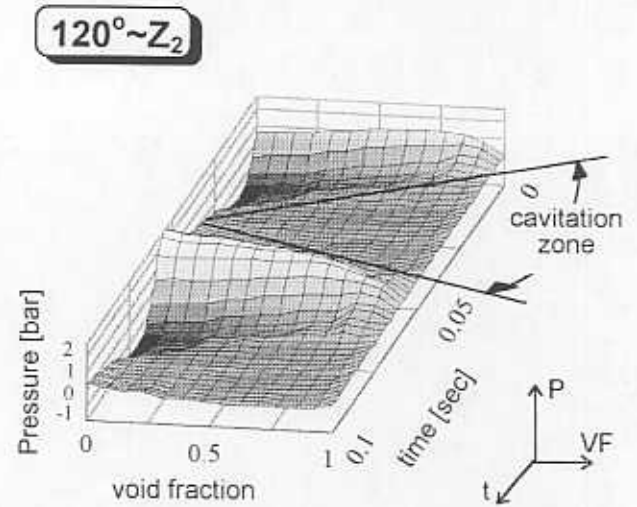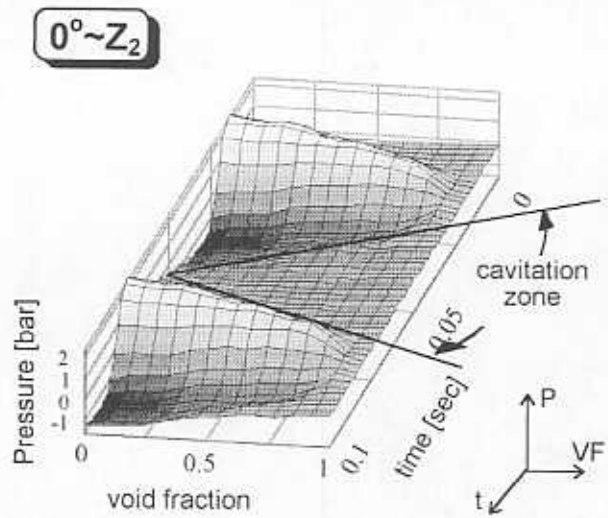
Fig. 18.- 3-D plots of the pressure fields versus the mixture void fraction for a whirl frequency of 16.67 Hz at different circumferential locations.
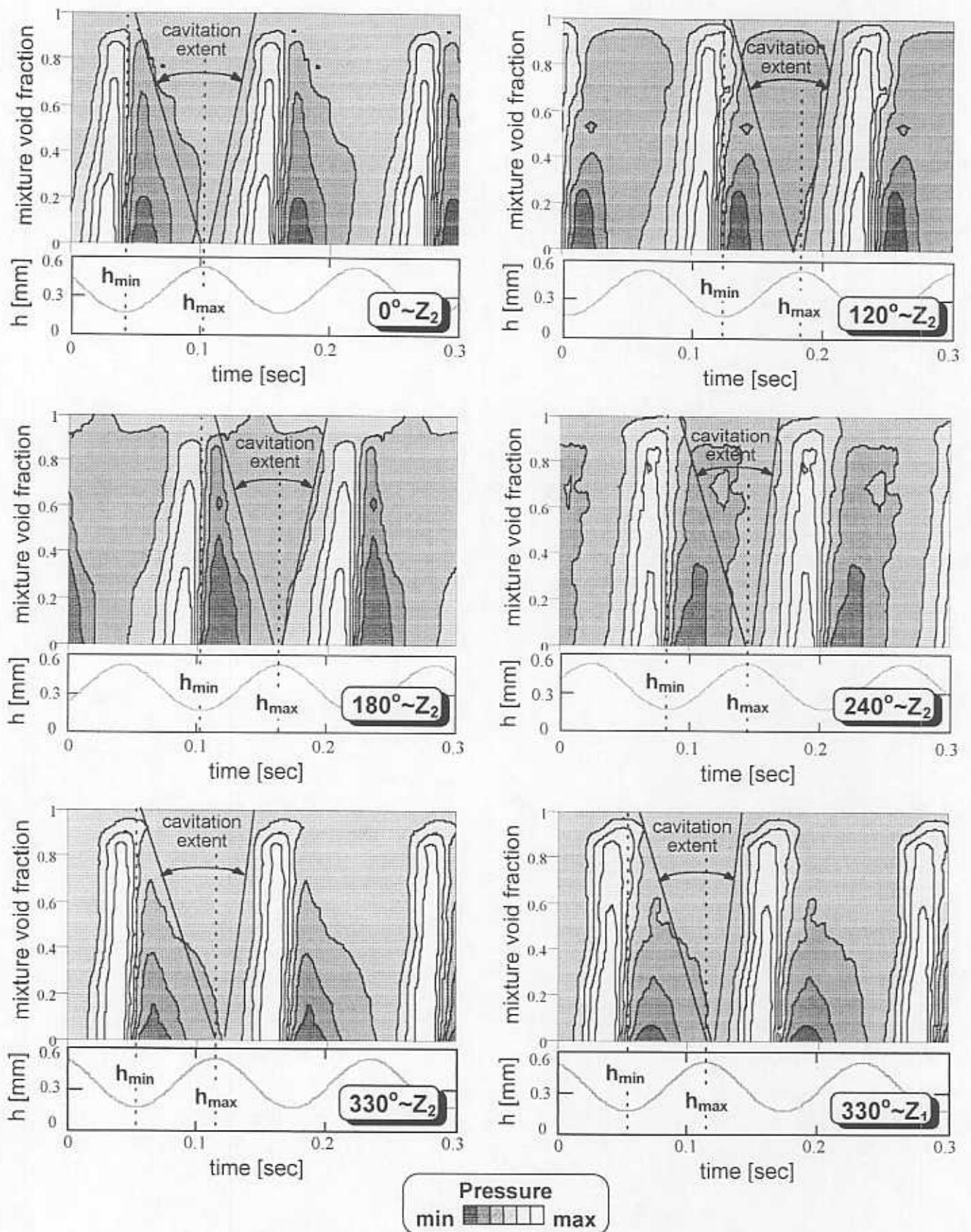
Fig. 19.- Contour plots of the squeeze film pressure fields versus the mixture void fraction for a whirl frequency of 8.33 Hz at different circumferential locations.
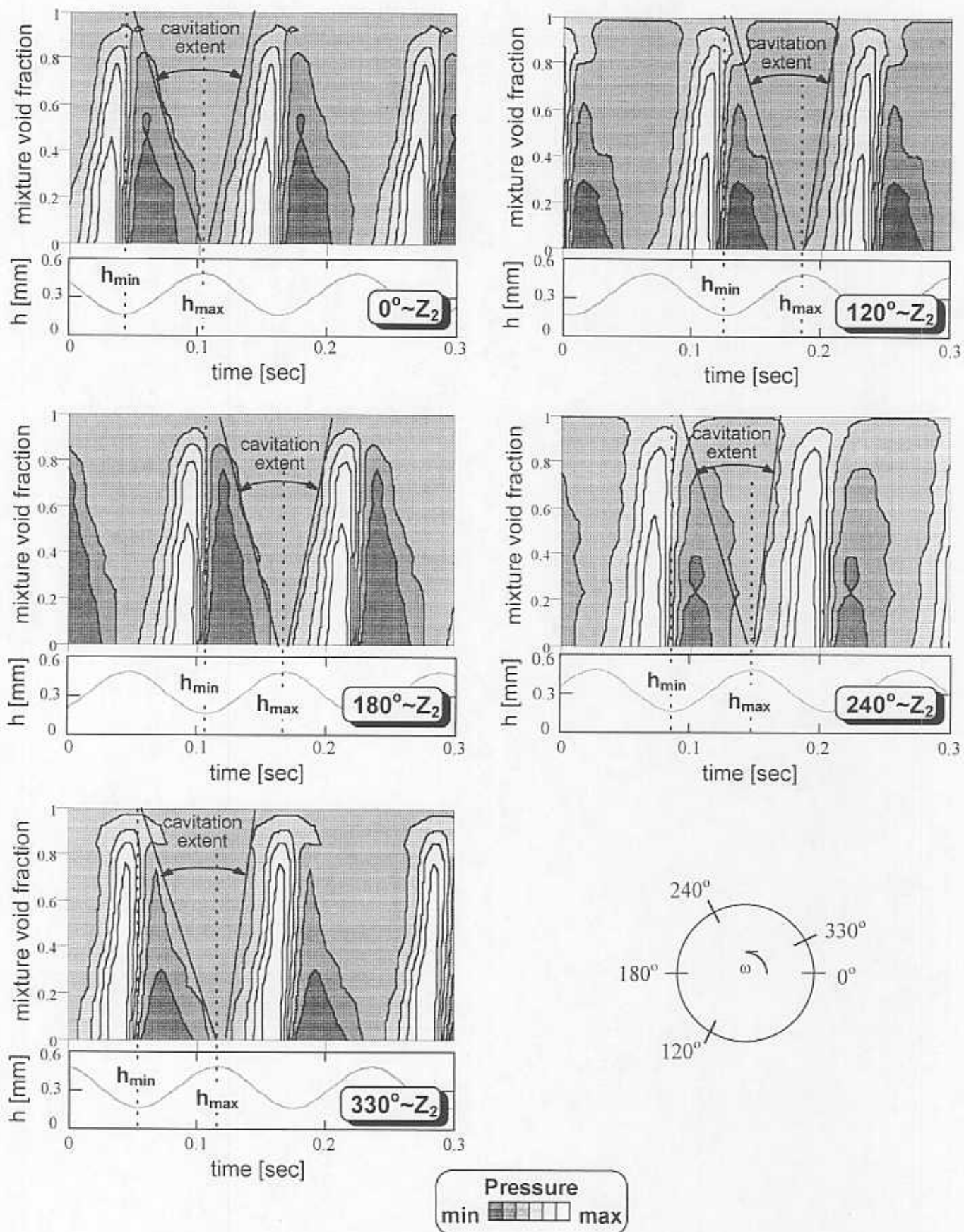
Fig. 20.- Contour plots of the squeeze film pressure fields versus the mixture void fraction for a whirl frequency of 16.67 Hz at different circumferential and axial locations.
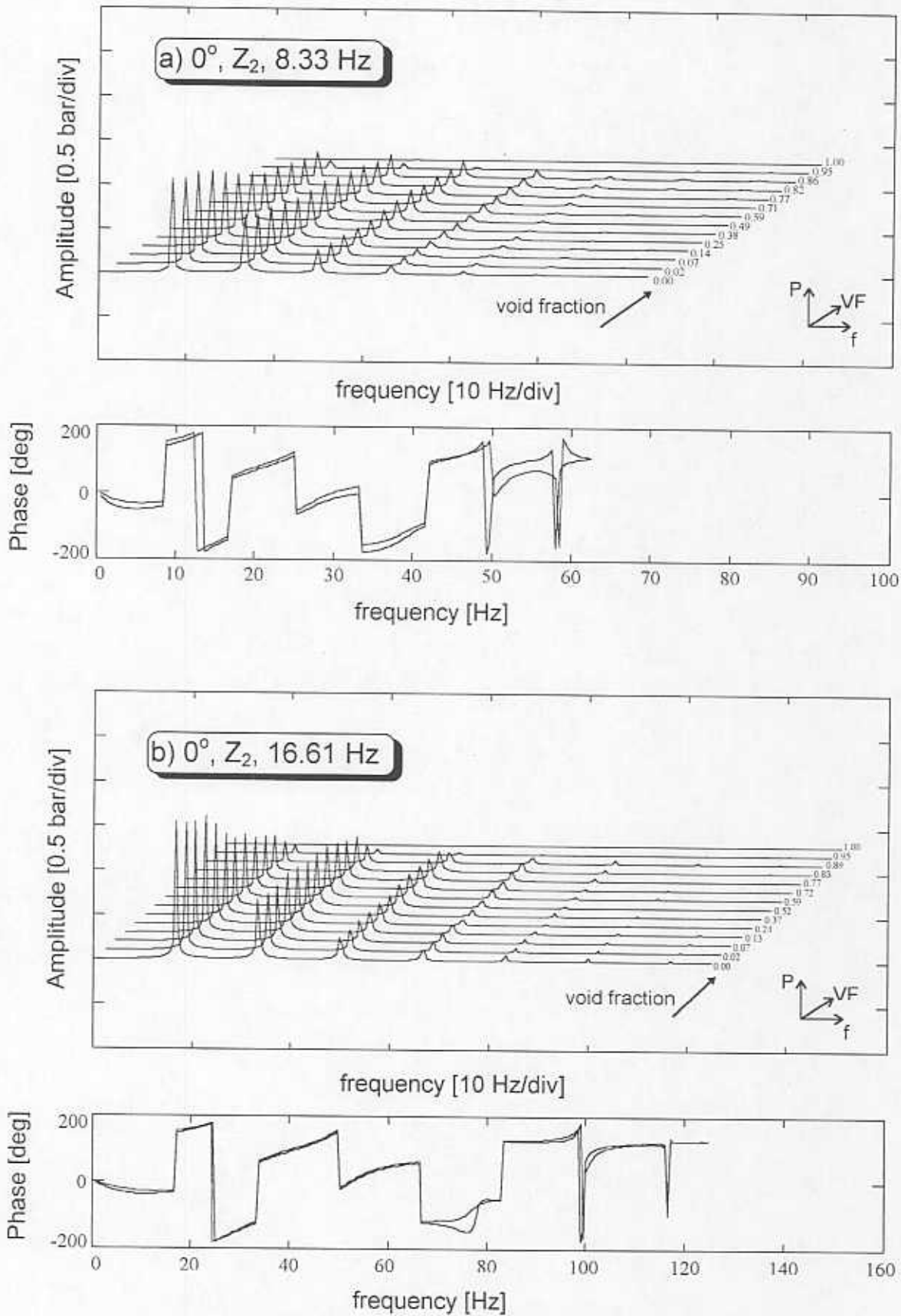
Fig. 21.- Waterfall plots of the frequency content (amplitude and phase) of the period-averaged-*dynamic* pressure for the location $(0°, Z_2)$, at (a) 8.33 Hz and (b) 16.67 Hz.
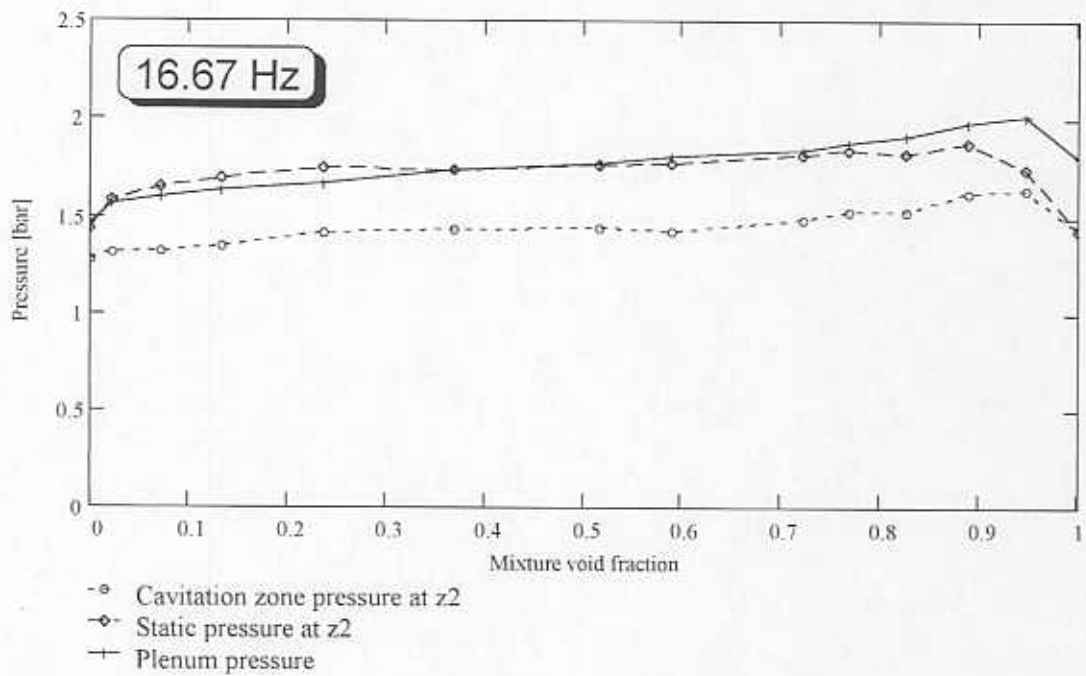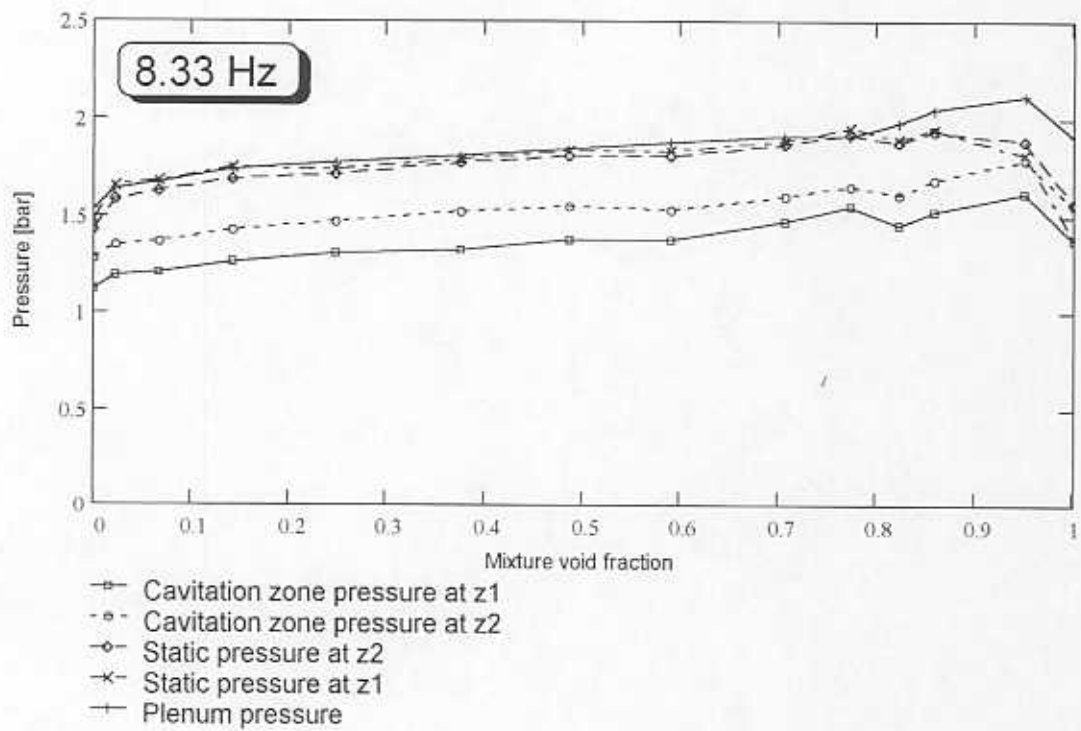
Fig. 22.- Plenum, cavitation and *static* film pressures vs. mixture void fraction at (a) 8.33 Hz and (b) 16.67 Hz.
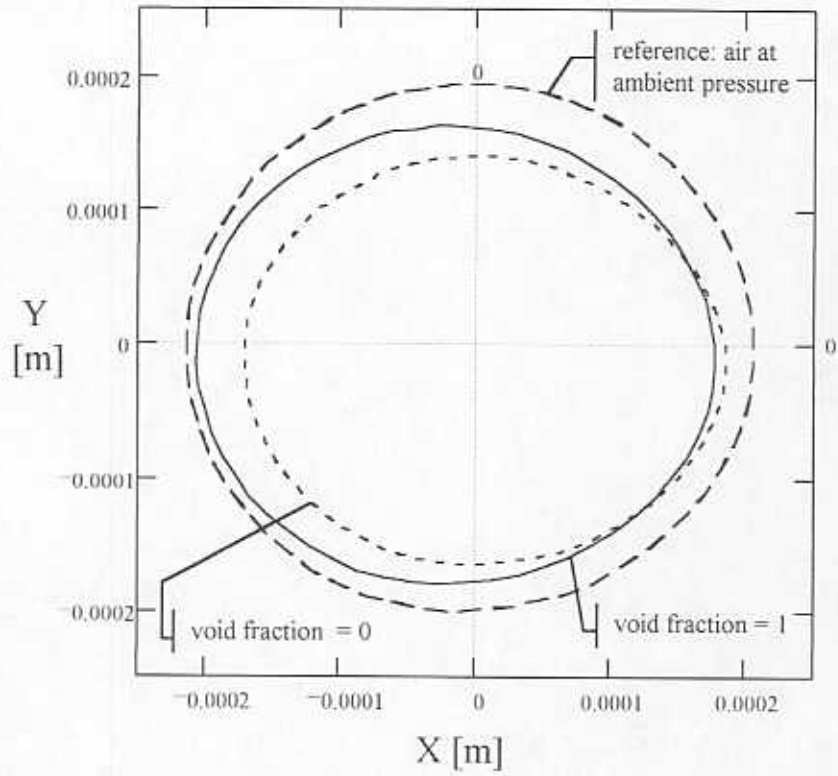
Fig. 23.- Change of the journal orbit of motion with the mixture void fraction.
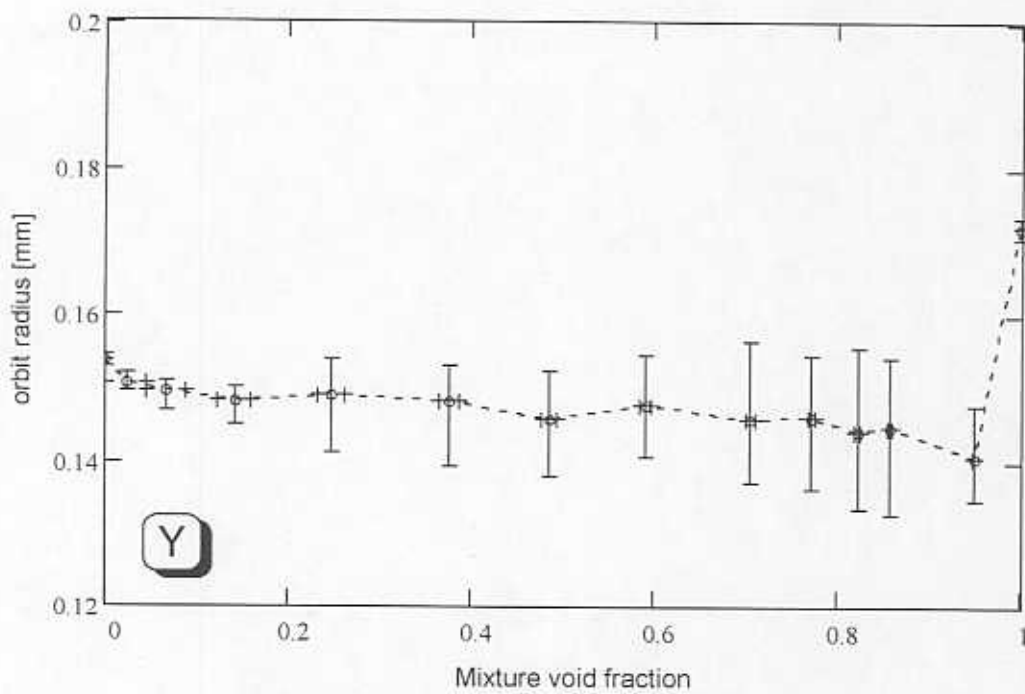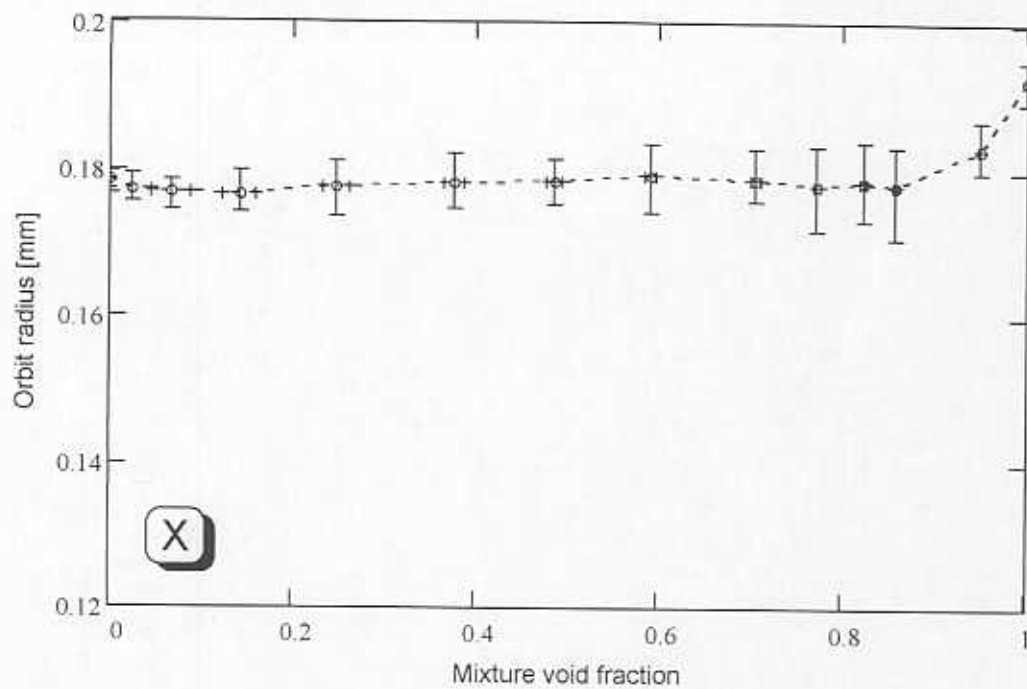
Fig. 24.- Orbit radius at 8.33 Hz based on measurements on
(a) horizontal-X direction and (b) vertical-Y direction
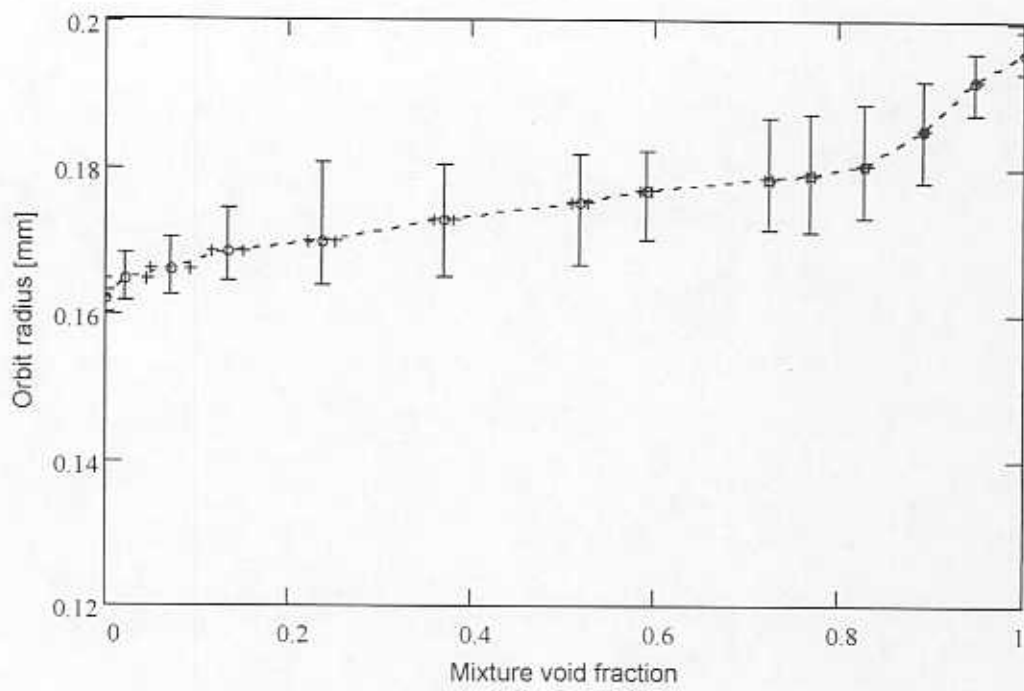
Fig. 25.- Orbit radius at 16.67 Hz based on measurements on
the horizontal-X direction
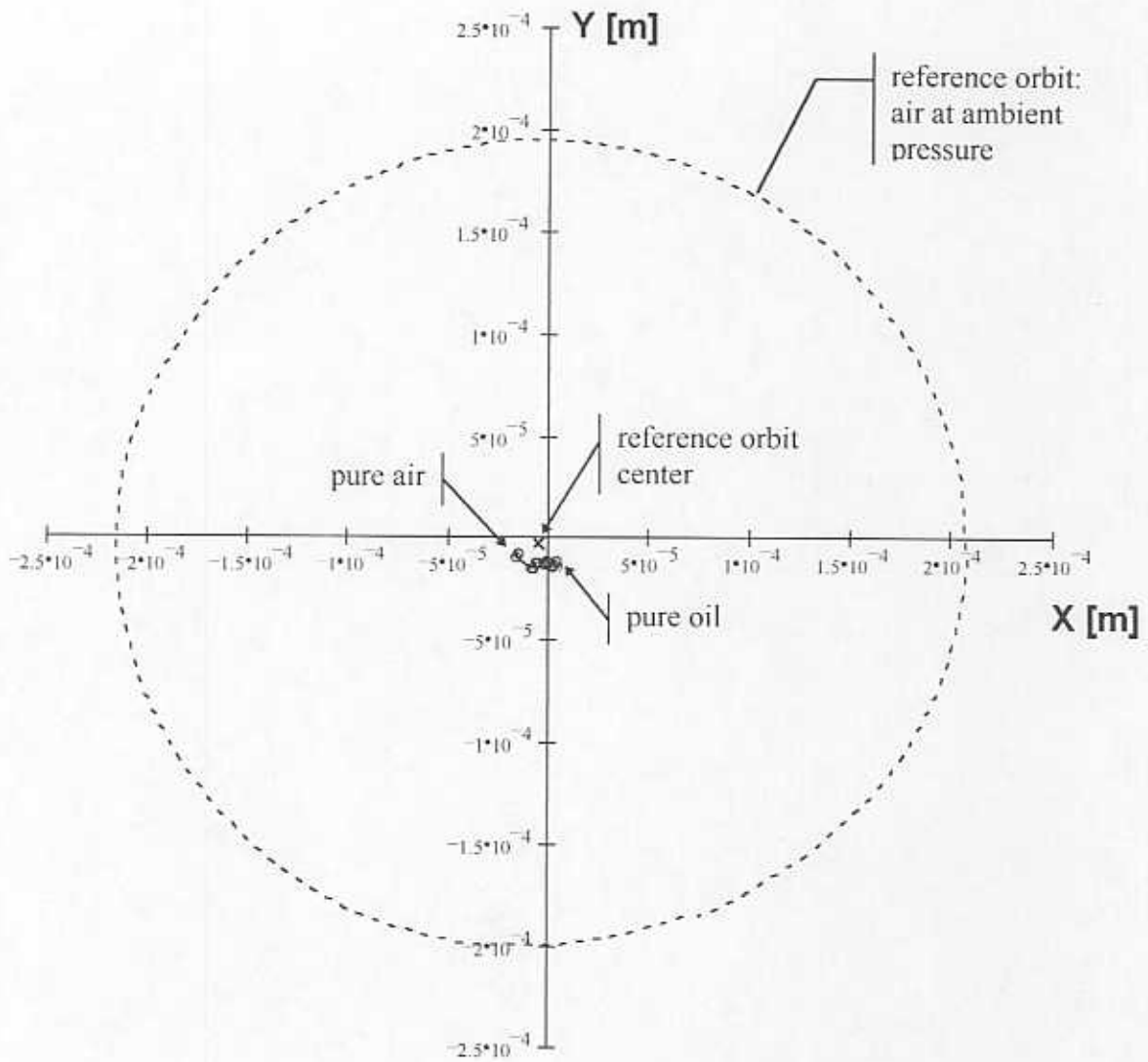
Fig. 26.- Orbit center locus as a function of the mixture void fraction
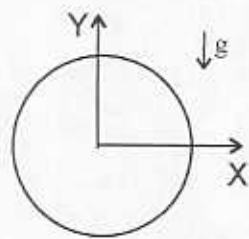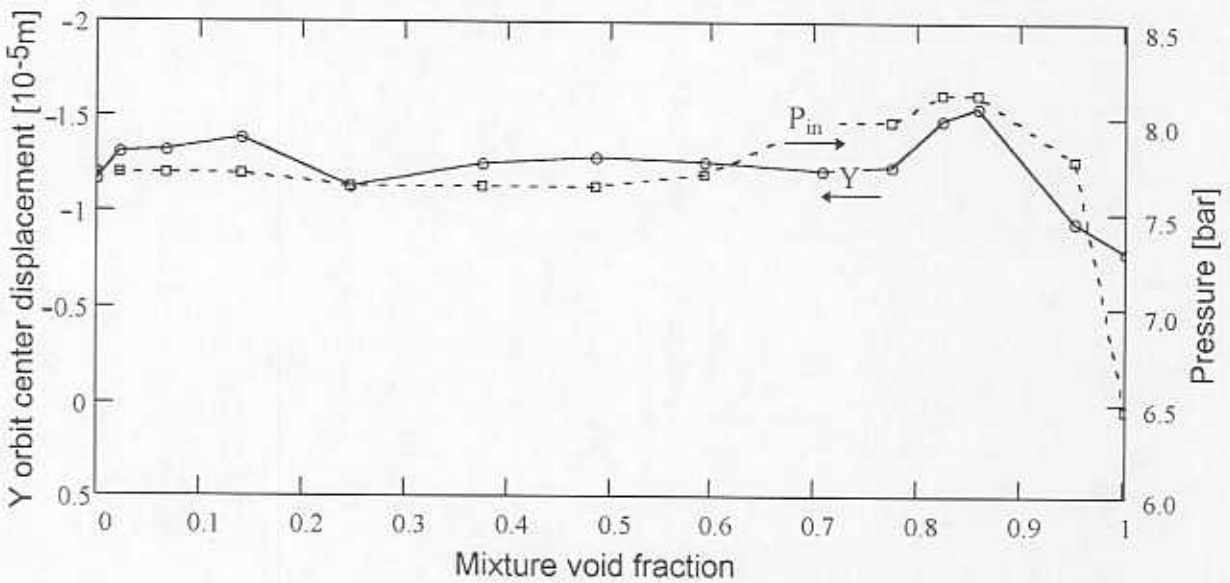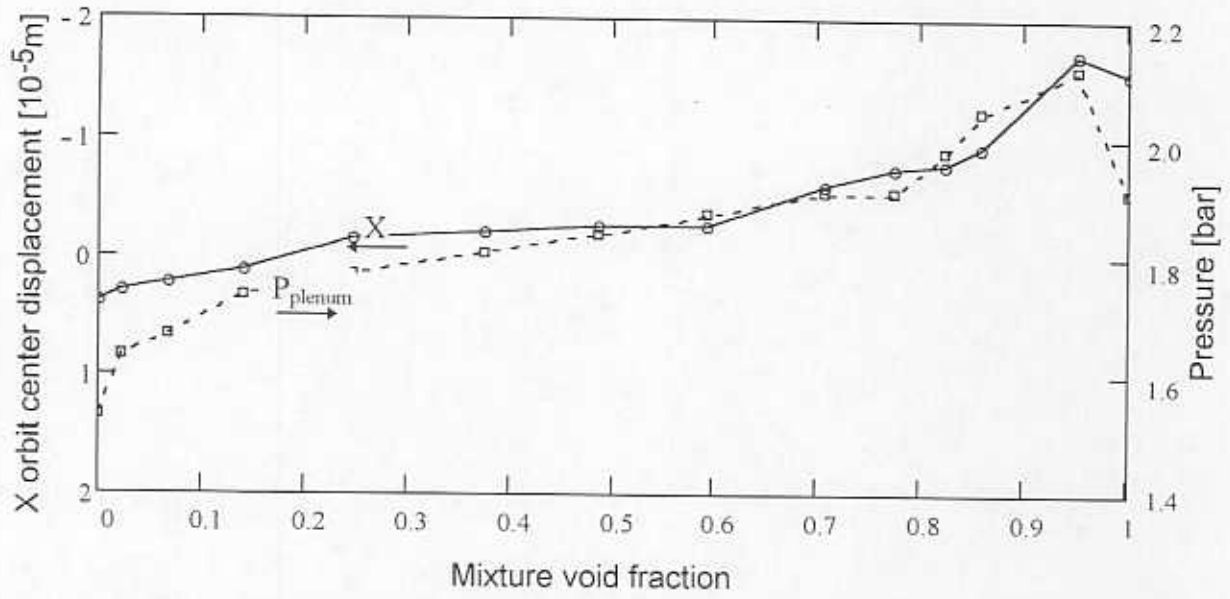
Fig. 27.- Relation between inlet and plenum pressures and
journal motion orbit center displacements at 8.33 Hz
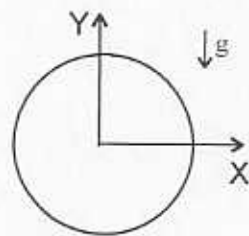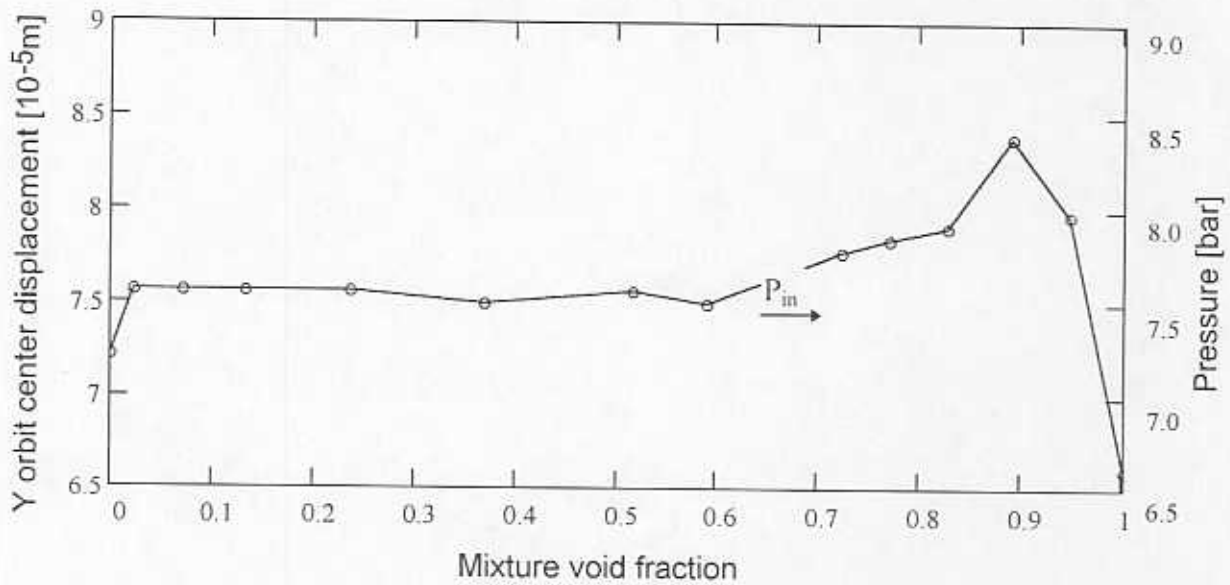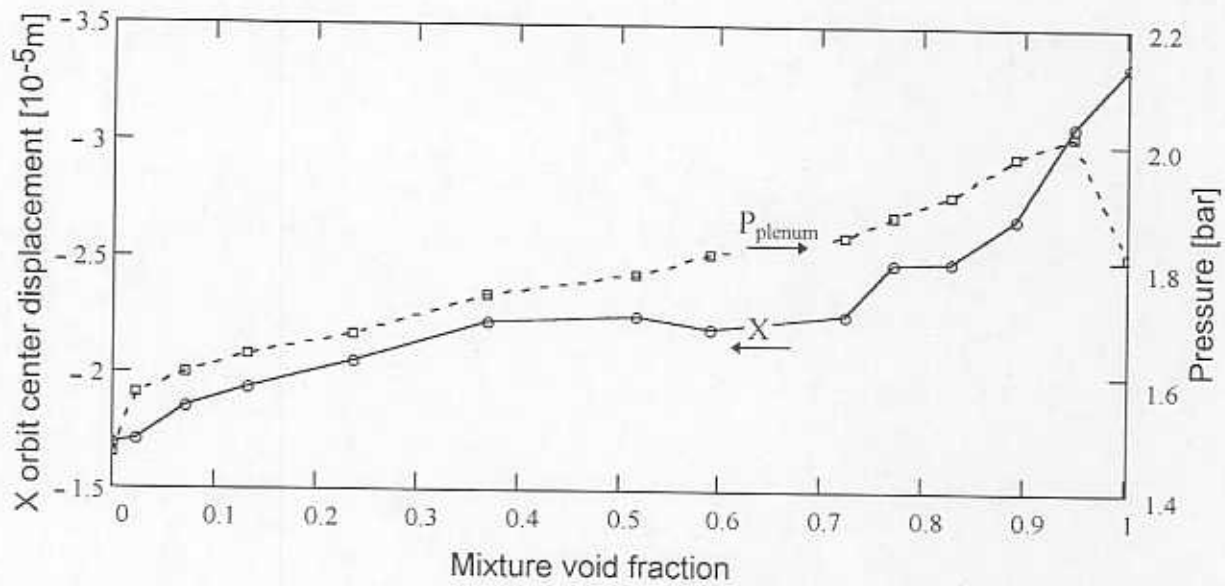
Fig. 28 .- Relation between inlet and plenum pressures and
journal motion orbit center displacements at 16.67 Hz
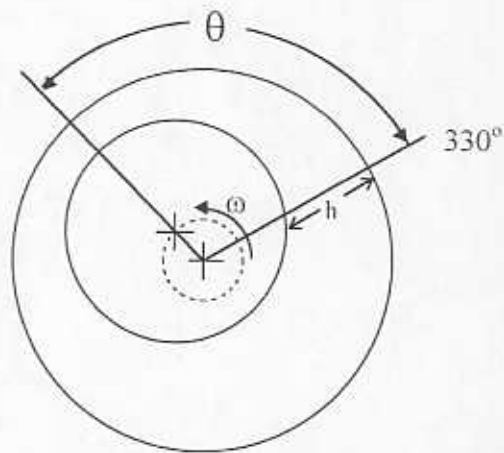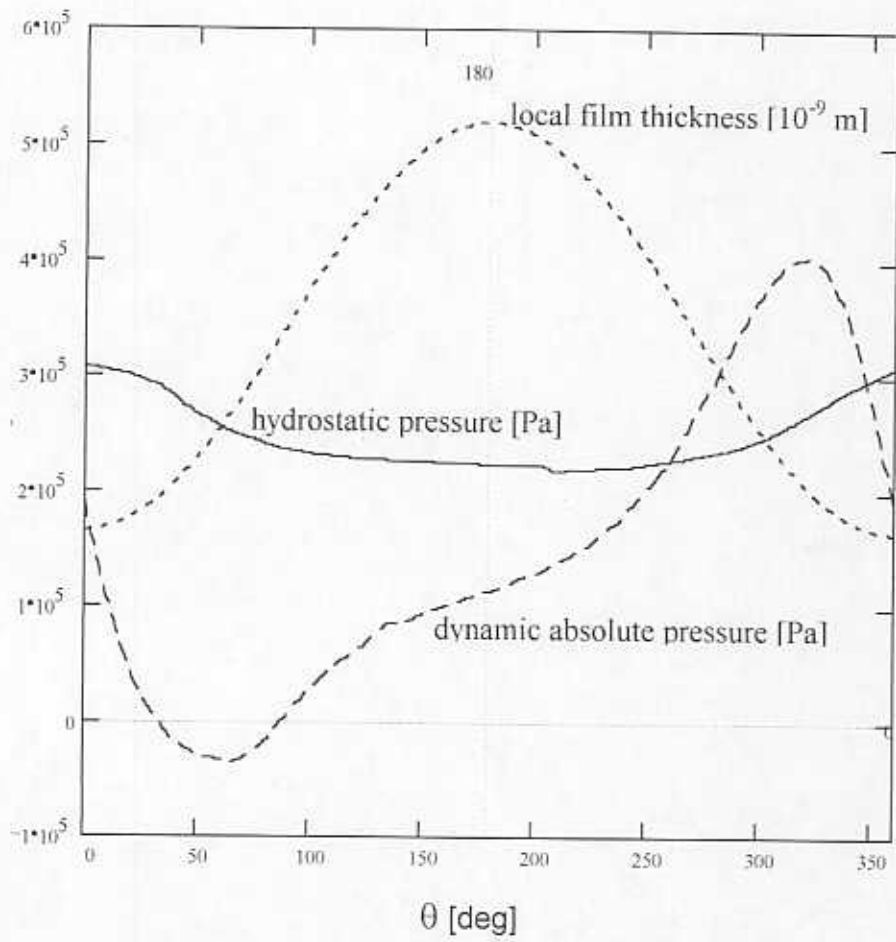
Fig. 29.- Hydrostatic and dynamic* absolute pressures and local film
thickness versus journal angular position at $(Z_1, 330°)$.
* Dynamic pressure at 8.33 Hz.
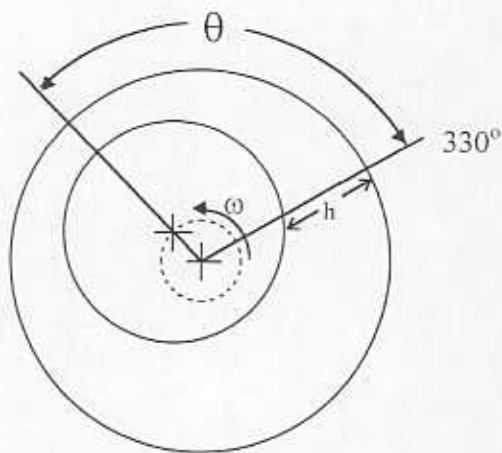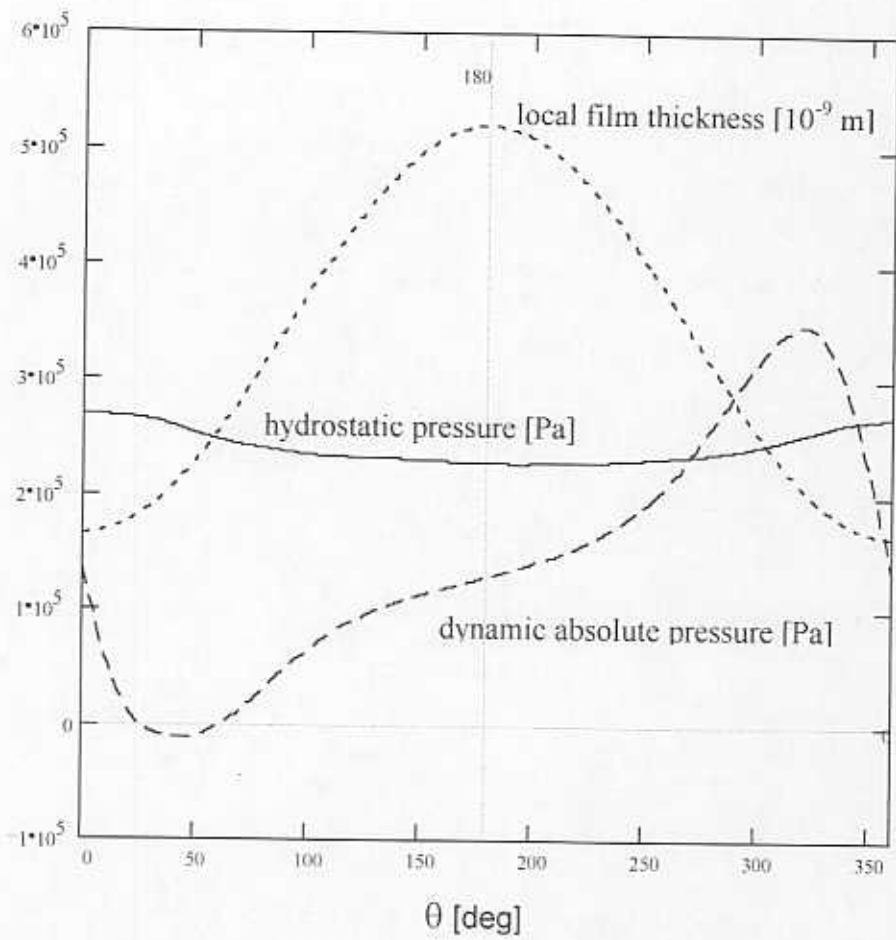
Fig. 30.- Hydrostatic and dynamic absolute pressures and local film thickness versus journal angular position at $(Z_2, 330°)$.
* Dynamic pressure at 8.33 Hz.
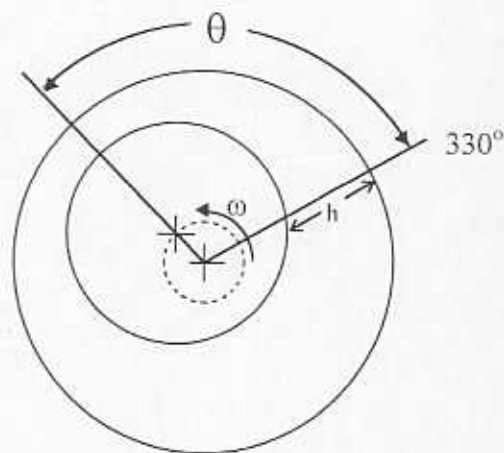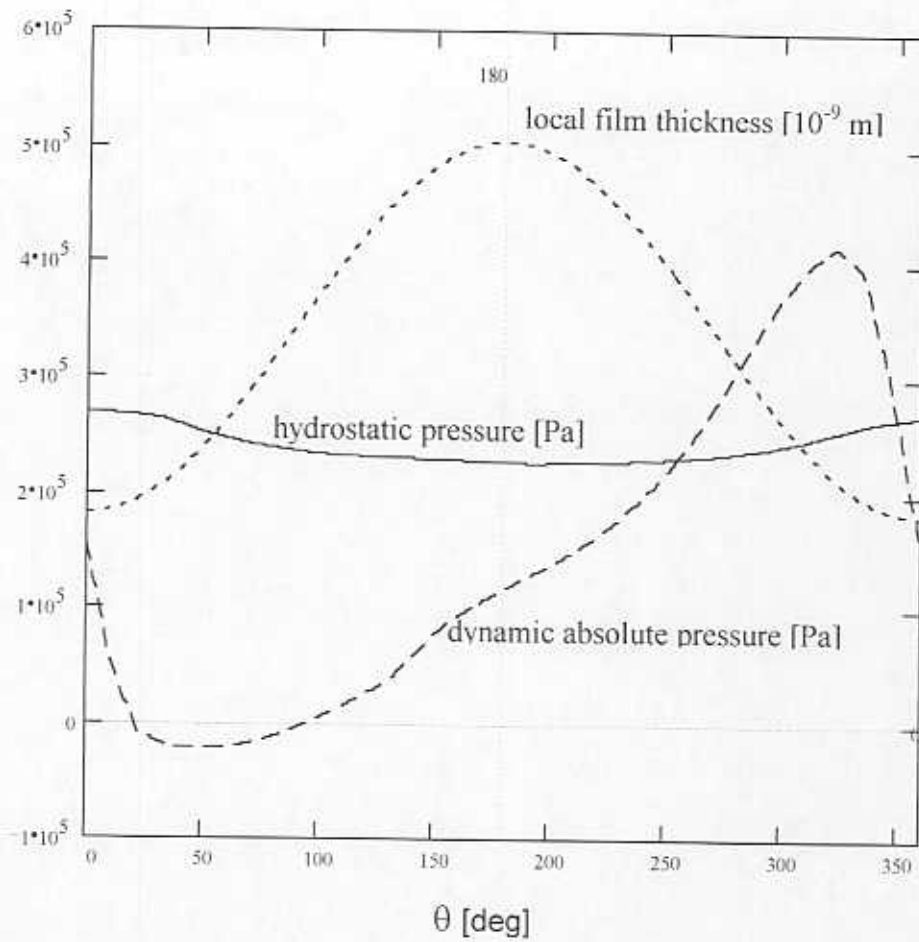
Fig. 31.- Hydrostatic and dynamic absolute pressures and local film thickness versus journal angular position at (Z_2, 330°).
* Dynamic pressure at 16.67 Hz.
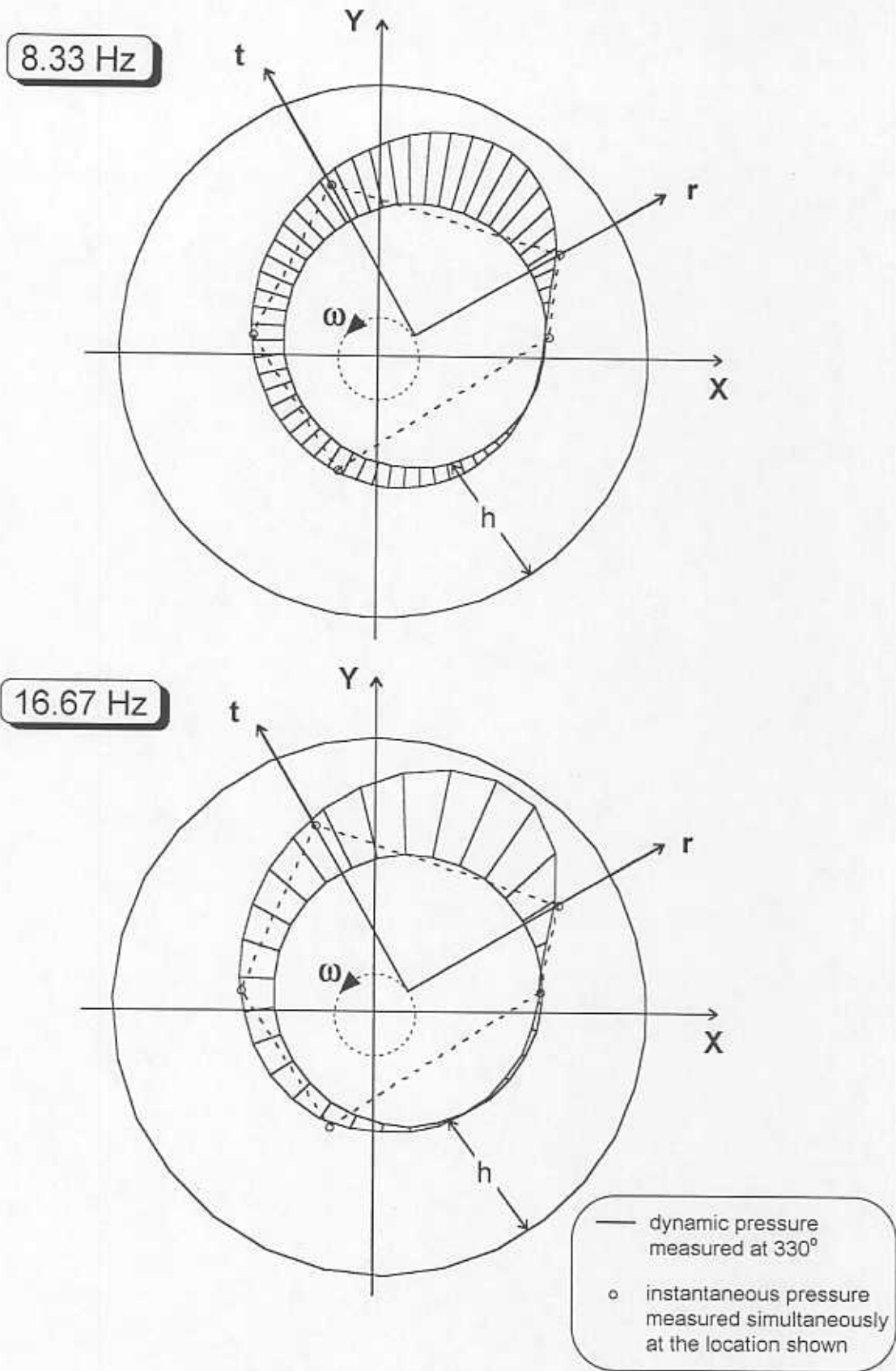
Fig. 32.- Pressure profile around the journal damper from measurements at
one fixed location over one cycle of motion and from simultaneous
measurements at different angular locations at the plane of Z_2.
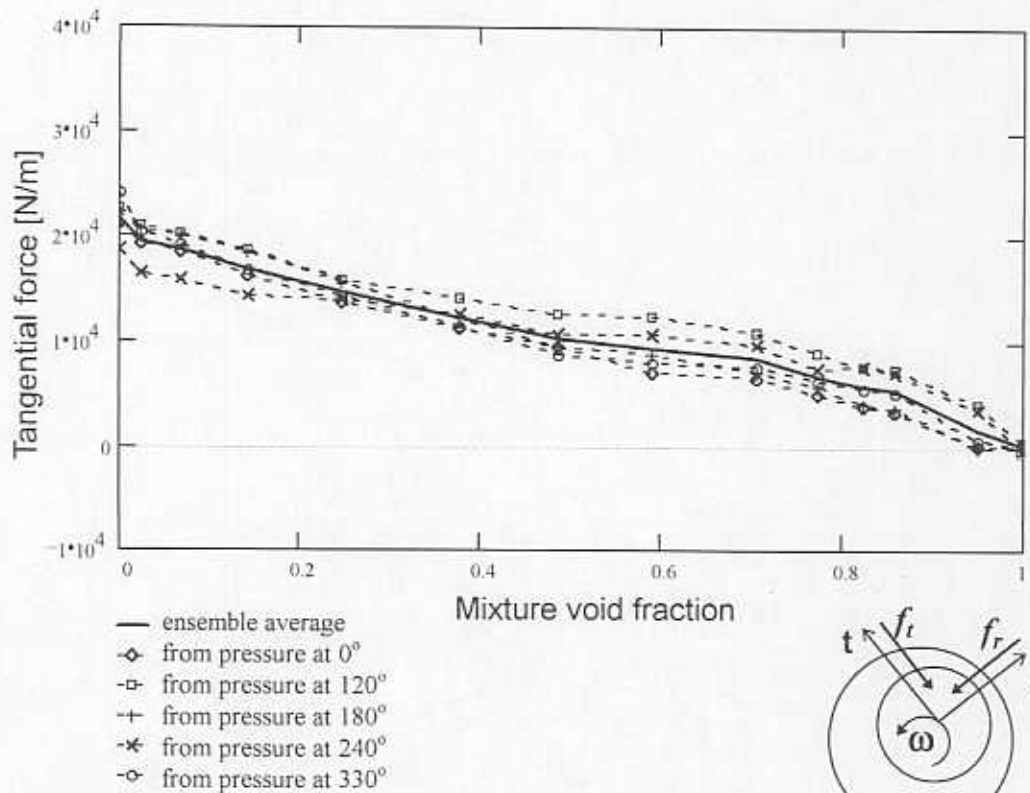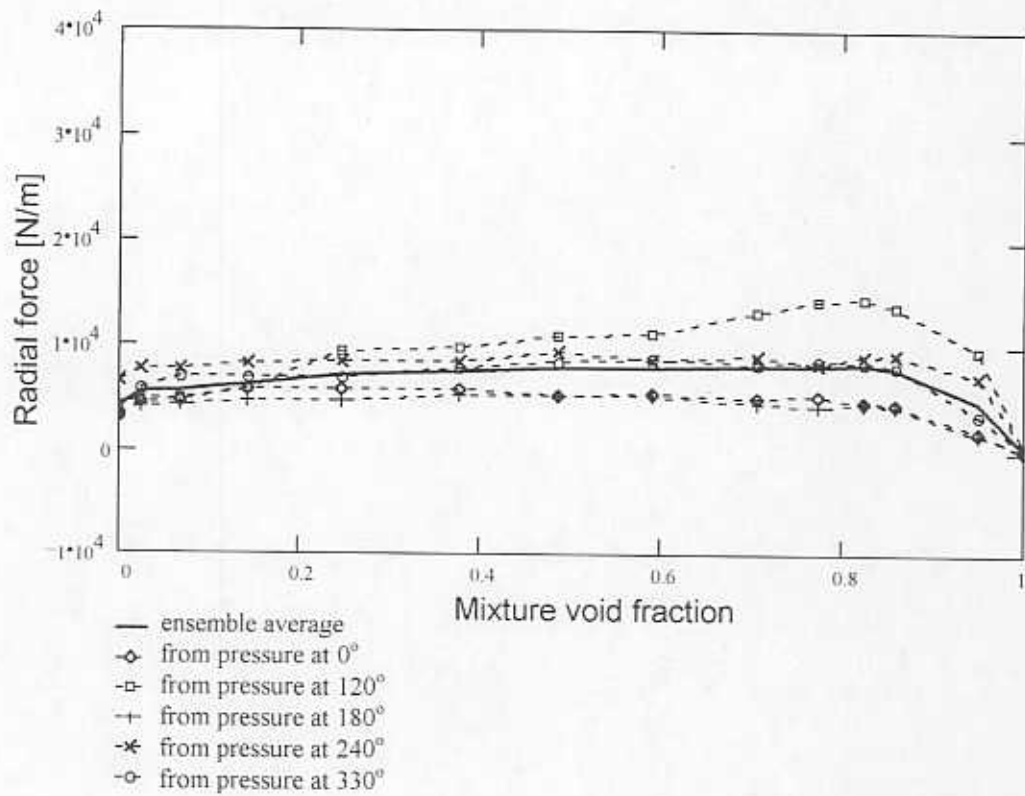
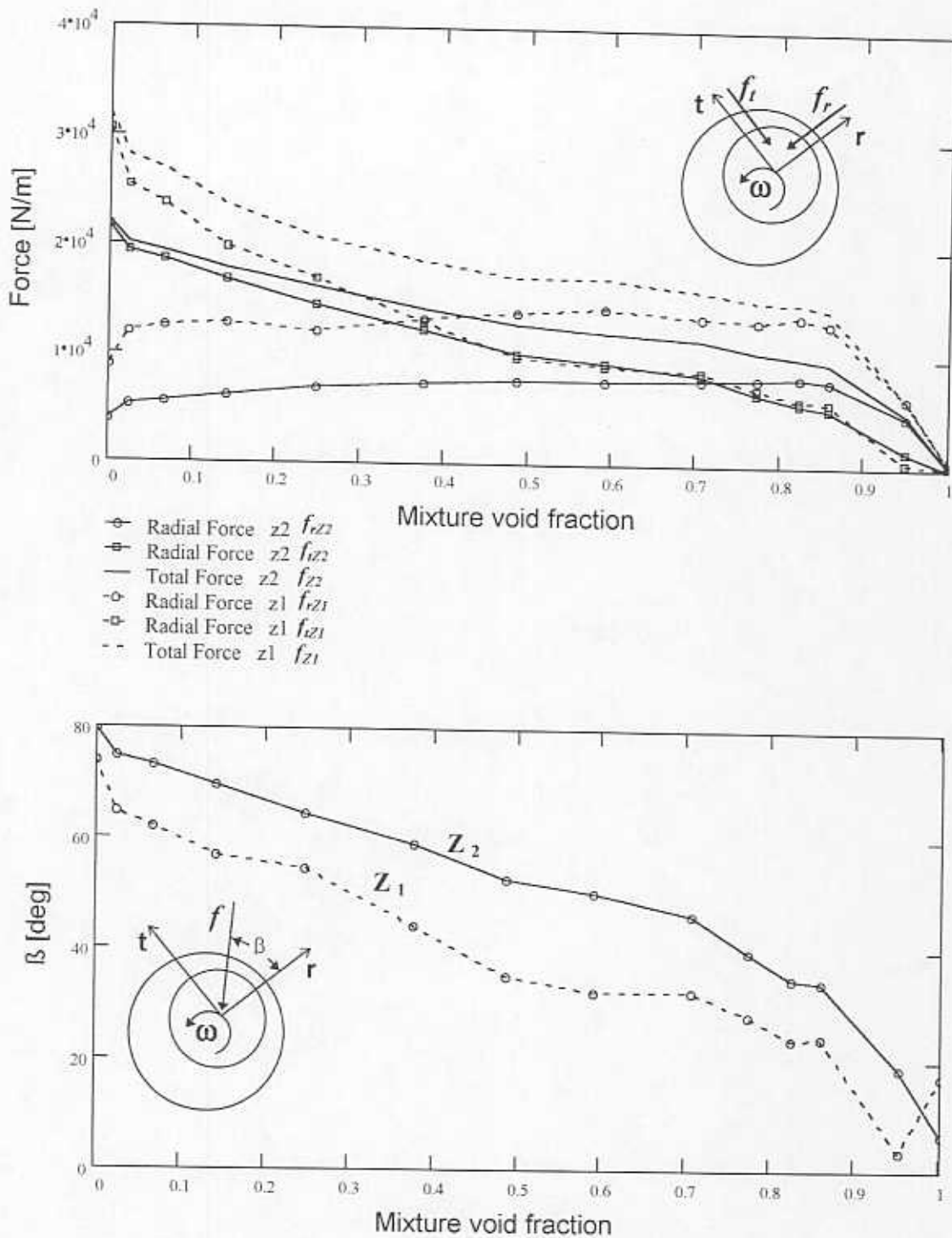Fig. 33.- Radial and tangential forces per unit length at the axial location Z_2 for a whirl frequency of 8.33 Hz.
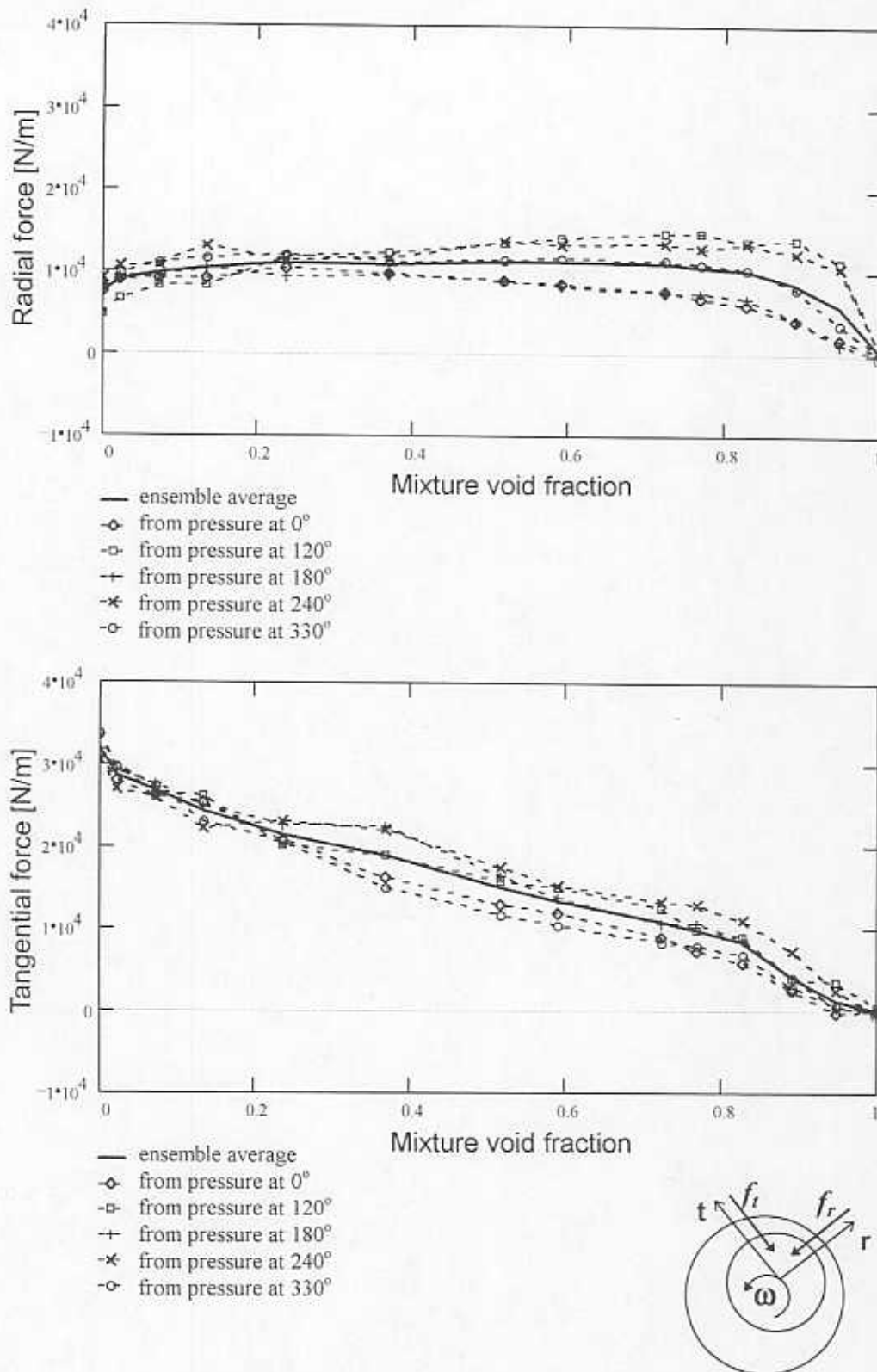
Fig. 34.- Radial and tangential forces per unit length at the axial location Z_2 for a whirl frequency of 16.67 Hz.

Fig. 35.- Ensemble squeeze film average forces per unit length at the axial locations Z_1 and Z_2, for a whirl frequency of 16.67 Hz.
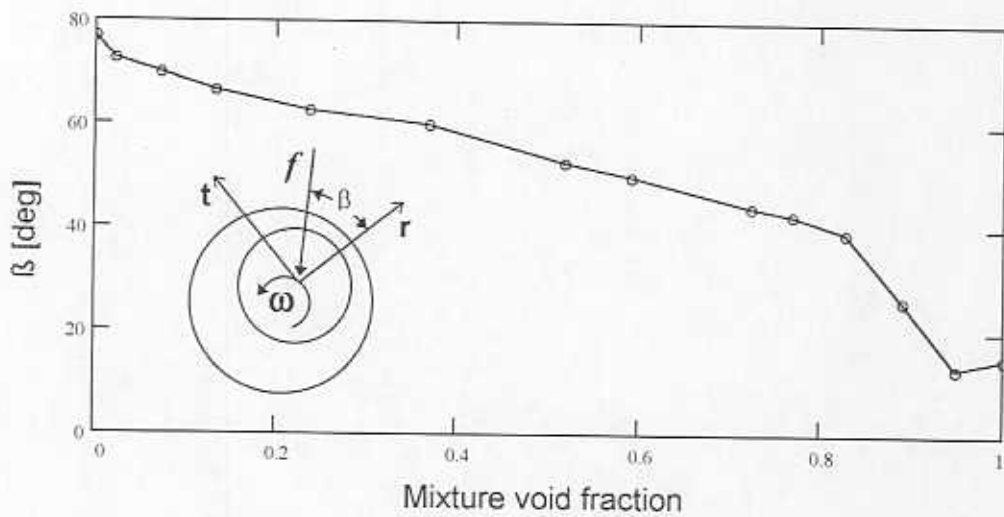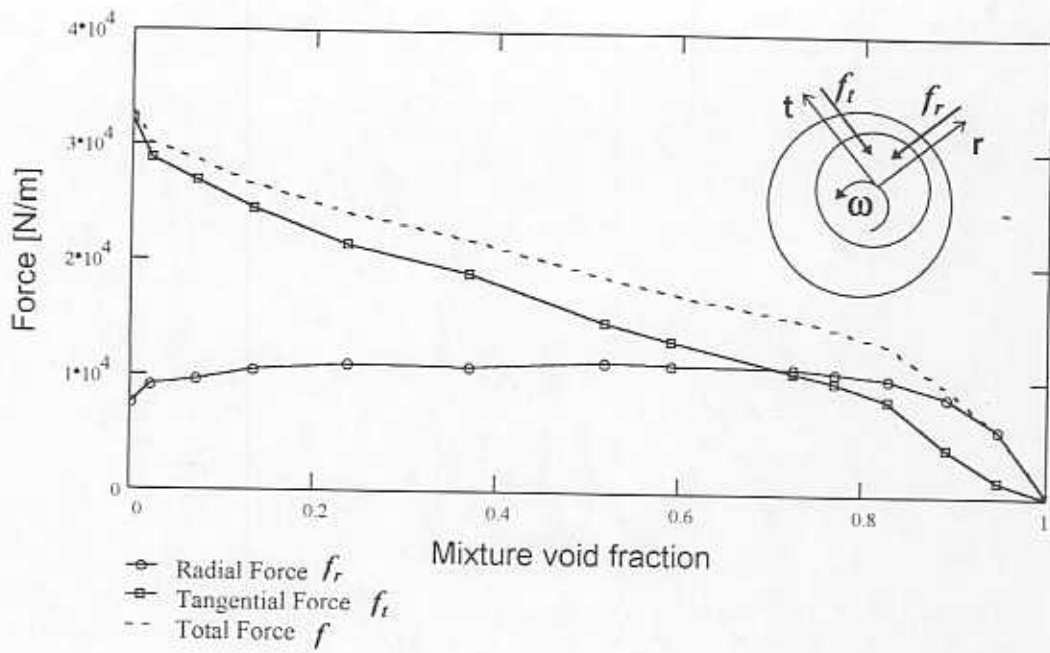
Fig. 36.- Ensemble squeeze film average forces per unit length at the axial location Z_2, for a whirl frequency of 16.67 Hz.
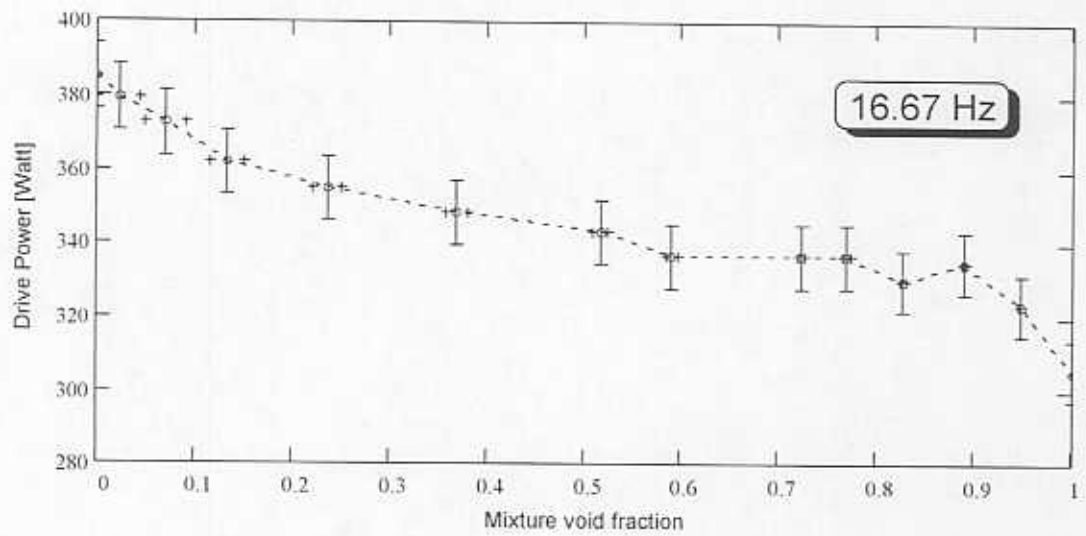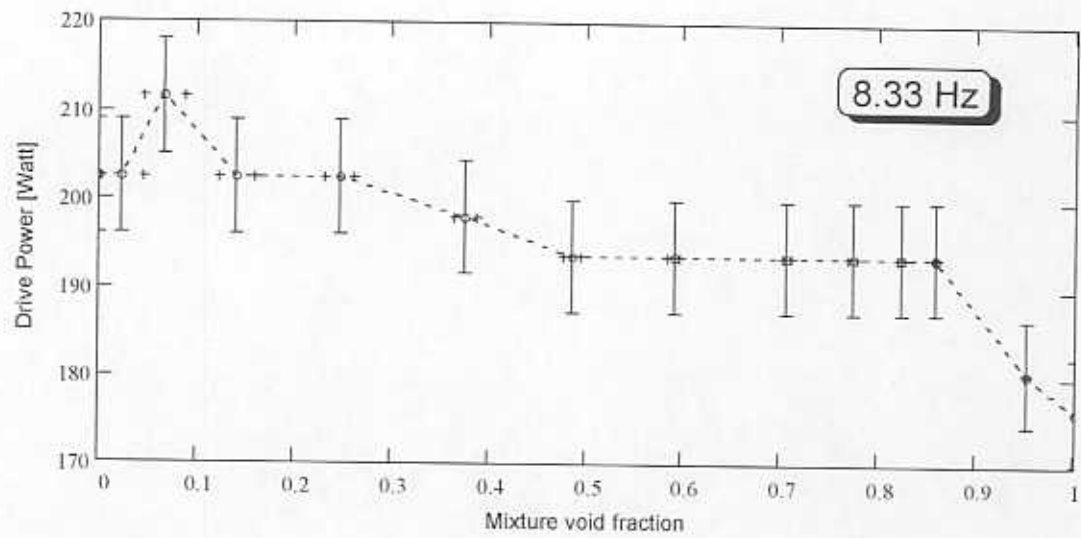
Fig. 37.- Electrical drive power vs. mixture void fraction at whirl
frequencies of 8.33 Hz and 16.67 Hz.